

Gas Phase Studies of Hydrocarbon Oxidation
by Chromium Oxide Cation

Thesis by
Heon Kang

In Partial Fulfillment of the Requirements
for the Degree of
Doctor of Philosophy

California Institute of Technology
Pasadena, California

1986

(Submitted October 15, 1985)

For my mother

Acknowledgment

Many thanks go to my research advisor Jack Beauchamp. His enthusiasm, understanding and friendship will always be appreciated.

I would also like to thank my friends at Caltech for all the good times, particularly the members of the Beauchamp group, past and present, for providing a stimulating and enjoyable learning environment as well as for their friendship. Among them, collaborators in the area of gas phase organometallic chemistry are especially thanked. Bruce Schilling and Maggie Tolbert have always provided valuable discussions related to this research. Denley Jacobson and Professor Mike Bowers have made significant contributions to the research on metal silylenes. I am also indebted to the members of the technical staff, in particular, Tom Dunn, Bill Schuelke, and Tony Stark. Georgia Alwan and Roberta Penska deserve special thanks for their artistic and speedy work in typing this manuscript.

I am grateful to the Korean Government for financial support during my graduate student career.

Finally, I am deeply indebted to Professor S. Chang for his assistance and encouragement in my early career. Above all, I thank my family for all the love, support and encouragement they have given me throughout my life. I wish my mom might be here to share my achievement.

Abstract

An ion beam reactive scattering technique is used to study organo-metallic reactions in the gas phase. Detailed investigations of the reactions of CrO^+ with hydrocarbons are reported. CrO^+ formed by surface ionization oxidizes both alkenes and alkanes larger than methane with a high degree of selectivity compared with other first-row transition metal oxides. Analyses of reaction energetics are facilitated by determination of ancillary thermochemical data, including Cr^+-O and CrO^+-H bond dissociation energies.

Chapter II presents an analysis of the reactions of CrO^+ with alkenes. Major reaction channels include allylic hydrogen abstraction by CrO^+ and oxidative cleavage of double bonds to form aldehydes and smaller alkenes.

Chapter III describes selective oxidation of saturated hydrocarbons by CrO^+ . Major product channels include alcohol formation, dehydrogenation, and loss of alkanes and alkenes. Reaction intermediates in which alkyl C-H bonds add across the Cr^+-O bond are proposed.

Chapter IV presents studies of reactions of transition metal ions (Ti, V, Cr, Fe, Co, and Ni) with organosilanes in the gas phase. These reactions often lead to formation of metal silylenes as major products. An examination of reaction thermochemistry provides estimates for metal-silylene bond dissociation energies. Relationships between the reactivities, metal-silylene bond energies, and the electronic structures of the metal ions are discussed.

Chapter V describes a novel source which generates metal atom and ion beams by focusing a CO_2 TEA laser onto a solid metal target. Kinetic energy distributions of laser-generated atoms and atomic ions are measured using time-of-flight techniques. Possible mechanisms for the

metal ion production as well as aspects of employing the laser-generated beams for gas phase reaction studies are discussed.

TABLE OF CONTENTS

		<u>Page</u>
CHAPTER I	Introduction	1
CHAPTER II	Gas Phase Studies of Alkene Oxidation by Transition Metal Oxides. Ion Beam Studies of CrO^+ .	9
CHAPTER III	Gas Phase Studies of Alkane Oxidation by Transition Metal Oxides. Selective Oxidation by CrO^+ .	43
CHAPTER IV	Reactions of Transition Metal Ions with Methyl Silanes in the Gas Phase; The Formation and Characteristics of Strong Transition Metal-Silylene Bonds.	89
CHAPTER V	Pulsed Laser Evaporation of Solid Metal Targets. Implications for Studying the Gas Phase Reactions of Laser-Generated Atoms and Ions.	139

CHAPTER I

INTRODUCTION

Introduction

Among the active areas of research in chemistry are investigations of oxidation processes involving metal oxide reagents. A desirable characteristic of a useful metal oxide reagent is an ability to effect selective oxidation processes.¹⁻⁵ Selectivity in oxidation reactions often varies in accordance with oxometal bond dissociation energies, making it possible to choose an appropriate oxometal compound for a desired transformation. This may be illustrated in the following two extreme examples. CrO_2Cl_2 is capable of delivering oxygen atoms to most types of oxidizable organic groups from its relatively weak Cr(V)=O bond.³ Therefore, selective oxidation can be achieved only at low temperatures in these reactions. On the other hand, W(IV) reagents⁵, forming a strong W(VI)=O bond, reduce epoxides to olefins. Correlations between the oxometal bond energies of oxidation reagents and their reactivity are certainly of fundamental importance. Unfortunately, most of the oxometal bond energies are not well enough known to predict the reaction thermochemistry of oxidation processes. Although they may endow oxidation reagents and catalysts with desirable properties, structural changes and cooperative bonding phenomena often complicate the detailed analysis of potential energy surfaces for oxidation processes. An ideal reagent for fundamental investigations, therefore, would be one in which a single oxometal bond can be isolated for a study. A practical alternative may be a diatomic metal oxide which has no other ligands attached. Even though these species are coordinatively unsaturated and may not directly resemble complex oxometal compounds, they make it possible to carry out detailed thermochemical and mechanistic studies.

Recent interests in gas phase organometallic chemistry have produced a variety of experimental methods that allow the investigation of such small unsaturated organometallic fragments. They include an ion beam reactive scattering experiment^{6,7}, ion cyclotron resonance spectroscopy,⁸⁻¹⁰ and several other mass spectroscopic techniques.^{11,12} These methods have proven to be very successful in obtaining specific metal ion-ligand bond energies,^{6,7} as well as energetic information relating to organometallic reaction intermediates.⁸⁻¹² In this respect, we have studied the gas phase reactions of a diatomic transition metal oxide species, CrO^+ , with hydrocarbons using ion beam reactive scattering techniques which is presented in Chapters II and III of this thesis. CrO^+ oxidizes both alkenes and alkanes larger than methane. In reactions with alkenes, CrO^+ abstracts hydrogen atom from allylic C-H bonds and adds to double bonds to yield aldehydes and other cleavage products. Reactions with alkanes exhibit alcohol formation, dehydrogenation, and loss of alkanes and alkenes. The patterns in which CrO^+ oxidizes alkenes and alkanes are rather selective compared with the other first-row transition metal oxides. This behavior is analyzed using related thermochemical data including M^+-O and MO^+-H bond dissociation energies.

Chapter IV presents an excursion into a new area of gas phase organometallic chemistry. The ion beam reactive scattering method is employed to investigate gas phase reactions involving transition metal-silicon bonds. Transition metal ions (Ti, V, Cr, Fe, Co, and Ni) are generated by surface ionization and reacted with organosilanes, including the methyl silanes $[(\text{CH}_3)_n\text{SiH}_{4-n}]$, $n = 0-4$ and hexamethyl disilane. A surprising observation, with no precedent in condensed phase chemistry, is prevalent formation of transition metal silylenes as major products.

Correlation of metal-silylene bond energies and the electronic structure of the metal ions provides interesting insights into the nature of transition metal-silylene bonds.

The success of experimental studies of gas phase organometallic reactions depends enormously on the availability of appropriate and dependable sources of reactant species. The development of a new method for generating metal ions and atoms for gas phase reaction studies is described in Chapter V. A high-power pulsed laser delivers energy to a target on a time scale sufficiently short to elevate the instantaneous surface temperature well above the boiling point of the metal, resulting in the generation of an intense pulse of metal atoms and ions. The interaction of high-power pulsed lasers with solid materials has been studied extensively and many reviews are available.^{13,14} Briefly, initial interaction of laser radiation with a surface increases the surface temperature. The reflectivity of the metal surface drops rapidly as the surface becomes heated by the laser. Hence, energy can be delivered to the surface effectively even with IR lasers which emit radiation in a wavelength region where most of the cold metal surfaces have high reflectivity. For example, a 500-nsec-duration pulse from a CO₂ TEA laser, which can deliver a power density of $\sim 10^8$ watts cm⁻² to a stainless steel target, drops the surface reflectivity rapidly over a time period comparable to the laser pulse.^{14(a)} The range of laser power density may be divided into four categories depending on the physical process which dominates the interaction between the high-power laser pulse and the solid material. At relatively low power densities, melting is the main effect. When the power densities are greater than ca. 10^6 watts cm⁻², the surface reaches its boiling temperature so rapidly that the dominant

physical process becomes vaporization. Target material is removed as a vapor, producing a hole in the target. If the laser light is intense enough ($>10^7$ - 10^8 watts cm^{-2}), the early portion of the laser pulse evaporates a small amount of material from the surface. This material is slightly thermally ionized and produces an opaque, high temperature plasma by absorbing more incoming laser light. Most of the laser light is cut off by the plasma, and little laser energy is delivered to the surface. The process of generating the high temperature plasma (inverse Bremsstrahlung) has a cross section which increases with the square of the laser wavelength. Hence, CO_2 lasers are expected to be more effective than visible or UV lasers in generating the plasma. Finally, when the power density becomes very high ($>10^{13}$ watts cm^{-2}), an additional absorption mechanism, which is called the collective plasma effect, may become operative.

An important application of this methodology is to use the laser-generated particles as a beam source for gas phase kinetic studies. Metal ions,¹⁵ atoms,^{16,17} and clusters¹⁸⁻²⁰ generated in this fashion are now being widely used in conjunction with beam and ICR experiments. In our laboratory, fundamental studies of physical phenomena related to the generation of metal atoms and ions have been undertaken. During the course of these studies, we observed that metal atoms are ejected from the source backwards along the laser light, with an angular distribution which narrows as the laser drills a small hole in the metal surface. These results indicate that a practical beam source should avoid fogging of the window through which the laser light is introduced and take advantage of the beam collimation which may develop as a channel is formed in the target. A novel source design is described in Chapter V which

addresses these desirable experimental conditions. A parabolic reflector focuses the laser beam onto a small target and particles emitted from the target are sampled through a small aperture in the mirror. Metal atoms and ions are generated by CO₂ TEA laser pulses with power density in the range 10^7 - 10^9 watts cm⁻². The laser-generated atoms have kinetic energies which range from thermal to as high as 10 eV, depending on the laser irradiation conditions and target geometry. Kinetic energy distributions of the metal ions and atoms produced from this source are presented and discussed.

Selected References

1. J.S. Pizey, "Synthetic Reagents", Vol. 2, pp. 143-174. Wiley, New York, 1974.
2. M. Schroeder, Chem. Rev. 80, 187 (1980).
3. K.B. Wiberg, in "Oxidation in Organic Chemistry" (K.B. Wiberg, ed.), Part A, p. 69. Acad. Press, New York, 1965.
4. K.B. Sharpless, A.Y. Teranish, J. Am. Chem. Soc., 93, 3120 (1977).
5. (a) K.B. Sharpless, M.A. Umbreit, M.T. Nieh, and T.C. Flood, J. Am. Chem. Soc., 94, 6538 (1972).
(b) A. Sattar, J. Forrester, M. Moir, J. S. Roberts, and W. Parker, Tetrahedron Lett. 1403 (1978).
6. (a) P.B. Armentrout and J.L. Beauchamp, J. Am. Chem. Soc., 103, 784 (1981).
(b) L.F. Halle, P.B. Armentrout, and J.L. Beauchamp, Organometallics, 1, 963 (1982).
(c) M.L. Mandich, L.F. Halle, and J.L. Beauchamp, J. Am. Chem. Soc., 106, 4403 (1984).
7. N. Aristov and P.B. Armentrout, J. Am. Chem. Soc., 106, 4065 (1984).
8. J. Allison and D.P. Ridge, J. Am. Chem. Soc., 101, 4998 (1979).
9. D.B. Jacobson and B.S. Freiser, J. Am. Chem. Soc., 107, 72 (1985) and references therein.
10. M.A. Hanratty, C.M. Paulsen, and J.L. Beauchamp, J. Am. Chem. Soc., 107, 5074 (1985).
11. M.A. Hanratty, J.L. Beauchamp, A.J. Illies, and M.T. Bower, J. Am. Chem. Soc., 107, 1788 (1985).
12. D.A. Peake, M.L. Gross, and D.P. Ridge, J. Am. Chem. Soc., 106, 4307 (1984).

14. (a) J.F. Ready, "Industrial Applications of Lasers", Acad. Press, New York, 1978.
(b) J.F. Ready, "Effects of High-Power Laser Radiation", Acad. Press, New York, 1971.
15. (a) R.B. Cody, R.C. Burnier, W.D. Reents, Jr., T.J. Carlin, D.A. McCrery, R.K. Lengel, and B.S. Freiser, Int. J. Mass Spectrom. and Ion Phys. 33, 37 (1980).
(b) D.B. Jacobson and B.S. Freiser, J. Am. Chem. Soc., 106, 3891 (1984).
16. (a) J.F. Friichtenicht, Rev. Sci. Instrum 45, 51 (1974).
(b) B.G. Wicke, J. Chem. Phys., 78, 6036 (1983).
17. P. Leismann, V. Henc-Bartolic, U. Rebhan, and H.J. Kunze, Physica Scripta, 30, 186 (1984).
18. M.D. Morse, G.P. Hansen, P.R.R. Langridge-Smith, Lan-Sun Zheng, M.E. Geusic, D.L. Michalopoulos, and R.E. Smalley, J. Chem. Phys. 80, 5400 (1984).
19. V.E. Bondybey and J.H. English, J. Chem. Phys. 80, 568 (1984).
20. R.L. Whetten, D.M. Cox, D.J. Trevor, and A. Kaldor, J. Phys. Chem. 89, 566 (1985).

CHAPTER II

GAS PHASE STUDIES OF ALKENE OXIDATION BY
TRANSITION METAL OXIDES.
ION BEAM STUDIES OF CrO^+

GAS PHASE STUDIES OF ALKENE OXIDATION BY TRANSITION
METAL OXIDES. ION BEAM STUDIES OF CrO^+

H. Kang and J.L. Beauchamp^{*}

Contribution No. from the Arthur Amos Noyes Laboratory of Chemical
Physics, California Institute of Technology, Pasadena, California 91125.

^{*} Author to whom correspondence should be addressed.

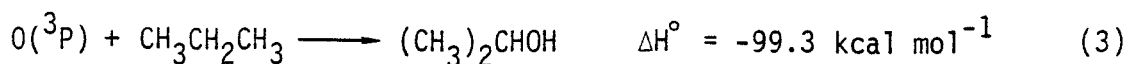
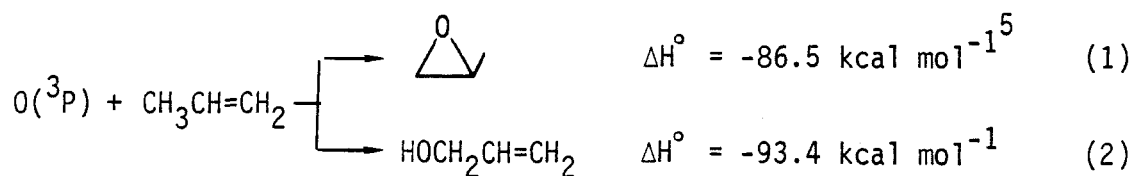
Abstract

An examination of reaction thermochemistry and metal oxide bond dissociation energies focuses attention on the chromium oxide ion as an interesting candidate for investigations of hydrocarbon oxidation processes. Reactions of this species, formed by surface ionization, have been examined using ion-beam reactive scattering techniques. In reactions with alkenes, CrO^+ abstracts allylic hydrogen to form CrOH^+ and adds to double bonds to yield aldehydes and other products which are rationalized by postulating metallacyclic intermediates. In comparison with other first-row transition metal oxides, which are either too stable (Sc, Ti, and V) or too reactive (Mn, Fe, Co, and Ni), CrO^+ exhibits a balance in being reactive but selective. Bond dissociation energies derived in this study include $D^0(\text{Cr}^+-\text{O}) = 85.3 \pm 1.3 \text{ kcal mol}^{-1}$ and $D^0(\text{Cr}-\text{O}) = 110 \pm 2 \text{ kcal mol}^{-1}$.

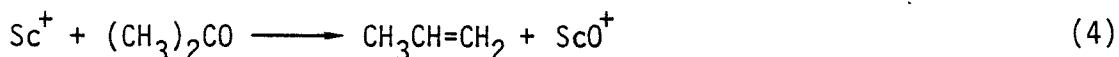
Introduction

Oxidation reactions involving metal oxide reagents¹ and catalysts² play an important role in organic synthesis owing to their capacity for selective oxygen transfer to a wide variety of substrates. A key mechanistic feature common in these reactions is the participation by one or more oxometal groups (M-O) in the transformation. Although the mechanisms of these reactions have received a considerable amount of attention, it is often difficult to completely characterize important reactive intermediates in condensed phase studies. In the present work, we report ion beam studies of the reactions of the simplest metal oxide reagent, which is a diatomic metal oxide ion, with alkenes in the gas phase, where the identities of reactants and nascent products are readily ascertained. Topics relating to selective oxidation of alkanes by CrO^+ in the gas phase will be presented in a subsequent paper.³ A discussion of the energetics and mechanisms of the observed reactions derives benefit from the growing thermochemical data base being obtained in recent gas phase studies of the reactions of atomic transition metal ions with various organic molecules.⁴

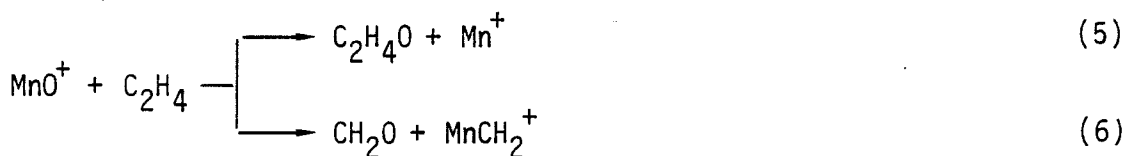
Several factors are important in selecting a metal oxide system for detailed studies. Consider the energetics of several oxidation processes involving alkenes and alkanes, including epoxidation (reaction 1), allylic oxidation (reaction 2), and formation of alcohols from saturated alkanes (reaction 3).



Reactions such as these in which oxygen is transferred from a transition metal center will be roughly thermoneutral when the metal-oxygen bond dissociation energy is in the range 85~100 kcal mol⁻¹. Consider next the available bond dissociation energies for transition metal oxide ions in Table I. The early transition metals, Sc, Ti, and V form stable metal oxide ions which would be unreactive with alkanes and alkenes. These atomic metal ions might be expected to react with oxygen containing organic molecules to regenerate hydrocarbons and metal oxide ions. This behavior is exemplified by reaction (4) in which Sc⁺ reacts with acetone to yield ScO⁺ and propene.⁶



The late transition metals Mn, Fe, Co, and Ni have metal oxide ion bond dissociation energies [$D^\circ(\text{M}^+-\text{O})$] which are low, leading to the possibility of exothermic processes for the reactions of these metal oxide ions with alkanes and alkenes. While favorable overall thermochemistry does not insure a facile reaction, a growing number of examples support the contention that barriers in exothermic reactions of transition metal oxide ions are rare. For example, MnO⁺ undergoes reactions (5) and (6)



with ethene.⁷ FeO⁺ reacts with various hydrocarbons, reactions (7)-(11) being examples.^{4(i),8} Freiser and co-workers have reported an extensive study of the reactions of FeO⁺ with alkanes, demonstrating the exceptional and relatively nonselective reactivity of this weakly bonded metal oxide. Bridging these extremes in behavior is the chromium oxide molecular ion,

Table I. Thermochemical Data of the First-row
Transition metal Oxides

Metal	$D^\circ (M^+ - O)$ kcal mol ⁻¹	$D^\circ (M - O)$ kcal mol ⁻¹	IP(MO) eV	$D^\circ (M^+ - OH)$ kcal mol ⁻¹	$D^\circ (MO^+ - H)$ kcal mol ⁻¹
Sc	159±7 ^a	161.5±3 ^a	6.6±0.3 ^a		
Ti	161±5 ^a	158.4±2 ^a	6.7±0.1 ^a		
V	131±5 ^{b,p}	146±4 ^c	7.4±0.3 ^o		
Cr	85.3±1.3 ^d	110±2 ^d	7.85±0.02 ^e	73±5 ^q	89±5 ^q
Mn	57±3 ^f	85±4 ^g	8.65±0.2 ^f		
Fe	69±3 ^f	93±3 ^{h,i}	8.9±0.16 ^{f,h,i}	73±3 ^{h,j}	106±4 ^{h,n}
Co	64±3 ^f	87±4 ^{k,l}	8.9±0.2 ^{f,k}	71±3 ^j	107±4 ⁿ
Ni	45±3 ^f	89±5 ^{l,m}	9.5±0.2 ^{f,m}		

^aE. Murad, J. Geophys. Res. **83**, 5525 (1978).

^bReference 4-h.

^cM. Farber, O. Manuel Uy, and R.D. Srivastava, J. Chem. Phys. **56**, 5312 (1972).

^dThis study.

^eReference 21.

^fReference 23.

^gC.J. Cheetam and R.F. Barrow, Adv. High. Temp. Chem. **1**, 7 (1967).

^hE. Murad, J. Chem. Phys. 73, 1381 (1980).

ⁱD.L. Hildenbrand, Chem. Phys. Lett. 34, 352 (1975).

^jC.J. Cassady and B.S. Freiser, J. Am. Chem. Soc. 106, 6176 (1984).

^kR.T. Grimley, R.P. Burns, and M.G. Inghram, J. Chem. Phys. 45, 4158 (1966).

^lS. Smoes, F. Mandy, A. Auwera-Mahieu, and J. Drowart, Bull. Soc. Chim. Belg. 81, 45 (1972).

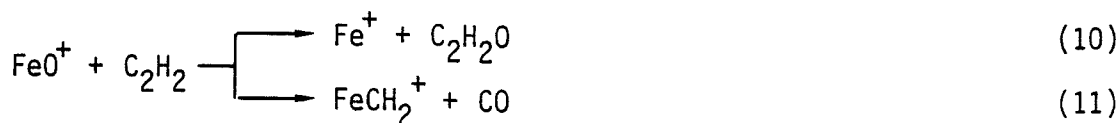
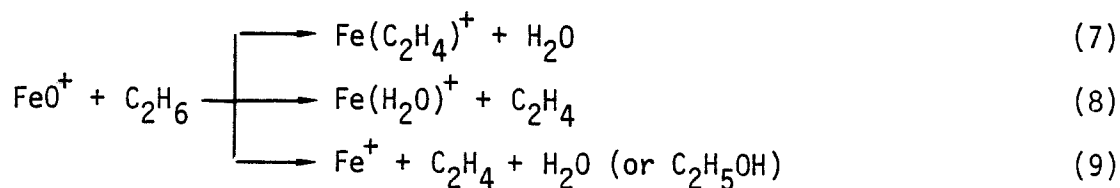
^mR.T. Grimley, R.P. Burns, and M.G. Inghram, J. Chem. Phys. 35, 551 (1961).

ⁿDerived from $D^{\circ}(\text{MO}^+ - \text{H}) = D^{\circ}(\text{M}^+ - \text{OH}) - D^{\circ}(\text{M}^+ - \text{O}) + D^{\circ}(\text{O} - \text{H})$.

^oDerived from $\text{IP}(\text{MO}) = D^{\circ}(\text{M} - \text{O}) - D^{\circ}(\text{M}^+ - \text{O}) + \text{IP}(\text{M})$.

^pReference 4-j.

^qReference 3.



with a metal oxide ion bond dissociation energy ($85.3 \text{ kcal mol}^{-1}$) which renders processes such as reactions 1-3 only slightly exothermic and possibly very selective. For this reason we considered this species an interesting subject for study, particularly in view of the many investigations of the oxidation reactions involving various chromium oxide reagents in solution.

Experimental

A detailed description of the ion beam apparatus used for these experiments is available elsewhere.⁹⁻¹¹ Briefly, ions generated from a source are accelerated and focused into a 60° sector magnet for mass separation. The mass selected beam is decelerated to a selected energy and focused into a collision chamber containing the reactant gas. Product ions scattered in the forward direction are focused into a quadrupole mass filter, and detected using a channeltron electron multiplier operated in a pulse counting mode. Ion signal intensities are corrected for the mass discrimination of the quadrupole mass filter.

CrO^+ beam is produced by surface ionization of CrO_2Cl_2 . CrO_2Cl_2 vapor is introduced through a leak valve onto a hot rhemium filament where dissociation and ionization of the resulting fragments occur. In order of decreasing yield, the three most abundant species observed are Cr^+ ,

CrO^+ , and CrCl^+ . No significant amounts of triatomic species are produced. CrO , having a relatively strong metal oxide bond and low ionization potential (Table I), yields the CrO^+ ion in greater abundance than can be obtained with the group 8-10 metal oxides. At the filament temperature used, $\sim 1300^\circ \text{K}$, it is estimated that over 97% of the CrO^+ and over 99% of the Cr^+ produced are in their electronic ground states (Table II). It is also estimated that 51% of the CrO^+ are in the vibrational ground state ($v = 0$), 25% are in $v = 1$ state, 12% are in $v = 2$ state, and the rest are in higher vibrational states.

Reaction cross sections for specific products, σ_i , are obtained by using Eq. 12 and 13 which relate the total reaction cross section, σ , the

$$I_0 = (I_0 + \sum I_i) \exp(-n_0 \sigma I) \quad (12)$$

$$\sigma_i = \sigma I_i / \sum I_i \quad (13)$$

number density of the target gas, n_0 , and the length of the collision chamber, I , to the transmitted reactant ion beam intensity, I_0 , and the sum of the product ion intensities, $\sum I_i$. The pressure of the target gas is kept low ($< 2 \times 10^{-3}$ torr) to minimize attenuation of the beam and ensure that reactions are the result of only a single bimolecular collision.

It is important to point out that neutral products are not detected in these experiments. However, except where noted below, the identity of these products can usually be inferred without ambiguity. In addition, these experiments provide no direct structural information about the ionic products. Thermochemical arguments can often distinguish possibilities for isomeric structures.

Table II. Low-lying States of Cr^+ and CrO^+

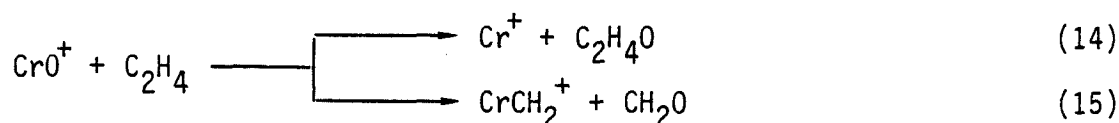
Ion	Low-lying states	Energy, eV	Vib. frequency cm^{-1}
$\text{Cr}^+,^a$	^6S	0.0	
	^6D	1.52	
$\text{CrO}^+,^b$	$^4\Sigma^-$	0.0	640±30
	$^4\Pi$	0.65	

^aReference 22.

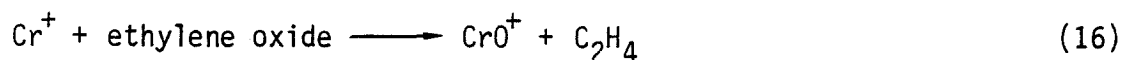
^bReference 21. Energies are ab initio SCF + CI calculational results.

Results and Discussion

Reaction of CrO^+ with Ethene. Reaction of CrO^+ with ethene yields Cr^+ as an exothermic ionic product, liberating $\text{C}_2\text{H}_4\text{O}$ as a neutral fragment (reaction 14). Formation of chromium carbene ion (reaction 15) is observed as an endothermic process (Fig. 1). To assign the structure of the neutral

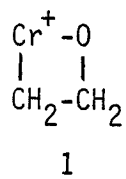


product, $\text{C}_2\text{H}_4\text{O}$, the reverse of reaction 14 was examined for two possible structural isomers, acetaldehyde and ethylene oxide. Cr^+ reacts with ethylene oxide to regenerate CrO^+ and ethene exothermically (reaction 16), cross section data of which are presented in Figure 3(a). On the other hand, no exothermic reaction is observed with acetaldehyde (reaction 17). Hence, the neutral product in reaction 14 must be acetaldehyde. It is



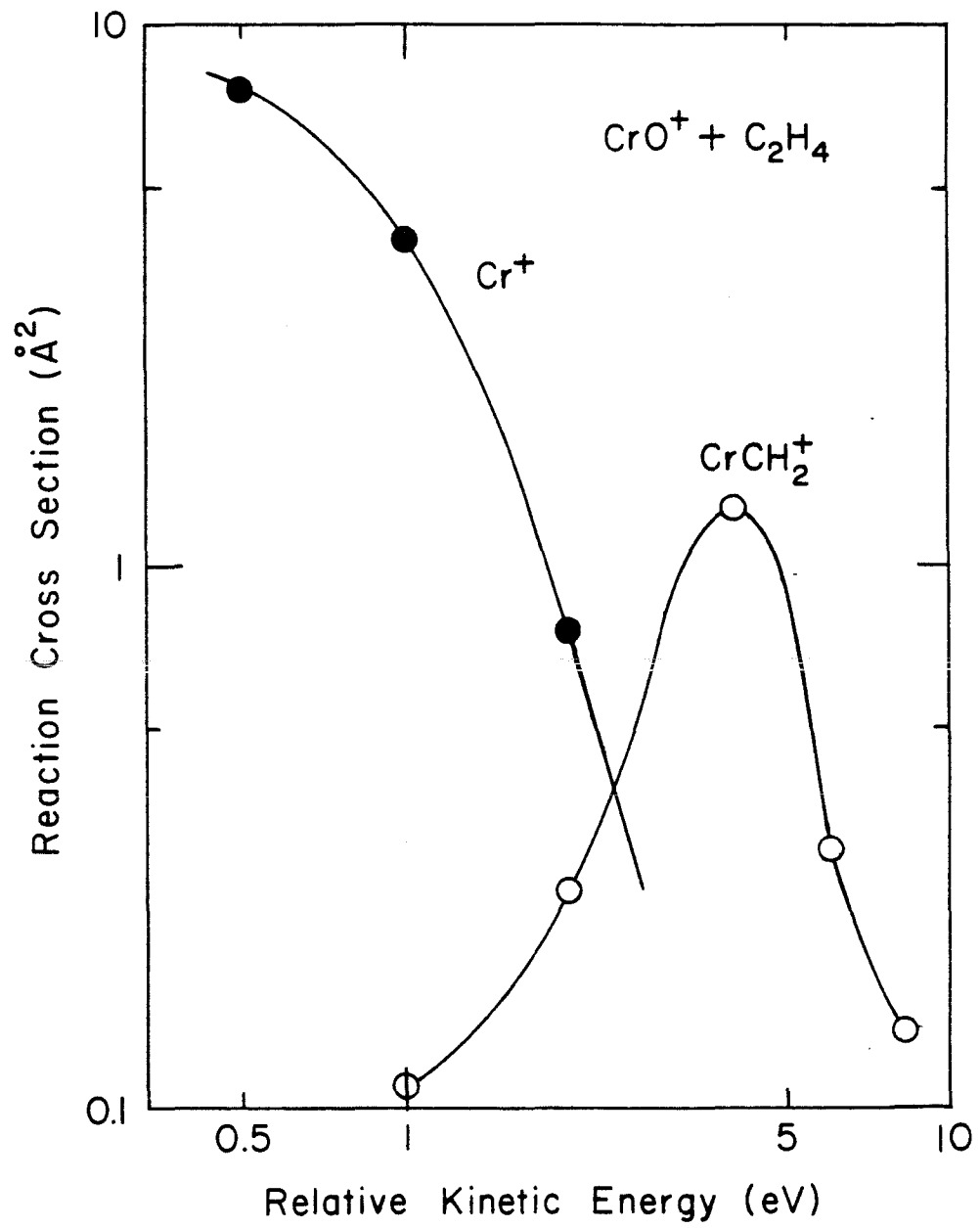
interesting to note that reactions 14 and 16 comprise a catalytic cycle which converts ethylene oxide into acetaldehyde with zero activation energy.¹²

A metallacycle intermediate 1, produced by a four-center cycloaddition of CrO^+ to ethene, may be postulated to account for the observed products



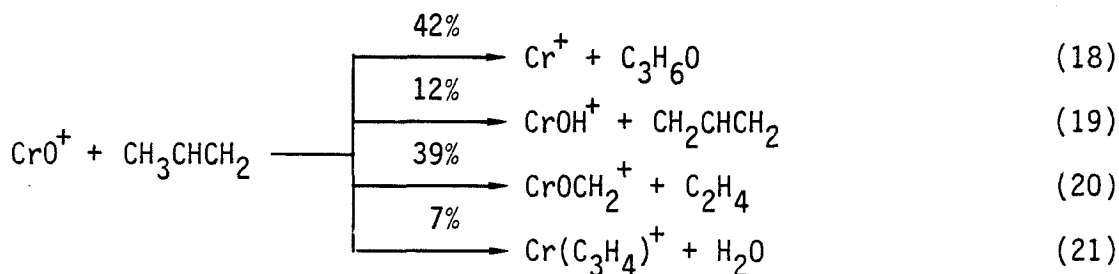
in the reaction of CrO^+ with ethene. Subsequent decomposition of the metallacycle intermediate may result in formation of Cr^+ (reaction 14),

Figure 1. Variation with relative kinetic energy of the experimental cross section for the reaction of CrO^+ with ethene. The products Cr^+ and CrCH_2^+ exhibit cross sections characteristic of exothermic and endothermic reactions, respectively.



CrCH_2^+ (reaction 15), or CrO^+ which is the reaction proceeding back to reactants. Generation of CrCH_2^+ in the reaction of CrO^+ with ethene (reaction 15) is calculated to be 28 kcal mol^{-1} endothermic.¹⁵

Reactions of CrO^+ with Larger Alkenes. Reactions of CrO^+ with larger alkenes yield a variety of products including Cr^+ , CrOH^+ , and other fragmentation products at low energy (Table III). The reaction with propene will be discussed in detail to exemplify the observed processes. CrO^+ reacts with propene to yield Cr^+ , CrOH^+ , CrOCH_2^+ , and $\text{Cr}(\text{C}_3\text{H}_4)^+$ (reactions 18-21). The formation of CrOH^+ very likely results



from abstraction of an allylic hydrogen (reaction 19). CrOH^+ is considered to be chromium hydroxide and not a metal hydride, since the allylic C-H bond dissociation energy, $D^\circ(\text{CH}_2\text{CHCH}_2\text{-H}) = 86.3 \text{ kcal mol}^{-1}$,¹³ is higher than any known metal ion-hydrogen bond dissociation energy. On the other hand, $\text{MO}^+\text{-H}$ bonds are usually strong enough to render abstraction of a hydrogen atom from the allylic C-H bond by a metal oxide ion an exothermic process (Table I).¹⁴

Observation of the facile allylic hydrogen abstraction process leads to a postulated mechanism shown in Scheme I. First, the initial association of propene and CrO^+ results in allylic hydrogen atom transfer to the oxygen center (Path A). Since the formation of CrOH^+ is an exothermic process by itself, the allyl radical could be either eliminated to yield CrOH^+ (6) or remain bonded to CrO^+ forming an energetic intermediate (2 or 3). Both

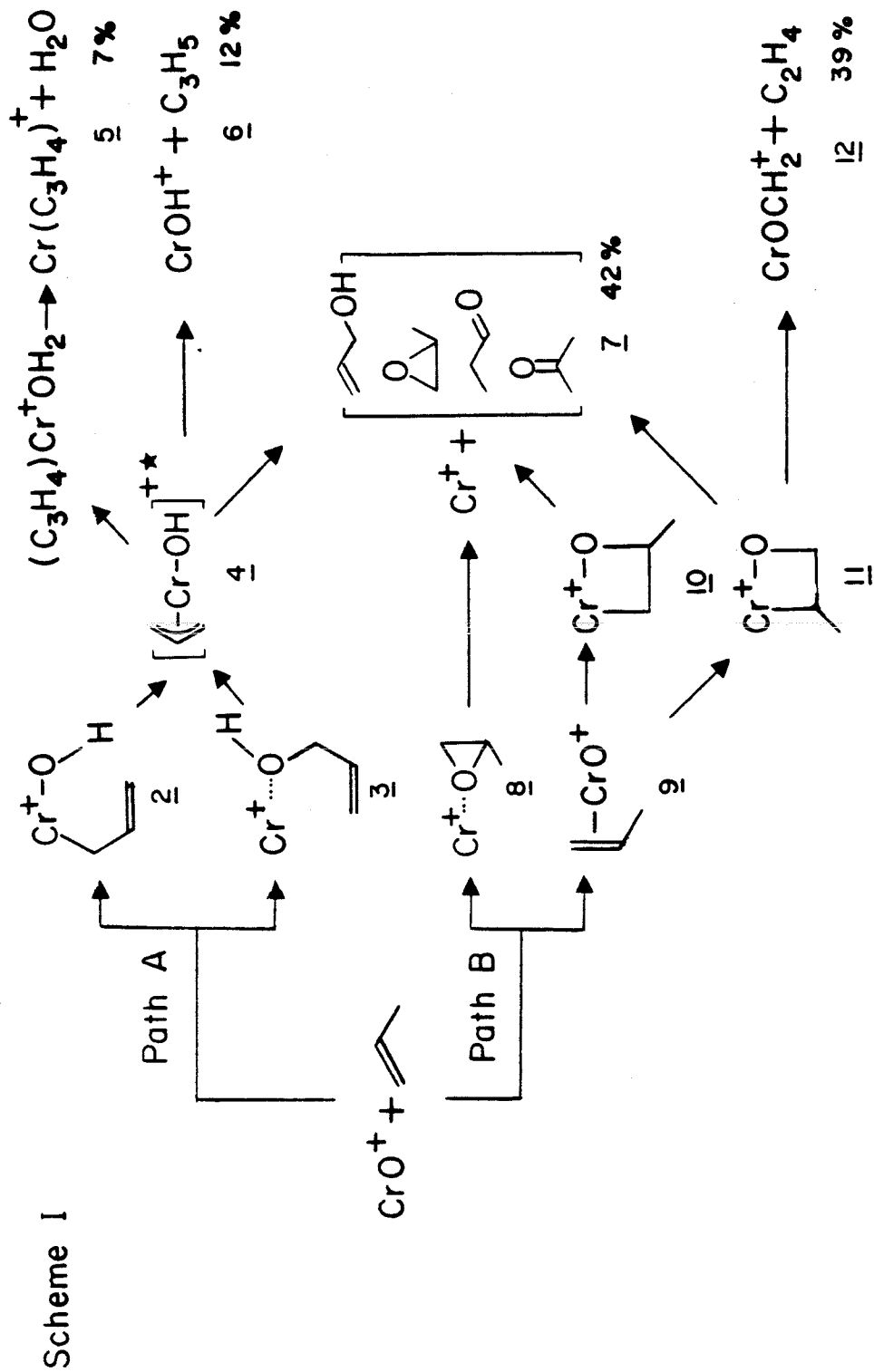
Table III. Product distributions for the exothermic reactions of CrO^+ with alkenes^a

<u>Alkene</u>	<u>Total cross section, Å²</u>	<u>Neutral lost</u>	<u>Ion Product</u>	<u>% of Total</u>
ethene	8	CH_3CHO	Cr^+	100
propene	70	H_2O	$\text{Cr}(\text{C}_3\text{H}_4)^+$	7
		C_2H_4	CrOCH_2^+	39
		CH_2CHCH_2	CrOH^+	12
		$\text{C}_3\text{H}_6\text{O}$	Cr^+	42
2-methyl propene	52	CH_3	$\text{Cr}(\text{C}_3\text{H}_5\text{O})^+$	11
		H_2O	$\text{Cr}(\text{C}_4\text{H}_6)^+$	11
		CH_3CHCH_2	CrOCH_2^+	9
		$\text{CH}_2\text{C}(\text{CH}_3)\text{CH}_2$	CrOH^+	34
		$\text{C}_4\text{H}_8\text{O}$	Cr^+	35
1-butene	88	CH_4	$\text{Cr}(\text{C}_3\text{H}_4\text{O})^+$	11
		H_2O	$\text{Cr}(\text{C}_4\text{H}_6)^+$	5
		C_2H_4	$\text{Cr}(\text{C}_2\text{H}_4\text{O})^+$	30
		CH_3CHCH_2	CrOCH_2^+	6
		C_4H_6	CrOH_2^+	5
		$\text{C}_4\text{H}_8\text{O}$	Cr^+	43

Table III, cont'd

<u>Alkene</u>	<u>Total cross section, Å²</u>	<u>Neutral lost</u>	<u>Ion product</u>	<u>% of total</u>
cis-2-butene	140	H ₂	Cr(C ₄ H ₆ O) ⁺	13
		CH ₄	Cr(C ₃ H ₄ O) ⁺	5
		H ₂ O	Cr(C ₄ H ₆) ⁺	4
		C ₂ H ₄	Cr(C ₂ H ₄ O) ⁺	40
		C ₄ H ₆	CrOH ₂ ⁺	7
		C ₄ H ₈ O	Cr ⁺	31

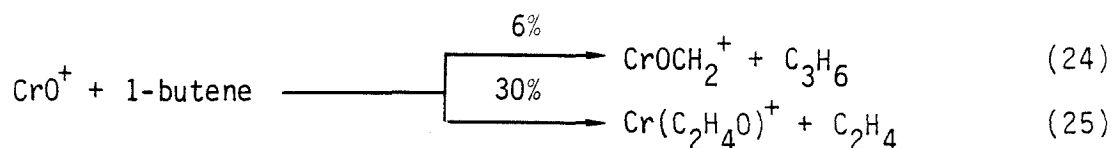
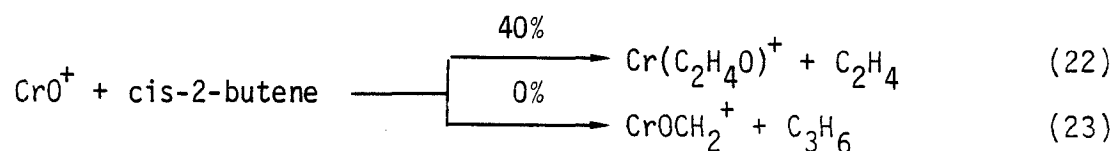
^aProduct distributions are measured at 0.5 eV relative kinetic energy.



2 and 3 can rearrange to an allyl hydroxy complex ion (4) and in turn to 5, 6, or 7. Hence, we consider Cr^+ , CrOH^+ , and $\text{Cr}(\text{C}_3\text{H}_4)^+$ as products which may be generated via this mechanism.

Another product of the reaction with propene, CrOCH_2^+ , which involves cleavage of the carbon-carbon bond of propene, cannot be explained by the mechanism proposed above. The product can be rationalized by postulating a metallacycle intermediate similar to 1 for the reaction with ethene. The initial step probably involves formation of an ion-molecule complex (9), which is followed by a four-center cycloaddition reaction to yield either 10 or 11. Decomposition of 11 can lead either to CrOCH_2^+ and ethene (12) or to Cr^+ and $\text{C}_3\text{H}_6\text{O}$ (7). Direct addition of an oxygen atom to the double bond is also possible (8), which probably yields Cr^+ and propylene oxide (7). Decomposition of metallacycle intermediate 10 into CrCH_2^+ and acetaldehyde is estimated to be 21 kcal mol^{-1} endothermic.¹⁵ Formation of the metal carbene product by decomposition of such metallacycle intermediate should become an energetically facile process as the metal oxide bond strength decreases relative to the metal carbene bond strength. This conjecture is substantiated by observation of metal carbene products in the reactions of ethene with MnO^+ ⁷ and ClCrO_2^+ .¹⁶

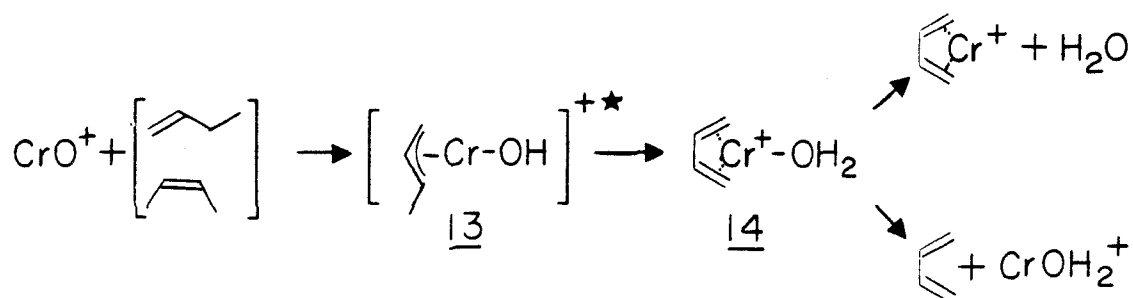
Several interesting points can be noted in the reactions of CrO^+ with 1-butene and cis-2-butene. Reactions 22-25 involve cleavage of C-C bonds



in the alkene, possibly via a mechanism similar to the one proposed for the reaction with propene (Scheme I). Reaction with *cis*-2-butene yields $\text{Cr}(\text{C}_2\text{H}_4\text{O})^+$ (reaction 22), representing cleavage of an internal double bond. This is an example of specific cleavage of an alkene double bond, the fragmented products containing information about the position of a double bond in the precursor molecule. The reaction with 1-butene yields CrOCH_2^+ , which can be simply accounted for the cleavage of the terminal double bond. This, however, is a minor product (reaction 24). The major product in which C-C bond cleavage occurs is $\text{Cr}(\text{C}_2\text{H}_4\text{O})^+$, which can be explained only by invoking rearrangement processes prior to cleavage. Therefore, cleavage of the double bond in 1-butene is nonspecific.

In comparing the reactivity of propene and 2-methyl propene to 1-butene and 2-butene, the reactions of CrO^+ with both propene and 2-methyl propene yield CrOH^+ , while the reactions with 1-butene and *cis*-2-butene do not. Since both 1-butene and *cis*-2-butene have allylic hydrogens, they might be expected to react with CrO^+ via the allylic oxidation pathway to form an allyl-hydroxy intermediate (13 of Scheme II). However, a facile

Scheme II



β -hydrogen transfer process, as shown in Scheme II, appears to be preferred to the loss of allyl radical in the reactions with 1-butene and cis-2-butene. The β -hydrogen transfer process is obviously not accessible for propene and 2-methyl propene. The water-butadiene ion complex (14) thus formed may lose either water or butadiene. Therefore, in the reactions of CrO^+ with 1- and 2-butenes, the allylic oxidation pathway leads to the products $\text{Cr}(\text{C}_4\text{H}_6)^+$ and CrOH_2^+ .

Reactions of Cr^+ with $\text{C}_3\text{H}_6\text{O}$ Isomers. Reaction intermediates such as 2, 3, 8 and 9 of Scheme I could resemble intermediates which might form in the reactions of Cr^+ with $\text{C}_3\text{H}_6\text{O}$ structural isomers. For this reason it is of interest to compare product distributions for such reactions with those observed for the reaction of CrO^+ with propene. Reactions examined for this purpose are listed in Table IV for the $\text{C}_3\text{H}_6\text{O}$ isomers trimethylene oxide, propylene oxide, propylene oxide, allyl alcohol, propanal, and acetone. An important consideration in comparing these reactions is the heat of formation of the reactants (Figure 2). If common intermediates are formed, then product distributions are expected to be identical only at the same level of internal excitation. For this reason, it is desirable to compare product distributions at different collision energies as well as at the same collision energy when the reactants have considerably different heats of formation.

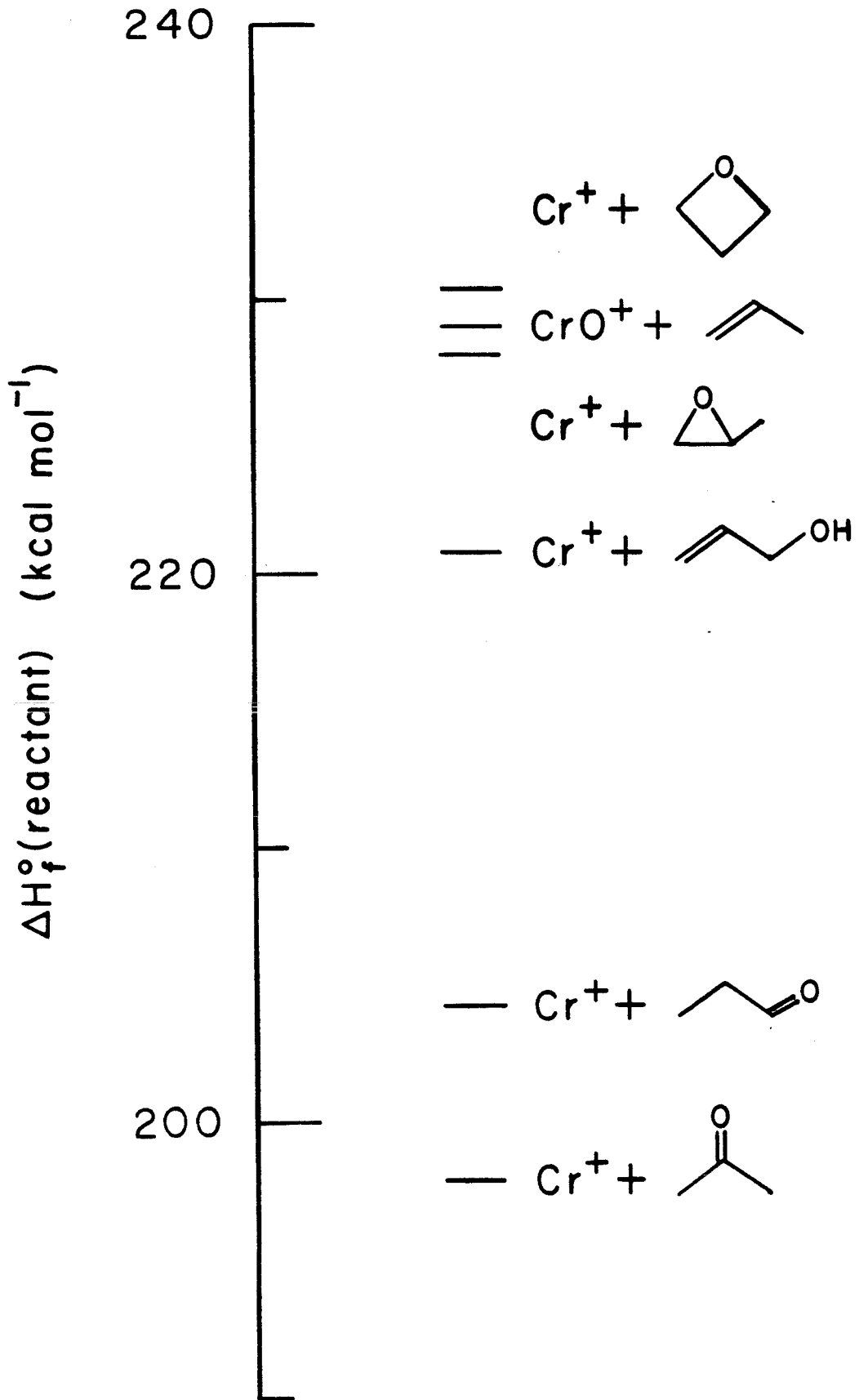
The reaction of Cr^+ with allyl alcohol, which is expected to involve an intermediate similar to 3 in Scheme I, yields $\text{Cr}(\text{C}_3\text{H}_4)^+$ and $\text{Cr}(\text{C}_3\text{H}_4\text{O})^+$ at low energy (Table IV). $\text{Cr}(\text{C}_3\text{H}_4)^+$ is proposed in Scheme I as an allylic oxidation product in the reaction of CrO^+ with propene. Formation of CrOH^+ in the reaction of Cr^+ with allyl alcohol is observed at higher

Table IV. Product distributions for the reactions of Cr^+ with several oxygen containing C_3 organic molecules.

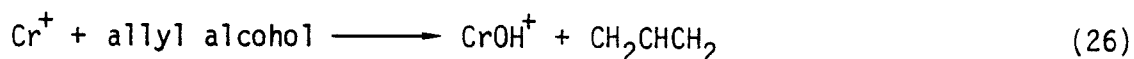
Reaction	Relative Kinetic Energy, eV	Total Cross Section, Å^2	Product, % of Total Cross Section							
			Cr^+	CrO^+	CrOH^+	CrOCH_2^+	$\text{Cr}(\text{C}_2\text{H}_4)^+$ &/or $\text{Cr}(\text{CO})^+$	CrOCH_2^+	$\text{Cr}(\text{C}_3\text{H}_4)^+$	$\text{Cr}(\text{C}_3\text{H}_4\text{O})^+$
$\text{CrO}^+ + \text{propene}$	0.5	70	42	0	12	0	0	39	7	0
$\text{Cr}^+ + \text{trimethylene oxide}$	1.0	12	40	0	10	0	0	30	0	20
$\text{Cr}^+ + \text{propylene oxide}$	0.5	140	0	0	0	0	30 ^a	70	0	0
$\text{Cr}^+ + \text{allyl alcohol}$	1.0	20	0	0	0	0	40	60	0	0
$\text{Cr}^+ + \text{propanal}$	0.5	50	0	0	0	6	7	60	16	11
$\text{Cr}^+ + \text{acetone}$	1.0	10	8	3	2	4	55	19	9	36
	0.5	14	0	0	0	0	0	0	64	36
	1.0	20	0	13	13	0	0	0	38	36
	0.5	N.R.								
	2.0	N.R.								
	0.5	N.R.								
	2.0	N.R.								

^aReaction of Cr^+ with trimethylene oxide -1, 1, 3, 3-d₄ yields $\text{Cr}(\text{C}_2\text{H}_2\text{D}_2)^+$, but $\text{Cr}(\text{CO})^+$ is not produced.

Figure 2. Heats of formation of various combinations of Cr^+ and CrO^+ with C_3 organic molecules.²⁰



energies (reaction 26), as expected from $D^\circ(\text{Cr}^+-\text{OH}) < D^\circ(\text{CH}_2\text{CHCH}_2-\text{OH}) = 78 \text{ kcal mol}^{-1}$,¹³ (Table I). This illustrates that the reaction



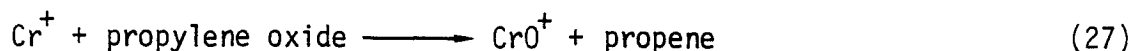
of Cr^+ with allyl alcohol, with excess translational energy, gives rise to all the allylic oxidation products proposed in Scheme I for the reaction of CrO^+ with propene, namely, CrOH^+ and $\text{Cr}(\text{C}_3\text{H}_4)^+$. Considering that this system has less energy available to the reactants than the reaction of CrO^+ with propene (Figure 2), these observations are consistent with the postulated intermediate 3 in Scheme I. We consider both 2 and 3 to be possible as an initial intermediate for the allylic oxidation process, since intermediates 2, 3, and 4 are expected to be easily interconvertible at the level of internal excitation provided when CrO^+ abstracts allylic hydrogen from propene.

Reaction of Cr^+ with propylene oxide yields products including CrOH_2^+ , $\text{Cr}(\text{C}_2\text{H}_4)^+$ and/or $\text{Cr}(\text{CO})^+$, CrOCH_2^+ , $\text{Cr}(\text{C}_3\text{H}_4)^+$, and $\text{Cr}(\text{C}_3\text{H}_4\text{O})^+$ [Table IV and see Figure 3(b)]. CrOCH_2^+ is the major product from this reaction. Since this is also the major product from the reaction of CrO^+ with propene, a common intermediate, the metallacycle 11 in Scheme I, may be implicated. The reaction of Cr^+ with propylene oxide yields several additional products which are not observed in the reaction of CrO^+ with propene, namely, CrOH_2^+ , $\text{Cr}(\text{C}_2\text{H}_4)^+$ and/or $\text{Cr}(\text{CO})^+$, and $\text{Cr}(\text{C}_3\text{H}_4\text{O})^+$. This indicates the availability of several reaction pathways in addition to metallacycle formation.

As an additional point, reactions of Cr^+ with trimethylene oxide, propylene oxide, and allyl alcohol, give rise to very different product distributions. This indicates that three different intermediates may be formed in these reactions which are not easily interconvertible. Propanal

and acetone do not react with Cr^+ in the energy ranges considered.

Chromium-Oxygen Bond Dissociation Energy. An examination of the thermochemistry for the reactions generating CrO^+ provides an estimate for the Cr^+-O bond energy. Observation of CrO^+ in the exothermic reaction of Cr^+ with ethylene oxide (reaction 16) provides a lower limit for $D^\circ(\text{Cr}^+-\text{O})$ of $84.0 \text{ kcal mol}^{-1,5}$. Reaction of CrO^+ with propylene oxide, on the other hand, yields CrO^+ as an endothermic product (reaction 27), providing an upper limit for $D^\circ(\text{Cr}^+-\text{O})$ of $86.5 \text{ kcal mol}^{-1}$. Figures 3(a) and (b) present

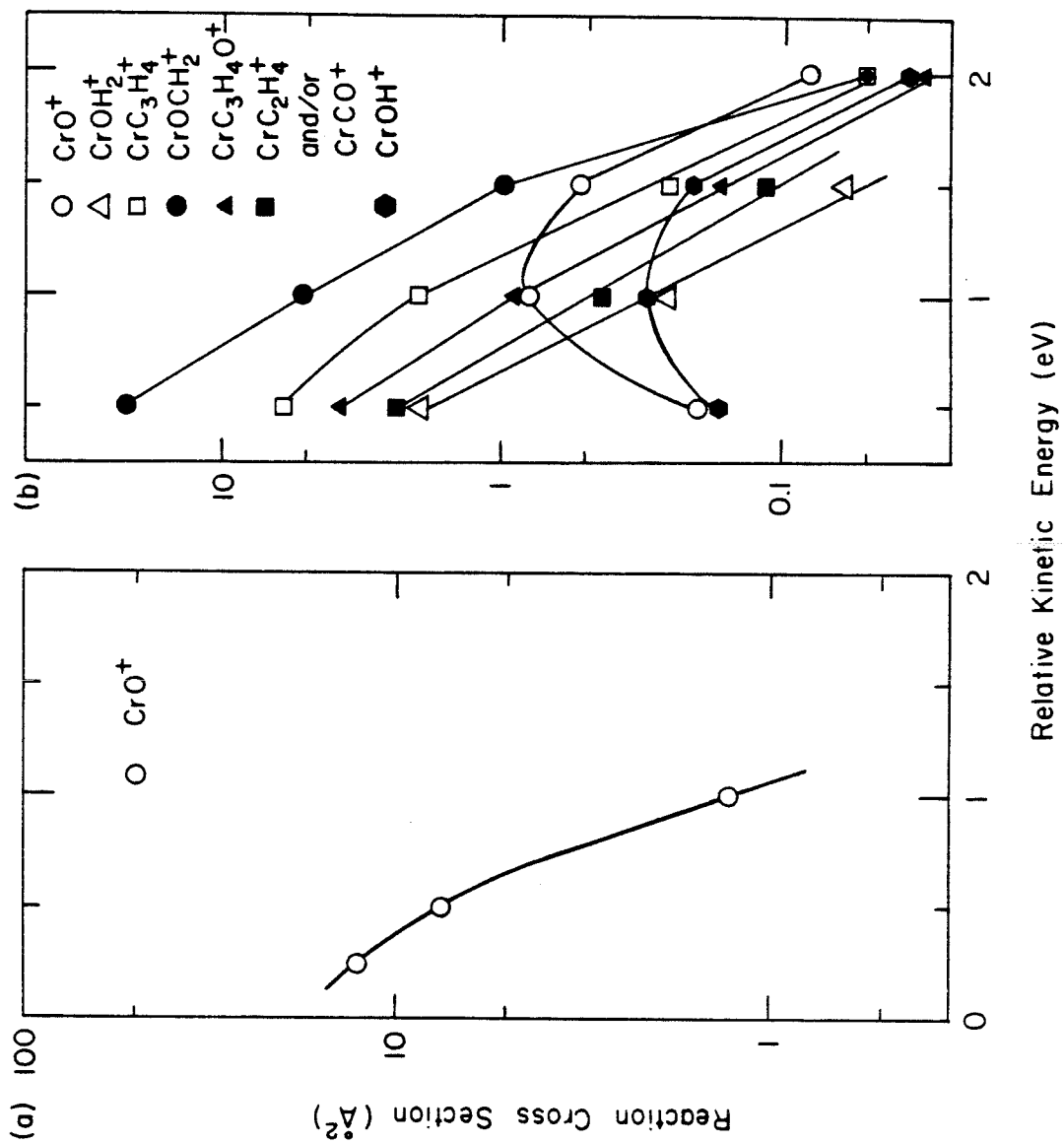


experimental cross section data for these reactions, which are consistent with exothermic and endothermic formation of CrO^+ from the reaction of Cr^+ with ethylene oxide (reaction 16) and propylene oxide (reaction 27), respectively.

Reaction 27 is one of the many competing product channels of the reaction with propylene oxide as shown in Figure 3(b). As a result, caution should be exercised in interpreting the experimental cross section for CrO^+ formation as indicating an endothermic reaction, since the observed increase in cross section with increasing kinetic energy might be due to competition with processes which are more favorable at lower levels of excitation. This possible complication seems remote, however, considering the similarity between reactions with ethylene oxide (reaction 16) and propylene oxide (reaction 27). Hence, we choose to interpret the data in Figure 3(b) as indicating that reaction 27 is endothermic.

Using $D^\circ(\text{Cr}^+-\text{O}) = 85.3 \pm 1.3 \text{ kcal mol}^{-1}$, the neutral $\text{Cr}-\text{O}$ bond dissociation energy can be derived from the thermodynamic cycle implied by Equation 28, which gives $D^\circ(\text{Cr}-\text{O}) = 110 \pm 2 \text{ kcal mol}^{-1}$. These values are

Figure 3. Variation in experimental cross section as a function of relative kinetic energy for (a) the reaction of Cr^+ with ethylene oxide. (b) the reaction of Cr^+ with propylene oxide.



$$D^{\circ}(\text{Cr}-\text{O}) = D^{\circ}(\text{Cr}^{+}-\text{O}) + \text{IP}(\text{CrO}) - \text{IP}(\text{Cr}) \quad (28)$$

compared with other literature values in Table V.

Conclusion

Gas phase CrO^{+} undergoes exothermic reactions with all of the alkenes considered in this study. CrO^{+} oxidizes ethene into acetaldehyde. Reactions with larger alkenes exhibit hydrogen abstraction, C-C bond cleavage, and formation of oxygen containing products including aldehydes. An examination of reactions of Cr^{+} with $\text{C}_3\text{H}_6\text{O}$ isomers provides useful information concerning reaction pathways involved in alkene oxidation by CrO^{+} . The major pathways include allylic oxidation, which proceeds via abstraction of allylic hydrogen by CrO^{+} , and formation of chemically activated metallacycle intermediates by cycloaddition of CrO^{+} and the double bond.

The present results exhibit interesting similarities to condensed phase alkene oxidations by oxometal reagents. The observation of allylic hydrogen abstraction by CrO^{+} parallels several studies of alkene oxidation by heterogeneous metal oxide catalysts.^{17,18} The formation of metallacycle intermediates has analogies in the mechanism proposed for reactions of CrO_2Cl_2 with alkenes in solution.¹⁹ In the gas phase, CrO^{+} oxidizes alkenes via both pathways, bridging the gap between the heterogeneous metal oxide catalysts and other solution phase oxometal reagents. Observation of such varieties of oxidation pathways from a simple diatomic metal oxide ion is quite surprising and suggests that even mechanistically complex heterogeneous allylic oxidation processes might be interpreted in terms of rather simple reactions involving specific active sites.

Table V. Cr^+-O and $\text{Cr}-\text{O}$ bond dissociation energies^a

<u>Bond Energy</u>	<u>This Study</u>	<u>Literature</u>
$D^\circ(\text{Cr}^+-\text{O})$	85.3 ± 1.3	76 ± 7^b 80 ± 3^c 86 ± 5^d
$D^\circ(\text{Cr}-\text{O})$	110 ± 2	101 ± 7^b

^aIn kcal mol^{-1} .

^b $D^\circ(\text{M}^+-\text{O}) = D^\circ(\text{M}-\text{O}) + \text{IP}(\text{M}) - \text{IP}(\text{MO})$.

$D^\circ(\text{Cr}-\text{O})$ from R.T. Grimley, R.P. Burns, and M.G. Inghram,
J. Chem. Phys., 34, 664 (1961).

^cRef. 23.

^dRecent measurement by P.B. Armentrout, et al. (to be published).

Acknowledgment

We gratefully acknowledge the support of the National Science Foundation under Grant CHE-8407857. Graduate fellowship support by the Korean Government (H.K.) is gratefully acknowledged.

References

1. For a review of oxidation reactions by oxometal reagents, see R.A. Sheldon and J.A. Kochi, "Metal Catalyzed Oxidations of Organic Compounds," Ch. 6. Academic Press, New York, 1981; K.B. Wiberg, "Oxidations in Organic Chemistry", Part A, Academic Press, New York, 1965, pp. 69-184.
2. B.C. Gates, J.R. Katzer, and G.C.A. Schuit, "Chemistry of Catalytic Processes", Ch. 4. McGraw-Hill, New York, 1974.
3. H. Kang and J.L. Beauchamp, J. Am. Chem. Soc. (submitted for publication).
4. a. L.F. Halle, P.B. Armentrout, and J.L. Beauchamp, Organometallics, 1, 963 (1982).
b. M.L. Mandich, L.F. Halle, and J.L. Beauchamp, J. Am. Chem. Soc., 106, 4403 (1984).
c. J. Allison and D.P. Ridge, J. Am. Chem. Soc., 101, 4998 (1979).
d. B.S. Larsen and D.P. Ridge, J. Am. Chem. Soc., 106, 1912 (1984).
e. R.C. Burnier, G.D. Byrd, and B.S. Freiser, J. Am. Chem. Soc., 103, 4360 (1981).
f. G.D. Byrd, R.C. Burnier, and B.S. Freiser, J. Am. Chem. Soc., 104, 3565 (1982).
g. D.B. Jacobson and B.S. Freiser, J. Am. Chem. Soc., 107, 4373 (1985) and references therein.
h. N. Aristov and P.B. Armentrout, J. Am. Chem. Soc., 106, 4065 (1984).
i. M.M. Kappes and R.H. Staley, J. Am. Chem. Soc., 103, 1286 (1981).

- j. M.M. Kappes and R.H. Staley, J. Phys. Chem., 85, 942 (1981).
5. J.D. Cox and G. Pilcher, "Thermochemistry of Organic and Organometallic Compounds", Academic Press, New York, 1970.
 6. M.A. Tolbert and J.L. Beauchamp, J. Am. Chem. Soc., 106, 8117 (1984).
 7. A.E. Stevens and J.L. Beauchamp, J. Am. Chem. Soc., 101, 6449 (1979).
 8. T.C. Jackson, D.B. Jacobson, and B.S. Freiser, J. Am. Chem. Soc., 106, 1252 (1984).
 9. P.B. Armentrout and J.L. Beauchamp, J. Chem. Phys., 74, 2819 (1981).
 10. P.B. Armentrout and J.L. Beauchamp, J. Am. Chem. Soc., 103, 784 (1981).
 11. P.B. Armentrout and J.L. Beauchamp, Int. J. Mass Spectrom. Ion Phys., 29, 375 (1979).
 12. Small activation barriers along the reaction coordinate can often be overcome by the ion-molecule association energy, rendering the overall activation energy to be nearly zero; for a discussion of the activation energy question, see J.M.S. Henis, J. Chem. Phys., 52, 282 (1970).
 13. D.F. McMillen and D.M. Golden, Ann. Rev. Phys. Chem., 33, 493 (1982).

14. Bond energies other than those listed in Table I include,
 $D^\circ(\text{CaO}^+-\text{H}) = 150 \pm 14$, $D^\circ(\text{SrO}^+-\text{H}) = 141 \pm 9$, and $D^\circ(\text{BaO}^+-\text{H}) = 134 \pm 9$
kcal mol⁻¹ from E. Murad, J. Chem. Phys., 75, 4080 (1981).
15. $D^\circ(\text{Cr}^+-\text{CH}_2) = 54 \pm 5$ kcal mol⁻¹ from; P.B. Armentrout, et al. (to be
published). $D^\circ(\text{M}_n^+-\text{CH}_2) = 94 \pm 7$ kcal mol⁻¹ from P.B. Armentrout,
L.F. Halle, and J.L. Beauchamp, J. Am. Chem. Soc., 103, 6501 (1981).
16. D.M. Walba, C.H. Depuy, J.J. Grabowski, and V.M. Bierbaum, Organo-
metallics, 3, 498 (1984). CrO_2Cl^+ is expected to have relatively
weak oxochromium bonds compared with CrO^+ . Since the number of
electrons involved in oxochromium bond may be same for both CrO_2Cl^+
and CrO_2Cl_2 , the bond dissociation energy of CrO_2Cl^+ is expected to
be close to that of CrO_2Cl_2 , which is 51 kcal mol⁻¹ with double bond
character (Ref. 24).
17. R.K. Grasselli and J.D. Burrington, Adv. Catal., 30, 133 (1981) and
references therein.
18. W. Martin and J.H. Lunsford, J. Am. Chem. Soc., 103, 3728 (1981);
J.C. Schultz and J.L. Beauchamp., J. Phys. Chem., 87, 3587 (1983).
19. K.B. Sharpless, A.Y. Teranishi, J. Org. Chem., 38, 185 (1973);
K.B. Sharpless, A.Y. Teranishi, and J.E. Backvall, J. Am. Chem. Soc.,
93, 3120 (1977).

20. $\Delta H_f^\circ(\text{Cr}^+) = 250.3 \text{ kcal mol}^{-1}$ from H.M. Rosenstock, K. Draxl, B.W. Steiner, and J.T. Herron, J. Phys. Chem. Ref. Data Suppl., 6 (1977).
Heats of formation for organic molecules are from Ref. 5.
21. J.M. Dyke, B.W.J. Gravenor, R.A. Lewis and A. Morris, J. Chem. Soc.,
Faraday Trans. 2, 79, 1083 (1983).
22. C.E. Moore, "Atomic Energy Levels", (National Bureau of Standards,
Washington, D.C., 1971).
23. P.B. Armentrout, L.F. Halle, and J.L. Beauchamp, J. Chem. Phys., 76,
2449 (1982).
24. A.K. Rappe and W.A. Goddard III, J. Am. Chem. Soc., 102, 5114 (1980);
J. Am. Chem. Soc., 104, 3287 (1982).

CHAPTER III

GAS PHASE STUDIES OF ALKANE OXIDATION
BY TRANSITION METAL OXIDES.
SELECTIVE OXIDATION BY CrO^+

GAS PHASE STUDIES OF ALKANE OXIDATION BY TRANSITION
METAL OXIDES. SELECTIVE OXIDATION BY CrO^+ .

H. Kang and J.L. Beauchamp^{*}

Contribution No. from the Arthur Amos Noyes Laboratory of Chemical
Physics, California Institute of Technology, Pasadena, California 91125.

*Author to whom correspondence should be addressed.

Abstract

The gas phase reactions of CrO^+ with alkanes have been studied using ion beam reactive scattering techniques. CrO^+ undergoes facile reactions with alkanes larger than methane. CrO^+ oxidizes ethane into ethanol selectively. In addition to the possibility of alcohol formation, reactions with larger alkanes are more complex, yielding products in which dehydrogenation and loss of alkenes and alkanes occur. In reactions with cyclic alkanes, cyclopropane and cyclobutane yield products characteristic of C-C bond cleavage. In contrast, reactions with cyclopentane and cyclohexane mainly involve dehydrogenation and elimination of H_2O . A series of hydrogen abstraction reactions are examined to determine the bond dissociation energy $D^\circ(\text{CrO}^+-\text{H}) = 89 \pm 5 \text{ kcal mol}^{-1}$. This bond energy has implications for the reaction mechanisms of CrO^+ with alkanes, leading to the suggestion of a multicenter reaction intermediate, in which alkyl C-H bonds add across the Cr^+-O bond as an initial step. This is supported by an examination of the reactions of Cr^+ with alcohols.

Introduction

The development of new reagents and catalysts for the selective oxidation of saturated hydrocarbons remains an active area of interest among chemists. Desirable targets include such possibilities as the activation of methane and terminal oxidation of an alkane chain.^{1,2} However, there is an intrinsic need for better understanding of the mechanisms of oxidation processes with particular emphasis being placed on elucidation of elementary processes. Of particular interest is the question as to whether or not oxidations of organic substrates involve intermediates with metal-carbon bonds. In the absence of any M-C bond formation, radical intermediates formed by hydrogen atom abstraction are likely to be the mode of hydrocarbon oxidation,²⁻⁴ a route which is not well designed for selectivity in general. On the other hand, reaction intermediates in which M-C bonds are formed offer the possibility of using the expanding body of knowledge in organometallic chemistry to design more selective alkane oxidation systems. The question of possible organometallic intermediates have been raised in a number of cases, but seldom answered unequivocally in condensed phase studies. In this paper, we report gas phase studies of simplified alkane oxidation systems which permit detailed examination of the reaction energetics as well as mechanisms.

In a previous study from our laboratory,⁴ arguments based on energetic considerations were presented which suggested that CrO^+ is an ideal reagent for studies of gas phase oxidation processes. The conjecture that this species would be both reactive and selective was generally supported by studies of alkene oxidation. In our earlier study, the bond dissociation energy $D^\circ(\text{Cr}^+-\text{O}) = 85.3 \pm 1.3 \text{ kcal mol}^{-1}$ was determined. With this value, the general oxidation process indicated in reaction 1 will typically be

Table I. Reaction Enthalpies Used In Text.

<u>Reaction</u>		<u>ΔH° rxn, kcal mol⁻¹,^a</u>
O (³ P) + H ₂	→ H ₂ O	-116.8
O + CH ₄	→ CH ₃ OH	-89.2
	→ CH ₂ O + H ₂	-67.1
	→ H ₂ O + CH ₂	-5.2 ^b
O + C ₂ H ₆	→ CH ₄ + CH ₂ O	-82.7
	→ CH ₃ CH ₂ OH	-95.0
	→ CH ₃ OCH ₃	-82.8
	→ C ₂ H ₄ + H ₂ O	-84.1
	→ CH ₃ OH + CH ₂	-6.9
O + CH ₃ CH ₂ CH ₃	→ 1-propanol	-95.3
	→ 2-propanol	-99.3
	→ CH ₃ OC ₂ H ₅	-85.9
	→ CH ₃ OH + C ₂ H ₄	-69.8
	→ H ₂ + allyl alcohol	-63.8
	→ H ₂ + propanol	-79.8
	→ H ₂ + acetone	-86.2
	→ Cyclopropane + H ₂ O	-79.3
	→ Propene + H ₂ O	-87.1
	→ C ₂ H ₆ + CH ₂ O	-80.4
	→ CH ₄ + CH ₃ CHO	-91.8

^aReference 10.

^bReference 30.



exothermic by 10-15 kcal mol⁻¹ when RH is a saturated hydrocarbon (Table I). It would be naive to believe that the criterion of reaction exothermicity alone can be used to identify processes deserving of further study. However, Freiser, et al. have shown that FeO⁺ reacts readily with saturated hydrocarbons.⁵ These results, along with our study of alkene oxidation by CrO⁺, lend support to the expectation that CrO⁺ will also oxidize saturated hydrocarbons. The present study demonstrates that this contention is indeed correct. Ion beam studies of the reactions of CrO⁺ with alkanes are reported in which the oxidation of alkanes to alcohols (reaction 1) is observed along with other reaction pathways. To better characterize the energetics of these reactions, the CrO⁺-H bond dissociation energy is determined by examining a series of hydrogen atom abstraction reactions. An intermediate in which alkyl C-H bonds add across the Cr⁺-O bond is proposed as an initial oxidation step. Reaction mechanisms are investigated using deuterium labeled alkanes. In addition, reactions of Cr⁺ with alcohols are investigated in an attempt to further elucidate the potential energy surfaces for these reactions and provide support for proposed reaction mechanisms.

Experimental

The experimental techniques employed in the present study are the same as those described in Reference 4, except that the Cr⁺ beam is generated using both electron impact ionization and surface ionization sources. The surface ionization source produces a Cr⁺ beam which is almost entirely in the ground electronic state (>99.9%, Table II) by thermal decomposition of CrO₂Cl₂ and ionization of Cr on the hot filament

Table II. Low-lying States of CrO^+ and Cr^+

Ion	Low-lying states	Energy, eV	Composition ^c	Vibrational Frequency $\bar{\omega}_e, \text{cm}^{-1}$
CrO^+, a	$X^4\Sigma^-$	0	97%	640±30
	4Π	0.65	3%	
Cr^+, b	X^6S	0	>99.9%	
	$6D$	1.52	0%	
	$4D$	2.46	0%	

^aReference 16. Energies are ab initio SCF + CI calculational results.

^bReference 31.

^cAt 1300 °K.

surface (~ 1300 °K). The electron impact ionization source is used to generate Cr^+ from $\text{Cr}(\text{CO})_6$, a process which is known to yield a significant fraction of the Cr^+ beam in excited electronic states.⁶ The CrO^+ beam, produced from CrO_2Cl_2 with the surface ionization source, is predominantly in the electronic ground state ($>97\%$), with 51% in the vibrational ground state, 25% in $v=1$ state, 12% in $v=2$ state, and the rest in higher vibrational states (Table II). The ions are collimated, mass and energy selected, and allowed to react with the target gas in a collision chamber. Product ions scattered in the forward direction are detected using a quadrupole mass spectrometer. Neutral products are not detected in these experiments.

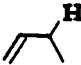
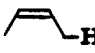
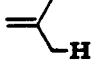



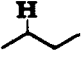
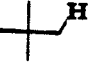
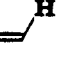
Results and Discussion

Determination of CrO^+ -H Bond Dissociation Energy. The CrO^+ -H bond dissociation energy is an important quantity in characterizing the reactivity of CrO^+ toward alkanes. Hence, the determination of $D^\circ(\text{CrO}^+-\text{H})$ will be presented first in order to permit logical development of discussions in later sections. $D^\circ(\text{CrO}^+-\text{H})$ can be obtained by examining hydrogen atom abstraction reactions (reaction 2) with a series of hydrocarbons of



varying C-H bond energies (Table III). The results for alkenes are taken from Reference 4. Hydrogen abstraction is observed from propene and 2-methyl propene which have allylic C-H bond dissociation energies ca. 86 kcal mol⁻¹.⁷ 1-Butene and cis-2-butene also have allylic C-H bonds with comparable bond dissociation energies, but they do not yield CrOH^+ . The study in Reference 4 suggested a mechanism in which hydrogen atom abstraction from these molecules results eventually in the formation of

Table III. Reactions Providing Limits for the Bond Dissociation Energies
 $D^{\circ}(\text{CrO}^+-\text{H})$ and $D^{\circ}(\text{CrO}^+-\text{H}^-)^{\text{a}}$

R-H	Total cross section, Å ²	Langevin cross section, Å ²	$D^{\circ}(\text{R-H})^{\text{b}}$ kcal mol ⁻¹	$D^{\circ}(\text{R}^+-\text{H}^-)^{\text{c}}$ kcal mol ⁻¹	Product, % of total yield		
					CrOH ⁺	CrOH ₂ ⁺	CrOH
	88	67	82.5 ± 1.3	241	0	5	0
	140	67	85.6 ± 1.5	244	0	7	0
	52	67	-86	250	34	0	0
	70	58	86.3 ± 1.5	256	12	0	0
C₆H₅CH₂-H	17	83	88.0 ± 1	238	0	0	100
	110	68	93.2 ± 2	233	0	0	0
	14	60	95.1 ± 1	252	0	13	0
	100	68	-95	248	0	11	0
	70	75	100 ± 2	264	0	0	0
	8	49	110 ± 2	287	0	0	0
C₆H₅-H	no reaction		110.9 ± 2	282			

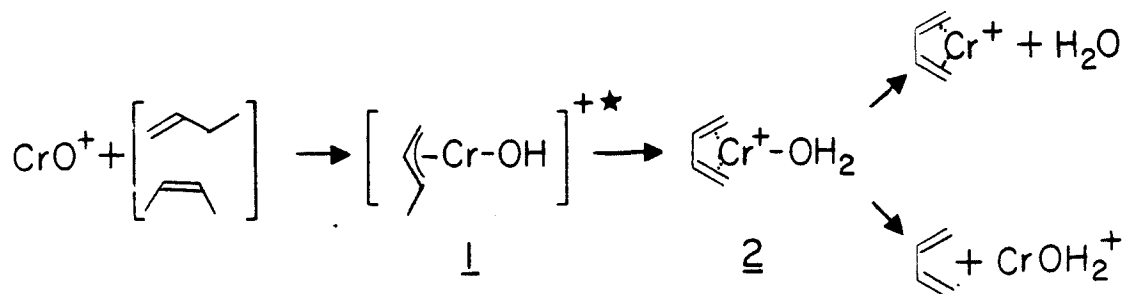
^aAt 0.5 eV relative kinetic energy.

^bReference 7.

^cReference 8.

CrOH_2^+ rather than CrOH^+ (Scheme I). Briefly, both 1-butene and cis-2-butene undergo H-abstraction to form an allyl-hydroxy ion complex (1),

Scheme I



followed by a facile B-H transfer from the allyl substituent to the Cr center to form a water-butadiene ion complex (2), which may lose either butadiene or H_2O . Hence, H-abstractions from 1-butene and cis-2-butene are considered to yield CrOH_2^+ . The analogous B-H transfer pathway is not available in the reactions of propene and 2-methyl propene, rendering generation of CrOH^+ a major process. The H-abstraction reactions from propene and 2-methyl propene exhibit the typical cross section behavior of an exothermic process.⁴ The exothermic hydrogen abstraction from propene provides a lower limit for $D^\circ(\text{CrO}^+-\text{H})$ of $86.3 \text{ kcal mol}^{-1}$.⁷ No hydrogen abstraction reaction is observed from the hydrocarbons with alkyl, vinyl, and phenyl C-H groups, which provides an upper limit of $93.2 \text{ kcal mol}^{-1}$ for the bond energy.

Reaction with toluene gives rise to C_7H_7^+ and CrOH , representing a formal hydride abstraction from toluene. Hydride abstraction is not

observed from the other hydrocarbons. The hydride abstraction from toluene provides a lower limit for the bond energy, $D^\circ(\text{CrO}^+-\text{H}^-) > D^\circ(\text{C}_6\text{H}_5\text{CH}_2^+-\text{H}^-) = 233 \text{ kcal mol}^{-1}$.⁹ The reaction with 2-methyl propene, which yields CrOH^+ and a neutral product 2-methyl propenyl radical, indicates $\text{IP}(\text{CrOH}) < \text{IP}[\text{CH}_2=\text{C}(\text{CH}_3)\text{CH}_2] = 7.90 \text{ eV}$.¹ This value, combined with $D^\circ(\text{CrO}^+-\text{H})$, yields an upper limit for $D^\circ(\text{CrO}^+-\text{H}^-)$ of $253 \text{ kcal mol}^{-1}$ from the thermodynamic cycle depicted by Equation 3.

$$D^\circ(\text{CrO}^+-\text{H}^-) = D(\text{CrO}^+-\text{H}) + \text{IP}(\text{CrOH}) - \text{EA}(\text{H}) \quad (3)$$

In the examination of the above hydrogen atom and hydride abstraction reactions, it is important to consider the internal excitation of the CrO^+ beam. A total cross section for the reactions with propene is 70 \AA^2 at 0.5 eV relative kinetic energy. For comparison, a theoretical cross section σ_r can be calculated using the Langevin-Gioumousis-Stevenson analysis for ion-molecule reactions (Eq.4),^{13,14} where α is the angle-averaged polarizability of the neutral reactant, e is the ion

$$\sigma_r = \pi(2\alpha e^2/E_t)^{1/2} \quad (4)$$

charge, and E_t is the relative kinetic energy. The calculated cross section at the same energy is 58 \AA^2 for propene. The process of hydrogen atom abstraction from propene exhibits a cross section of 8 \AA^2 , which corresponds to 12% of the observed total cross section and 14% of the calculated Langevin cross section. For 2-methyl propene, the reaction cross section for hydrogen abstraction corresponds to 34% of the observed total cross section and 25% of the Langevin cross section. Therefore, the observed hydrogen abstraction reactions cannot be attributed to electronically excited CrO^+ which comprises 3% of the beam. Possible

complications due to the presence of vibrationally excited CrO^+ also deserves consideration. The second vibrationally excited state ($v=2$) of CrO^+ , being only 12% of the total beam population, is unlikely to give rise to the observed cross sections for hydrogen atom abstraction. Hence, we may consider that only the $v=0$ and $v=1$ states are responsible for the reactions. For the possible participation of the $v=1$ state, we may add uncertainty of $1.8 \text{ kcal mol}^{-1}$ to the lower limit values of $D^\circ(\text{CrO}^+-\text{H})$ and $D^\circ(\text{CrO}^+-\text{H}^-)$ (Table II), which gives $D^\circ(\text{CrO}^+-\text{H}) = 89 \pm 5 \text{ kcal mol}^{-1}$ and $253 \text{ kcal mol}^{-1} > D^\circ(\text{CrO}^+-\text{H}^-) > 231 \text{ kcal mol}^{-1}$.

Using the value for $D^\circ(\text{CrO}^+-\text{H})$, the Cr^+OH bond dissociation energy can be calculated using Equation 5, which gives $D^\circ(\text{Cr}^+-\text{OH}) = 73 \pm 5 \text{ kcal mol}^{-1}$.¹⁵ The proton affinity of CrO is calculated using Equation 6,

$$D^\circ(\text{Cr}^+-\text{OH}) = D^\circ(\text{CrO}^+-\text{H}) + D^\circ(\text{Cr}^+-\text{O}) - D^\circ(\text{O}-\text{H}) \quad (5)$$

$$\text{PA}(\text{CrO}) = D^\circ(\text{CrO}^+-\text{H}) + \text{IP}(\text{H}) = \text{IP}(\text{CrO}) \quad (6)$$

which gives $\text{PA}(\text{CrO}) = 221 \pm 5 \text{ kcal mol}^{-1}$. The lower limit for $D^\circ(\text{CrO}^+-\text{H}^-)$, obtained from the exothermic hydride abstraction from toluene, can be used to derive a lower limit for $\text{IP}(\text{CrOH})$ from Eq.3. In turn, neutral bond dissociation energies $D^\circ(\text{CrO}-\text{H})$ and $D^\circ(\text{Cr}-\text{OH})$ can be derived by combining these values with $\text{IP}(\text{CrO})$ and $\text{IP}(\text{Cr})$, and using Equations 7 and

$$D^\circ(\text{CrO}-\text{H}) = D^\circ(\text{CrO}^+-\text{H}) + \text{IP}(\text{CrOH}) - \text{IP}(\text{CrO}) \quad (7)$$

$$D^\circ(\text{Cr}-\text{OH}) = D^\circ(\text{Cr}^+-\text{OH}) + \text{IP}(\text{CrOH}) - \text{IP}(\text{Cr}) \quad (8)$$

8.¹⁶ Derived thermochemical data are summarized in Table IV.

The measured CrO^+-H bond dissociation energy is $\sim 18 \text{ kcal mol}^{-1}$ less

Table IV. Summary of Thermochemical Data^a

$D^\circ (\text{CrO}^+ - \text{H})$	89 ± 5	$D (\text{FeO}^+ - \text{H})$	106 ± 4^e
$D^\circ (\text{Cr}^+ - \text{OH})$	73 ± 5	$D^\circ (\text{Fe}^+ - \text{OH})$	73 ± 3^d
$\text{PA}(\text{CrO})$	221 ± 5	$D^\circ (\text{CoO}^+ - \text{H})$	107 ± 4^e
$D^\circ (\text{Cr}^+ - \text{O})$	85.3 ± 1.3^b	$D^\circ (\text{Co}^+ - \text{OH})$	71 ± 3^d
$D^\circ (\text{CrO} - \text{H})$	$90 > > 67$		
$D^\circ (\text{Cr} - \text{OH})$	$99 > > 76$		
$D^\circ (\text{CrO}^+ - \text{H}^-)$	$253 > > 231$		
$D^\circ (\text{Cr}^+ - \text{OH}^-)$	$212 > > 189$		
$\text{IP}(\text{CrOH})$	$7.9 > > 6.9$		

^aBond energies in kcal mol^{-1} , IP's in eV.

^bReference 4.

^cDerived from $D^\circ (\text{Cr}^+ - \text{OH}^-) = D^\circ (\text{Cr} - \text{OH}) + \text{IP}(\text{Cr}) - \text{EA}(\text{OH})$.

^dReference 32.

^eDerived from $D^\circ (\text{MO}^+ - \text{H}) = D^\circ (\text{M}^+ - \text{OH}) - D^\circ (\text{M}^+ - \text{O}) + D^\circ (\text{O} - \text{H})$.

than the corresponding FeO^+-H and CoO^+-H bond dissociation energies (Table IV). Abstraction of a hydrogen atom from an alkyl C-H bond by CrO^+ is slightly endothermic. Thus, unlike CoO^+ and FeO^+ , reactions of CrO^+ with alkanes cannot yield radical products directly by hydrogen abstraction. As a result, reaction energetics require that any exothermic process which might involve hydrogen atom transfer from C-H bonds of alkanes to CrO^+ as a first step must proceed via a multicenter mechanism. The analogous hydrogen abstraction reactions involving FeO^+ or CoO^+ are exothermic processes. Reactions of these metal oxide ions with alkanes lead to radical products, as illustrated by recent studies of the reactions of FeO^+ with alkanes.⁵

Similarly, hydride abstraction from primary C-H bonds of alkanes by CrO^+ is slightly endothermic. Direct hydride abstractions from secondary and tertiary alkyl C-H bonds are not observed even though the range estimated for the CrO^+-H^- heterolytic bond dissociation energy overlaps with their R^+-H^- bond dissociation energies. This implies that the hydride transfer, if it occurs as a first step in a complex reaction, may also involve a multicenter transition state.

Reactions of CrO^+ with Linear and Branched Alkanes. CrO^+ undergoes facile reactions with linear and branched alkanes larger than methane at low energies. The product distributions measured at 0.5 eV relative kinetic energy are summarized in Table V.

Neither H_2 nor CH_4 are observed to react with CrO^+ , although processes involving formation of Cr^+ and H_2O in the reaction with H_2 (reaction 9) and formation of Cr^+ and methanol in the reaction with methane (reaction 10) are estimated to be exothermic by 32 kcal mol^{-1} and 4 kcal mol^{-1} , respectively (Table I).

Table V.

Product distributions for the exothermic reactions
of
 CrO^+ with Linear and Branched Alkanes.^a

<u>Alkane</u>	<u>Total Cross Section, Å²</u>	<u>Neutral lost</u>	<u>Ion product</u>	<u>% of Total</u>
H ₂	<0.7	N.R.	N.R.	
methane	<0.7	N.R.	N.R.	
ethane	8	C ₂ H ₅ OH	Cr ⁺	100
propane	14	H ₂	Cr(C ₃ H ₆ O) ⁺	47
		C ₂ H ₄	Cr(CH ₄ O) ⁺	20
		C ₃ H ₆	CrOH ₂ ⁺	13
		C ₃ H ₈ O	Cr ⁺	20
butane	100	H ₂	Cr(C ₄ H ₈ O) ⁺	10
		CH ₄	Cr(C ₃ H ₆ O) ⁺	10
		H ₂ O, H ₂	Cr(C ₄ H ₆) ⁺	34
		C ₂ H ₄	Cr(C ₂ H ₆ O) ⁺	32
		C ₄ H ₈	CrOH ₂ ⁺	11
		C ₄ H ₁₀ O	Cr ⁺	3
2-methyl propane	110	H ₂	Cr(C ₄ H ₈ O) ⁺	58
		CH ₄	Cr(C ₃ H ₆ O) ⁺	22
		H ₂ O, H ₂	Cr(C ₄ H ₆) ⁺	11
		C ₄ H ₁₀ O	Cr ⁺	9
2,2-dimethyl propane	70	·CH ₃	Cr(C ₄ H ₉ O) ⁺	11
		CH ₄	Cr(C ₄ H ₈ O) ⁺	57
		H ₂ O, H ₂	Cr(C ₅ H ₈) ⁺	4
		CH ₄ , H ₂ O	Cr(C ₄ H ₆) ⁺	3

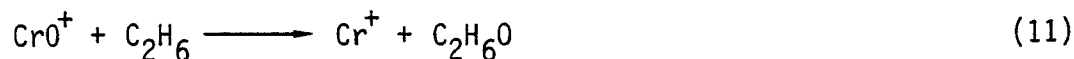
Table V. (cont'd.)

<u>Alkane</u>	<u>Total Cross Section, Å²</u>	<u>Neutral lost</u>	<u>Ion product</u>	<u>% of Total</u>
		CrOCH ₃	C(CH ₃) ₃ ⁺	4
		C ₅ H ₁₂ O	Cr ⁺	21

^aMeasured at 0.5 eV relative kinetic energy.

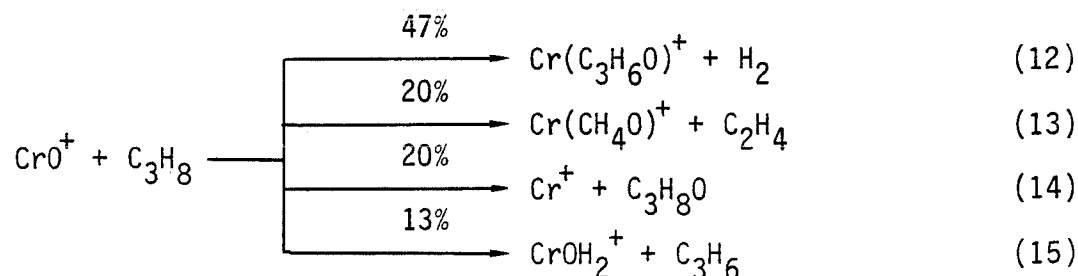


Ethane reacts with CrO^+ to yield Cr^+ and $\text{C}_2\text{H}_6\text{O}$ (reaction 11). The product $\text{C}_2\text{H}_6\text{O}$ can only be ethanol, since the other feasible products



including dimethyl ether, H_2O and ethene, and CH_2O and CH_4 are expected to involve slightly endothermic processes (Table I).

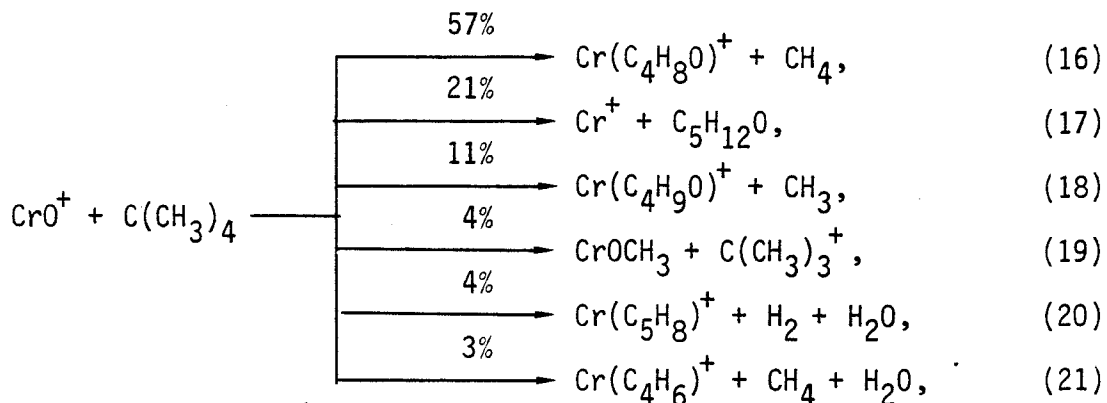
Reaction of CrO^+ with propane leads to the formation of several products in processes which appear to be exothermic, including dehydrogenation, elimination of ethene, propene, and $\text{C}_3\text{H}_8\text{O}$ (reactions 12-15). The structure of $\text{C}_3\text{H}_8\text{O}$ may be inferred from the reaction thermochemistry



presented in Table I. If the structure of $\text{C}_3\text{H}_8\text{O}$ in reaction 14 involved fragmented molecules, the adducts of the fragment with Cr^+ would also have appreciable yields. Only the products CH_4 and CH_3CHO can be formed in a significantly exothermic process ($\Delta H^\circ = -6.5 \text{ kcal mol}^{-1}$). The absence of $\text{Cr}(\text{C}_2\text{H}_4\text{O})^+$ as a product suggests that $\text{C}_3\text{H}_8\text{O}$ formed in reaction 14 is either a propanol or ethyl methyl ether.

Reaction 13 is of interest since loss of ethene requires the cleavage of a C-C bond in the alkane. Products involving C-C bond cleavage become even more prevalent with larger alkanes. For example, in the reaction

of CrO^+ with 2,2-dimethyl propane, the most prominent reaction pathway involves loss of methane (reactions 16-21). Reactions 18, 19, and 21 also involve C-C bond cleavage.

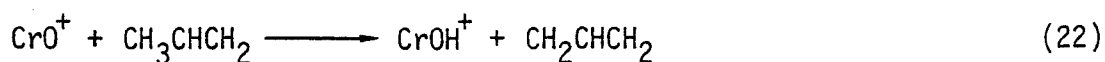


Reactions of CrO^+ with alkanes to yield alcohols (reactions 11, 14, 17) are exothermic by 10-15 kcal mol⁻¹ for the formation of the ground electronic state $\text{Cr}^+(\text{6S})$. Formation of electronically excited Cr^+ requires an extra energy of at least 35 kcal mol⁻¹ (Table II) and hence the product Cr^+ must be in the ground state. Since CrO^+ ($4\Sigma^-$ electronic ground state) and $\text{Cr}^+(\text{6S})$ have different spin states, reactions of CrO^+ with alkanes occur via a quartet-sextet surface crossing. The fact that these processes are only slightly exothermic suggests that activation barriers for the surface crossing may not be significant in the interactions of CrO^+ with alkanes.¹⁷

Formation of ethanol in the reaction with ethane (reaction 11) indicates that primary C-H bonds in saturated alkanes can react with CrO^+ . The reactivity of primary C-H bonds is further illustrated by the fact that the reaction with 2,2-dimethyl propane, which has only primary C-H bonds, exhibits loss of H_2 and H_2O (reaction 20). Reactions in which C-C bonds are cleaved by CrO^+ to yield smaller alkanes have extensive analogies in studies of the reactions of atomic transition metal ion with alkanes.^{11,18-20} Although definitive proof is lacking, the loss of alkanes

has been rationalized in these studies by a mechanism involving a first step in which the atomic metal ion inserts into a C-C bond.

Of particular interest is the structure of an intermediate which is formed when CrO^+ attacks an alkyl C-H or C-C bond. Studies of the gas phase reactions of CrO^+ with alkenes⁴ have suggested an initial reaction step in which CrO^+ abstracts an allylic-H from the alkene to form CrOH^+ (e.g., reaction 22). An analogous pathway may be considered for the reactions of CrO^+ with alkanes, which is the transfer of alkyl-H to CrO^+ . The



mechanism involving alkyl hydrogen transfer is supported by the formation of ethanol in the reaction of CrO^+ with ethane (reaction 11), which suggests that an intermediate is formed in which either H or C_2H_5 is initially bonded to oxygen. An examination of the reaction energetics in the previous section has illustrated that while the hydrogen transfer from allylic C-H bonds to CrO^+ is exothermic, the analogous process involving alkyl C-H bonds requires a multicenter intermediate. These arguments suggest an initial reaction intermediate in which CrO^+ is inserted into a C-H bond, with 3 and 4 being considered the most viable candidates. The possibility of initial insertion into alkyl C-C bonds



is not ruled out. In the case of ethane this process would be non-productive. With larger alkanes, however, product formation involving cleavage of C-C bonds may be better explained by insertion into alkyl C-C bonds.

Reactions of Ground and Excited States Cr^+ with Alcohols. Intermediates involved in the reaction of CrO^+ with alkanes could resemble intermediates which might form in the reactions of Cr^+ with alcohols, making it interesting to compare product distributions between these reactions. In this section, reactions of ground and excited state Cr^+ with 1-propanol and 2-propanol are examined to explore the viability of the intermediates 3 and 4, which might be formed in the reaction of CrO^+ with propane. Initial association of Cr^+ and propanol leads to an ion-molecule adduct with a structure analogous to the intermediate 4. Therefore, the adducts of 1-propanol and 2-propanol with Cr^+ could represent oxidative addition of primary and secondary C-H bonds of propane across an oxygen atom of CrO^+ , respectively. Reaction of Cr^+ with 2-propanol yields $\text{Cr}(\text{OH}_2)^+$ and $\text{Cr}(\text{C}_3\text{H}_6)^+$ (Table VI). In order to rationalize these products, a mechanism which involves an initial attack of the metal ion at the oxygen center and heterolytic cleavage of the $i\text{-C}_3\text{H}_7^+\text{-OH}^-$ bond may be postulated as shown in Scheme II. Cr^+ is envisioned to act

Scheme II

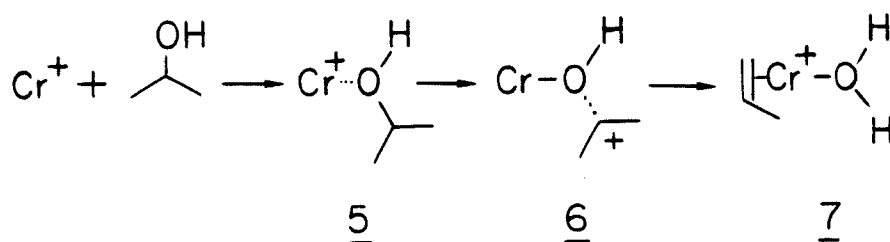


Table VI. Product distributions for the reactions: $\text{CrO}^+ + \text{propane}$,
 $\text{Cr}^+ + 1\text{-propanol}$, and $\text{Cr}^+ + 2\text{-propanol}$.

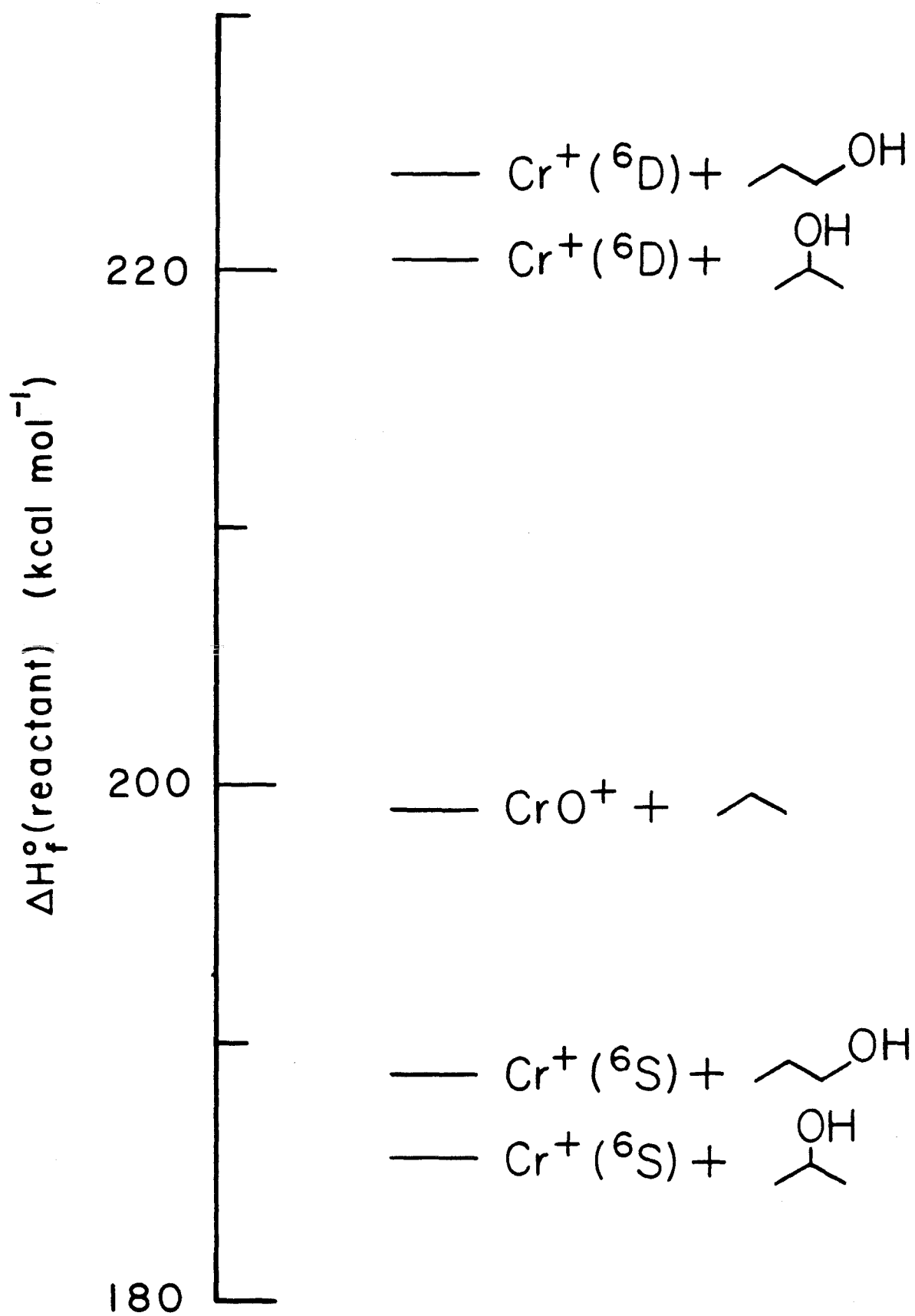
Reaction	Relative Kinetic Energy eV	Total Cross Section \AA^2	Product Yield (% of Total Cross Section)							
			Cr^+	$\text{Cr}(\text{OH})^+$	$\text{Cr}(\text{OH}_2)^+$	$\text{Cr}(\text{CH}_4\text{O})^+$	$\text{Cr}(\text{C}_3\text{H}_6)^+$	$\text{Cr}(\text{C}_2\text{H}_4\text{O})^+$	$\text{Cr}(\text{C}_3\text{H}_6\text{O})^+$	
(H) $\text{CrO}^+ + \text{propane}$	0.5	14	20	0	13	20	0	0	0	47
(I) $\text{Cr}^+ + 1\text{-propanol}$	0.5	0.6	-*	0	0	0	0	0	55	45
	1.0	0.06	-	0	0	0	0	0	70	30
	2.0	0.12	-	40	0	0	0	0	50	10
(J) $\text{Cr}^+ + 2\text{-propanol}$	0.5	7	-	0	54	0	0	46	0	0
	1.0	3	-	0	57	0	0	43	0	0
	2.0	0.2	-	0	100	0	0	0	0	0

* Product cannot be distinguished from reactant beam.

as a Lewis acid, binding to the oxygen center of 1-propanol (5). The hydroxide anion is transferred to the metal generating 2-propyl cation (6), which then undergoes proton transfer to the oxygen atom forming an intermediate 7.²¹ Competitive loss of H₂O and propene from 7 gives rise to the observed products. For comparison, analogous mechanisms which involve heterolytic cleavage of polar R-X bonds have been proposed by Allison and Ridge²² in studies of reactions of metal ions (Li, Na, Fe, Co, and Ni) with alkyl halides and alcohols. The mechanism proposed in Scheme II for the reaction with 2-propanol, which involves heterolytic cleavage of the R-OH bond, suggests that the different reactivity of 1-propanol might result from the energetically more demanding heterolytic bond cleavage with 1-propanol [$D^{\circ}(\text{n-C}_3\text{H}_7^+ - \text{OH}^-) = 237 \text{ kcal mol}^{-1}$] compared to 2-propanol [$D^{\circ}(\text{s-C}_3\text{H}_7^+ - \text{OH}^-) = 220 \text{ kcal mol}^{-1}$].²³ The products from the reaction with 1-propanol exhibit small reaction cross sections, but certainly exclude the possibility of an excited state Cr⁺ reaction.

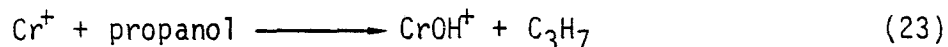
No combination of the product distributions for reactions of Cr⁺ with propanols resembles that of reaction of CrO⁺ with propane. Most significantly, Cr(C₃H₆)⁺ and Cr(C₂H₄O)⁺ are not formed in the reaction of CrO⁺ with propane. When we consider the higher heats of formation of the reactants in the interaction of CrO⁺ with propane than in the interaction of Cr⁺ with propanols (Figure 1), a common intermediate for these reactions should allow the reaction of CrO⁺ with propane to yield products which include those from the reactions of Cr⁺ with propanols. The failure to observe Cr(C₂H₄O)⁺ and Cr(C₃H₆)⁺ in the reaction of CrO⁺ with propane thus contradicts the assumption of a common intermediate. This

Figure 1. Heats of formation of reactants for the reactions Cr^+ + propanol and CrO^+ + propane. Values from references 10 and 34.



rules out the possibility of an initial C-H bond addition across an oxygen atom (4) and leaves the addition across the Cr^+-O bond (3) as a feasible initial step in the reaction of CrO^+ with propane.

It is of further interest to examine the reactions of Cr^+ with propanols at different levels of total reactant energy. Two methods are employed to control the available reactant energy. One is to change the collision energy, and the other is to generate Cr^+ in electronically excited states. As expected, the total reaction cross section decreases as the collision energy is increased. However, the overall product distribution does not change significantly compared with that of the low energy reaction (Table VI). In contrast, Cr^+ generated by electron impact from $\text{Cr}(\text{CO})_6$ reacts with propanols to yield a variety of products in addition to those from the reaction of ground electronic state Cr^+ (Table VII). These additional products undoubtedly result from the reaction of electronically excited Cr^+ , which constitutes a significant fraction of the beam when it is formed using electron impact ionization. For example, formation of CrOH^+ in the reactions of Cr^+ with propanols (reaction 23) must involve electronically excited Cr^+ , since this process



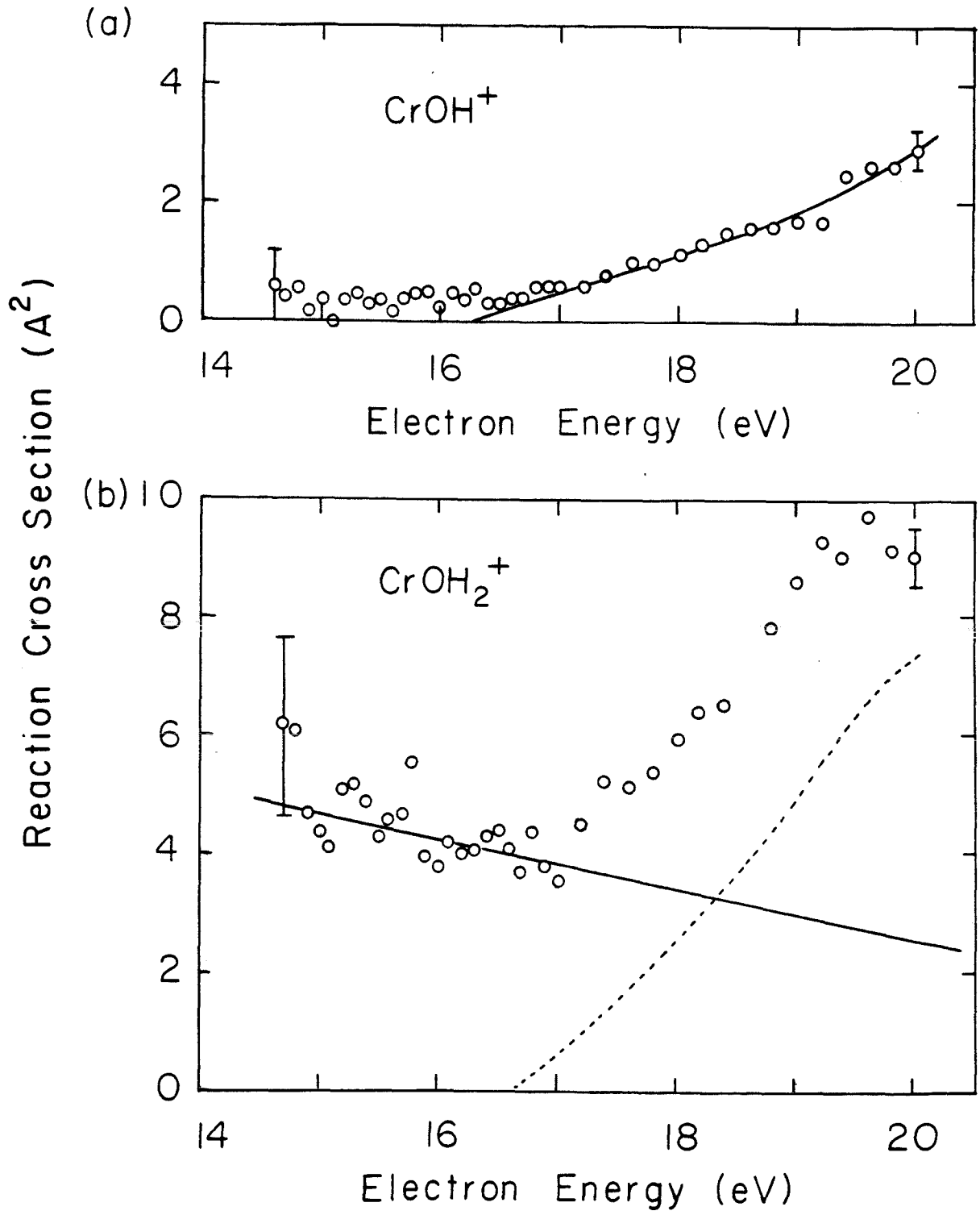
is endothermic by 18-20 kcal mol⁻¹ for the ground state. This product exhibits an experimental cross section which increases with increasing electron impact energy, representing an increasing fraction of excited state Cr^+ in the beam [Figure 2(a)]. CrOH^+ is observed as a product only when electron impact energy exceeds 16.5 ± 0.5 eV, indicating that formation of the excited electronic state Cr^+ occurs above this threshold energy. The product CrOH_2^+ exhibits an apparent reaction cross section which is constant at low electron energies and starts to increase around

Table VII. Product distributions for the reactions of Cr^+ with alcohols using the electron impact source.^a

Reaction	Electron Impact Energy, eV	Total Cross Section, Å ²	Product Yield (% of Total Cross Section)									
			C_3H_7^+	Cr^+O	Cr^+OH	Cr^+OH_2	$\text{Cr}^+(\text{CH}_3\text{O})$	$\text{Cr}^+(\text{C}_3\text{H}_4)$	$\text{Cr}^+(\text{C}_3\text{H}_6)$	$\text{Cr}^+(\text{C}_2\text{H}_4\text{O})$	$\text{Cr}^+(\text{C}_2\text{H}_5\text{O})$	$\text{Cr}^+(\text{C}_3\text{H}_6\text{O})$
Cr^+ + 1-propanol	16	9	5	0	5	40	19	4	0	3	3	21
	30	17	12	8	52	9	6	3	0	1	3	7
	70	30	7	8	60	8	5	3	0	0	2	7
Cr^+ + 2-propanol	SI	0.6	0	0	0	0	0	0	0	55	0	45
	16	18	6	0	6	21	13	9	21	0	10	14
	18	25	9	0	13	30	14	8	9	0	4	13
	70	64	21	8	41	13	8	1	1	0	2	5
	SI	7	0	0	0	54	0	0	46	0	0	0

^aMeasured at 0.5 eV relative kinetic energy.

Figure 2. Variation in experimental cross section as a function of electron impact ionization energy. Reactions of Cr^+ with 2-propanol at a relative kinetic energy of 0.5 eV. a) Formation of CrOH^+ exhibits a threshold at 16.5 ± 0.5 eV. The cross section increases with the electron impact energy representing an increasing portion of excited state Cr^+ in the beam. b) Formation of CrOH_2^+ results from the reactions of both ground state (solid line) and excited state (dotted line) Cr^+ .



the same threshold energy recorded for CrOH^+ [Figure 2(b)], indicating that this product results from the reactions of both ground and excited state Cr^+ . Since the threshold energy lies ca. 1-2 eV above appearance potential of Cr^+ ,²⁵ this may suggest that the first excited electronic state (${}^6\text{D}$) of Cr^+ (Table II), which is located 1.52 eV above the ground electronic state (${}^6\text{S}$), can give rise to these products. The ${}^6\text{D}$ state of Cr^+ should have a relatively long lifetime and persist in the beam on a microsecond time scale. Interestingly, the observed products in the reaction of $\text{Cr}^+({}^6\text{D})$ with propanol include those from the reaction of CrO^+ with propane. Since $\text{Cr}^+({}^6\text{D})$ can provide much more energy to reaction intermediates than the ground state Cr^+ (Figure 1), this might imply that intermediate 4, generated in the reaction of $\text{Cr}^+({}^6\text{D})$ with propanol, could rearrange to 3, yielding products of the reaction of CrO^+ with propane.

Reactions of CrO^+ with Deuterium Labeled Alkanes. Product distributions measured in the reaction of CrO^+ with several deuterium labeled alkanes, including propane-2,2- d_2 , 2-methyl propane-2- d_1 , and butane-1,1,1,4,4,4- d_6 are listed in Table VIII. In studying reactions of deuterium labeled compounds, scrambling processes sometimes result in products with a statistical distribution of hydrogen and deuterium. For example, if isotope effects are ignored, complete scrambling in the reaction with butane-1,1,1,4,4,4- d_6 would yield dehydrogenation products in the ratio of $\text{H}_2 : \text{HD} : \text{D}_2 = 2 : 8 : 5$ (Table IX). This is very different from the observed isotopic product distribution for this reaction ($\text{H}_2 : \text{HD} : \text{D}_2 = 1 : 1 : 0$), suggesting a specific process in which H_2 loss occurs mainly across the central C-C bond. Product formation involving loss of HD in the reaction with 2-methyl propane-2- d_1 is more favored ($\text{HD}/\text{H}_2 = 1$) than

Table VIII. Isotopic product distributions for neutral lost in the exothermic reactions of deuterated alkanes with CrO^+ .

Alkane	σ_T $^\circ\text{A}^2$	Neutral Lost (% of Total)
propane-2,2-d ₂ ^a	22	H ₂ (25), HD(24), C ₂ H ₃ D(10), C ₂ H ₂ D ₂ (13), C ₃ H ₄ D ₂ (11), C ₃ H ₅ D ₂ O(17)
2-methyl propane-2-d ₁ ^b	150	H ₂ (23), HD(23), CH ₄ (29), H ₂ O + H ₂ (13), HDO + H ₂ and H ₂ O + HD(5), C ₄ H ₁₀ O(7)
butane-1,1,1,4,4,4-d ₆ ^a	110	H ₂ (5), HD(5), CD ₄ (10), H ₂ O + H ₂ (27), HDO + H ₂ and H ₂ O + HD(7), C ₂ H ₂ D ₂ (23), C ₂ HD ₃ (9), C ₄ H ₄ D ₄ (5), C ₄ H ₃ D ₅ (6), C ₄ H ₄ D ₆ O(3)

^aMeasured at 0.5 eV relative kinetic energy.

^bMeasured at 0.25 eV relative kinetic energy.

Table IX. Isotopic Distribution of Dehydrogenation Products in the Reactions of CrO^+ with Deuterated Alkanes ($\text{H}_2:\text{HD}:\text{D}_2$)

Alkane	Loss of $\text{H}_2:\text{HD}:\text{D}_2$	
	Statistical ratio	Observed Ratio
propane-2,2-d ₂ ^a	15:12:1	1:1:0
2-methylpropane-2d ₁ ^b	4:1:0	1:1:0
n-butane-1,1,1,4,4,4-d ₆ ^a	2:8:5	1:1:0

^aMeasured at 0.5 eV relative kinetic energy.

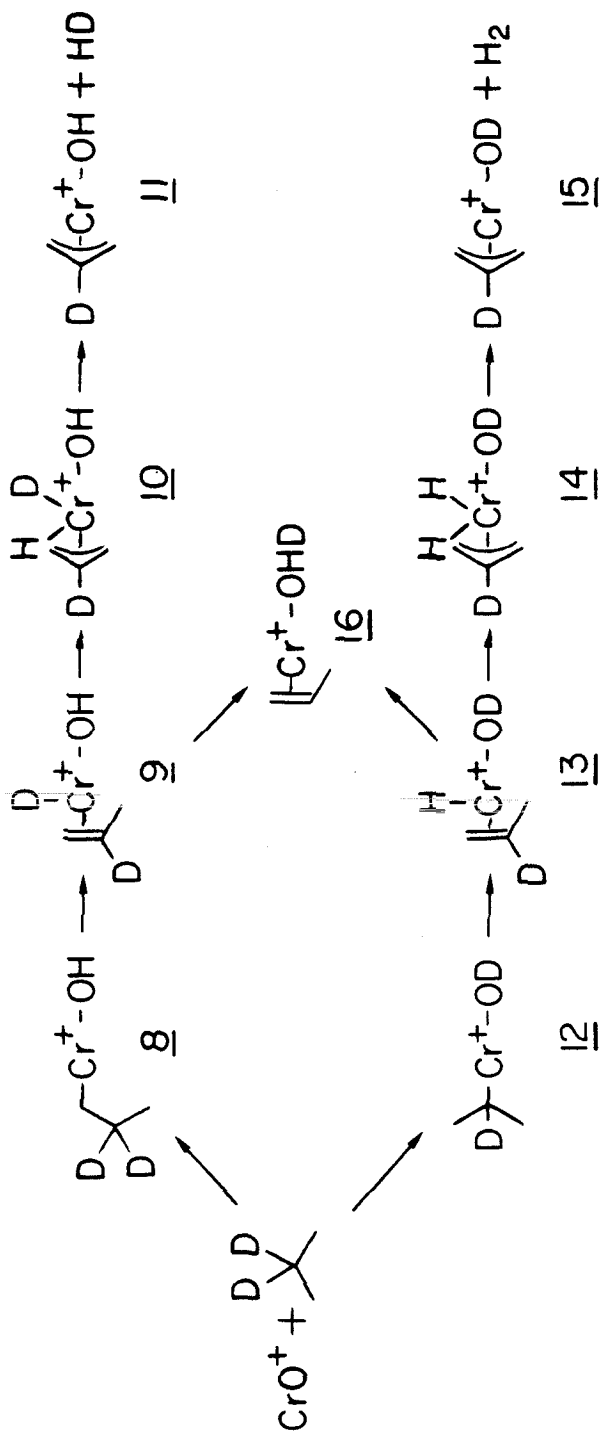
^bMeasured at 0.25 eV relative kinetic energy.

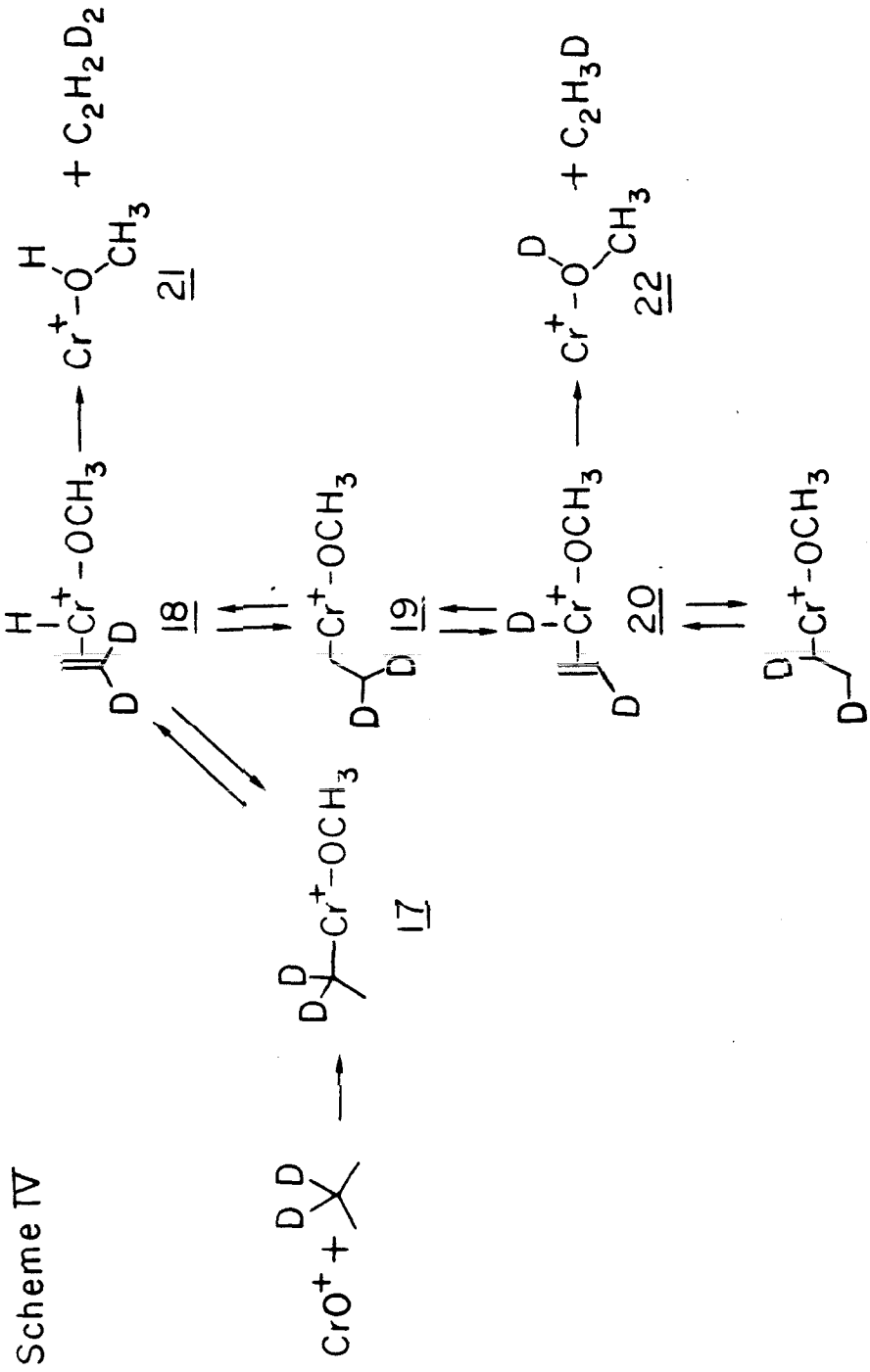
the statistical ratio ($\text{HD}/\text{H}_2 = 0.25$), indicating that 1,2-dehydrogenation occurs preferentially. CH_4 loss in this reaction is highly specific. These observations, along with the proposed initial intermediate 3, provide a guide to investigate plausible mechanisms for the reaction of CrO^+ with alkanes.

Scheme III presents a postulated mechanism for the dehydrogenation of propane, which is the major product channel in the reaction of CrO^+ with propane-2,2- d_2 . The first step is insertion of CrO^+ into either a primary C-H bond or secondary C-D bond. The C-H insertion intermediate 8 undergoes β -D transfer to the Cr center to generate 9, and in turn 10 by another β -H transfer, which reductively eliminated HD leaving an allyl hydroxy complex (11). Insertion into a secondary C-D bond (12) follows an analogous process to eliminate H_2 (15). The overall mechanism is consistent with the fact that D_2 loss is not observed in the reaction. Formation of allyl hydroxy complexes has been postulated in the previous study of the reactions of CrO^+ with alkanes (1 of Scheme I).⁴ We assume that the preferred pathway for rearrangement of intermediate 9 is the β -H transfer which leads to 10 and 11, rather than the transfer of D to the oxygen center to generate 16. In general, loss of H_2 is observed without loss of H_2O in the reactions with alkanes. However, loss of H_2O is always accompanied by loss of H_2 . This may suggest that loss of H_2 precedes loss of H_2O , supporting the argument that the process $\text{9} \rightarrow \text{10}$ prevails. In the case of propane-2,2- d_2 , if intermediate 16 were formed, loss of either $\text{C}_3\text{H}_5\text{D}$ or HDO would be expected. Exclusive $\text{C}_3\text{H}_4\text{D}_2$ loss in this reaction thus contradicts the possible formation of intermediate 16, supporting the proposed mechanism.

Scheme IV presents a mechanism which invokes initial insertion of

Scheme III

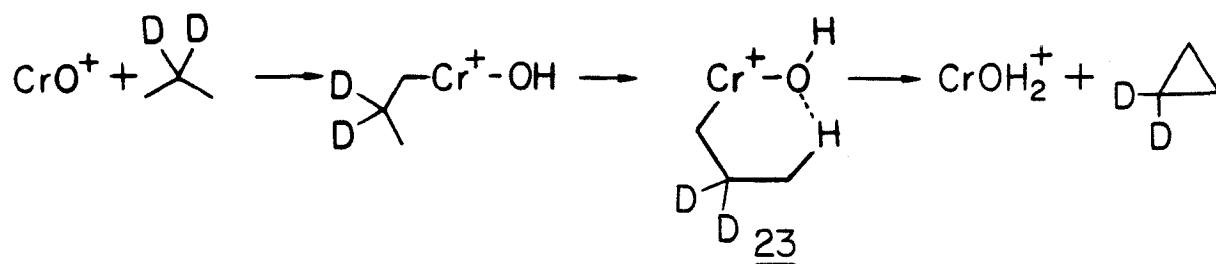




CrO^+ into a C-C bond in order to provide a plausible explanation for the processes leading to ethene loss in the reaction with propane-2,2-d₂. The C-C insertion intermediate 17 undergoes β -H transfer to form 18, which may assume an equilibrium with 20 via reversible ethene insertion into the Cr^+ -H bond. The analogous reversible olefin insertion into a M^+ -H bond (M = Fe, Co, Ni, and Rh) has been suggested in several studies.^{26,27} The intermediates 18 and 20 result in loss of $\text{C}_2\text{H}_2\text{D}_2$ and $\text{C}_2\text{H}_3\text{D}$, respectively.

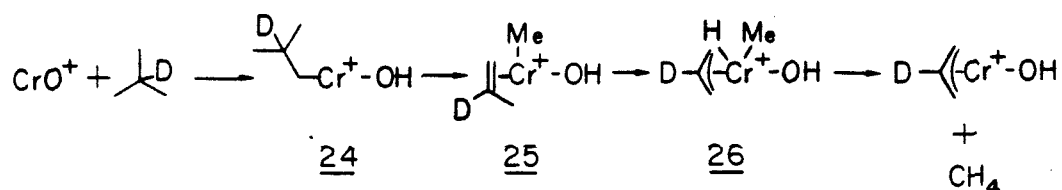
The process of propene loss in the reaction with propane shows unique features. Despite the fact that the corresponding ionic product CrOH_2^+ is most likely a chromium-water complex, loss of H_2O is not observed from this reaction. Intermediate 16 of Scheme III might be expected to account for the propene loss, as we postulated for the reaction of Cr^+ with 2-propanol (7 of Scheme II). However, the absence of H_2O loss, which might be expected from the competitive bond cleavage of intermediate 16,²⁸ as well as the arguments used to propose the mechanism shown in Scheme III do not support the possibility of this intermediate. Moreover, the observed isotopic product distribution for the reaction using propane-2,2-d₂ shows exclusive 1,3-dehydrogenation from propane. A mechanism involving cyclic intermediate 23 may be postulated for a plausible explanation, which is shown in Scheme V. Initial insertion into a C-H bond leads to a six-membered cyclic intermediate 23, which permits hydrogen transfer from the terminal C-H bonds of propane to the oxygen atom, and in turn, dissociation of $\text{C}_3\text{H}_4\text{D}_2$. The preferential loss of $\text{C}_3\text{H}_4\text{D}_2$ compared with H_2O loss suggests that the neutral product in this reaction might be cyclopropane, since cyclopropane is expected to have less binding energy to Cr^+ than H_2O .

Scheme V

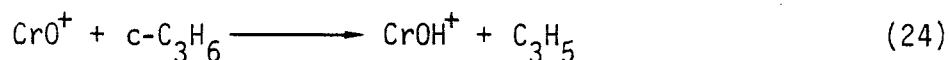


A major product channel common in the reactions of CrO^+ with 2-methyl propane, 2,2-dimethyl propane, and butane is the loss of methane. In order to rationalize these processes, mechanisms which involve initial C-H insertion and β -Me group transfer may be postulated, with an example being shown in Scheme VI for the reaction with 2-methyl propane-2- d_1 . The initial C-H insertion intermediate 24 undergoes β -Me transfer to form 25, and β -H transfer to form 26, which then eliminates CH_4 . This mechanism is consistent with the isotopic product distribution which shows exclusive loss of CH_4 .

Scheme VI



Reactions of CrO^+ with Cyclic Alkanes. Reactions of CrO^+ with cyclic alkanes and propene are summarized in Table X. Interaction of CrO^+ with cyclopropane yields CrOH^+ as a major product (reaction 24),



representing formal hydrogen atom abstraction from cyclopropane. Since cyclopropyl C-H bonds are stronger than the CrO^+-H bond (Table XI), the hydrogen abstraction implies that the neutral lost in reaction 24 is an allyl rather than cyclopropyl radical. If this rearrangement occurs in the reaction intermediate prior to dissociation, then similar results might be expected in comparing the reactions of cyclopropane and propene. The nearly identical product distributions confirm this argument. The additional product $\text{Cr}(\text{C}_3\text{H}_4\text{O})^+$ observed in the reaction with cyclopropane

Table X. Product distributions for the exothermic reactions of CrO^+ with cyclic alkanes and propene.^a

<u>Reactant</u>	<u>Total Cross Section, Å²</u>	<u>Neutral Lost</u>	<u>Ion product</u>	<u>% of Total</u>
Cyclopropane	48	H ₂	$\text{Cr}(\text{C}_3\text{H}_4\text{O})^+$	5
(propene) ^b	(70)	H ₂ O	$\text{Cr}(\text{C}_3\text{H}_4)^+$	6 (7)
		C ₂ H ₄	CrOCH_2^+	25 (39)
		C ₃ H ₅	CrOH^+	20 (12)
		C ₃ H ₆ O	Cr^+	44 (44)
Cyclobutane	90	C ₂ H ₄	$\text{Cr}(\text{C}_2\text{H}_4\text{O})^+$	78
		C ₄ H ₈ O	Cr^+	22
Cyclopentane	80	2H ₂	$\text{Cr}(\text{C}_5\text{H}_6\text{O})^+$	91
		C ₅ H ₁₀ O	Cr^+	9
Cyclohexane	80	2H ₂	$\text{Cr}(\text{C}_6\text{H}_8\text{O})^+$	10
		3H ₂	$\text{Cr}(\text{C}_6\text{H}_6\text{O})^+$	14
		H ₂ O	$\text{Cr}(\text{C}_6\text{H}_{10})^+$	5
		H ₂ O, H ₂	$\text{Cr}(\text{C}_6\text{H}_8)^+$	25
		H ₂ O, 2H ₂	$\text{Cr}(\text{C}_6\text{H}_6)^+$	18
		C ₆ H ₁₂ O	Cr^+	28

^aMeasured at 0.5 eV relative kinetic energy.

^bThese data are taken from Reference 4.

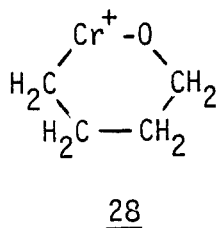
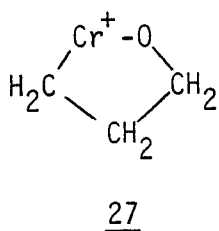
Table XI. C-H and C-C Bond Energies of Cyclic Alkanes

Alkane	<u>Bond Energies, kcal mol⁻¹</u>	
	C-H ^a	C-C ^b
cyclopropane	106.3 ± 0.3	54
cyclobutane	96.5 ± 1	55
cyclopentane	94.5 ± 1	75
cyclohexane	95.5 ± 1	81

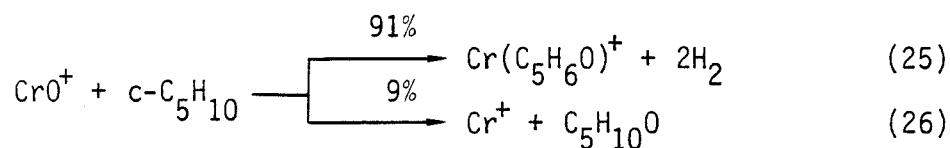
^aReference 7.

^bEstimated values from ring strain energies: Ref. 33.

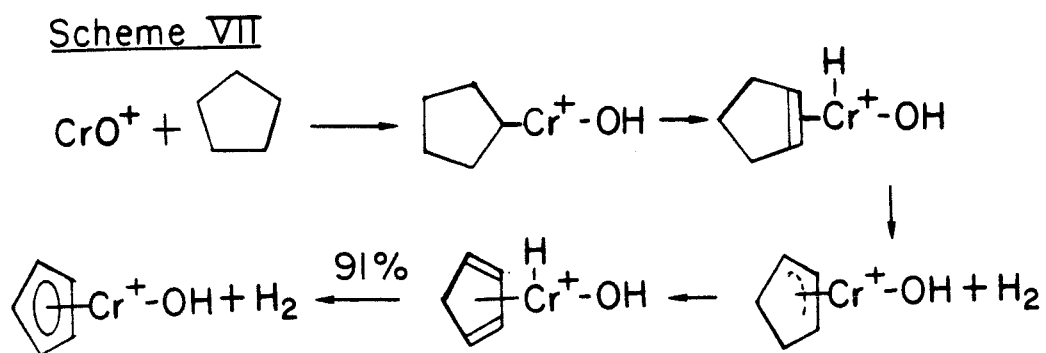
can be rationalized by the fact that cyclopropane has a higher heat of formation than propene.²⁹ Reaction with cyclobutane is highly specific yielding $\text{Cr}(\text{C}_2\text{H}_4\text{O})^+$ as the only product in addition to Cr^+ . The loss of C_2H_4 in the reactions of CrO^+ with cyclopropane and cyclobutane may result from rearrangement and decomposition of the intermediates 27 and 28, respectively, formed by insertion of CrO^+ in the strained C-C bonds of these cycloalkanes.



Reaction with cyclopentane eliminates two moles of H_2 to yield $\text{Cr}(\text{C}_5\text{H}_6\text{O})^+$ exclusively (reaction 25). This multiple dehydrogenation



product can be rationalized by a mechanism analogous to Scheme III, which involves initial insertion into a C-H bond followed by successive β -H transfers to the Cr center to eliminate H_2 (scheme VII). This mechanism suggests a structure of $(\text{C}_5\text{H}_5) - \text{Cr}^+ - \text{OH}$ for the double dehydrogenation product. Cyclohexane yields products resulting from dehydrogenation and elimination of H_2O in various intermediate steps.



Summary

1. A single bimolecular encounter between CrO^+ and an alkane provides energetically facile pathways for alkane oxidation. CrO^+ undergoes exothermic reaction with ethane to oxidize ethane into ethanol selectively. In addition to the possibility of alcohol formation, reactions of CrO^+ with larger alkanes provide a variety of product channels for alkane oxidation, which include dehydrogenation and loss of alkenes and alkanes.

2. Reactions of CrO^+ with cyclopropane and cyclobutane yield products characteristic of C-C bond cleavages. Reaction of CrO^+ with cyclopropane is unique, exhibiting a product distribution which closely resembles that of the reaction with propene. In contrast, reactions

with cyclopentane and cyclohexane exhibit multiple dehydrogenation and H_2O loss.

3. A $\text{CrO}^+\text{-H}$ bond dissociation energy of 89 kcal mol^{-1} , determined by examining a series of hydrogen abstraction reactions, implies that the reaction between CrO^+ and an alkyl C-H bond involves multicenter intermediates. This argument, supported by an examination of the reactions of Cr^+ with alcohols, suggests an initial intermediate in which a C-H bond adds across the $\text{Cr}^+\text{-O}$ bond.

Acknowledgment

We gratefully acknowledge the support of the National Science Foundation under Grant CHE-8407857.

Graduate fellowship support by the Korean Government (H.K. 1980-84) is gratefully acknowledged.

REFERENCES

1. Report of the International Workshop on "Activation of Dioxygen Species and Homogeneous Catalytic Oxidations." ed. T.J. Collins (Galzignano, Italy, 1984).
2. R.A. Sheldon and J.A. Kochi, "Metal Catalized Oxidations of Organic Compounds" (Academic Press, New York, 1981).
3. W. Martir and J.H. Lunsford, J. Am. Chem. Soc., 103, 3728 (1981); J.C. Schultz and J.L. Beauchamp, J. Phys. Chem., 87, 3587 (1983).
4. H. Kang and J.L. Beauchamp, J. Am. Chem. Soc. (submitted).
5. T.C. Jackson, D.B. Jacobson, and B.S. Freiser, J. Am. Chem. Soc., 106, 1252 (1984).
6. L.F. Halle, P.B. Armentrout, and J.L. Beauchamp, J. Am. Chem. Soc., 103, 962 (1981).
7. D.F. McMillen and D.M. Golden, Ann. Rev. Phys. Chem., 33, 493 (1982).
8. F.P. Lossing and J.L. Holmes, J. Am. Chem. Soc., 106, 6917 (1984).
9. The product $C_7H_7^+$ can be either benzyl or cycloheptatrienyl cation. $D^\circ(C_6H_5CH_2^+ - H^-) = \Delta H_f^\circ(C_7H_7^+) + \Delta H_f^\circ(H^-) - \Delta H_f^\circ(C_6H_5CH_3)$ is used to calculate the bond dissociation energy, which gives $233 \text{ kcal mol}^{-1}$ when the product is cycloheptatrienyl cation. For the formation of benzyl cation, it gives $237 \text{ kcal mol}^{-1}$ for the bond energy.
10. J.D. Cox and G. Pilcher, "Thermochemistry of Organic and Organometallic Compounds" (Academic Press, New York, 1970).
11. In the dissociation of such a charged intermediate, the preferred ionic product is the fragment having the lower ionization potential (IP), P.B. Armentrout and J.L. Beauchamp., J. Am. Chem. Soc., 103, 784, (1981). IP's are from Ref. 12.
12. J.C. Schultz, Ph.D. Thesis (California Institute of Technology, 1984).

13. Polarizabilities of hydrocarbons are from S.C. Chan, B.S. Rabinovitch, J.T. Bryant, L.D. Spicer, T. Fujimoto, Y.N. Lin, and S.P. Pavlou, *J. Phys. Chem.*, 74, 3160 (1970).
14. R.D. Levine and R.B. Bernstein, "Molecular Reaction Dynamics" (Oxford University Press, 1974).
15. $D^{\circ}(\text{O-H}) = 101.3 \text{ kcal mol}^{-1}$ from K.P. Huber and G. Herzberg, "Constants of Diatomic Molecules" (Van Nostrand Reinhold, New York, 1979).
16. $\text{IP}(\text{Cr}) = 6.76 \text{ eV}$ and $\text{IP}(\text{CrO}) = 7.85 \pm 0.02 \text{ eV}$; J.M. Dyke, B.W.J. Gravenor, R.A. Lewis, and A. Morris, *J. Chem. Soc., Faraday Trans. 2*, 79, 1083 (1983).
17. This may be compared with an activation energy of 25 kcal mol^{-1} measured in the reaction of Cr^+ with N_2O forming CrO^+ and N_2 ; P.B. Armentrout, L.R. Halle, J.L. Beauchamp., *J. Chem. Phys.*, 76, 2449 (1982).
18. L.F. Halle, P.B. Armentrout, and J.L. Beauchamp, *Organometallics*, 1, 963 (1982) and references therein.
19. G.D. Byrd, R.C. Burnier, and B.S. Freiser, *J. Am. Chem. Soc.*, 104, 3565 (1982).
20. B.S. Larsen and D.P. Ridge, *J. Am. Chem. Soc.*, 106, 1912 (1984) and references therein.
21. $\text{PA}(\text{CH}_2\text{CH}=\text{CH}_2) = 184.9 \text{ kcal mol}^{-1}$ from D. H. Aue and M.T. Bowers, "Gas Phase Ion Chemistry", vol. 2, Chapter 9, ed. M.T. Bowers (Academic Press, 1979).
22. J. Allison and D.P. Ridge, *J. Am. Chem. Soc.*, 101, 4998 (1979).
23. $D^{\circ}(\text{R}^+-\text{OH}^-)$ is calculated using $D^{\circ}(\text{R}^+-\text{OH}^-) = D^{\circ}(\text{R-OH}) + \text{IP}(\text{R}\cdot) - \text{EA}(\text{OH}^-)$. $D^{\circ}(\text{R-H})$ is from ref 20. $\text{IP}(\text{n-C}_3\text{H}_7\cdot) = 8.15 \text{ eV}$ and $\text{IP}(\text{i-C}_3\text{H}_7\cdot) =$

- 7.36 eV from Ref.9. EA(OH) = 1.825 eV from B.K. Janousek and J.I. Brauman, Chapter 10 of Ref. 21.
24. $D^\circ(i\text{-C}_3\text{H}_7\text{-OH}) = 92.8 \text{ kcal mol}^{-1}$ and $D(n\text{-C}_3\text{H}_7\text{-OH}) = 91.6 \text{ kcal mol}^{-1}$ from Ref. 7 and 10.
25. AP(Cr^+) from $\text{Cr}(\text{CO})_6$ is measured using our current instrument to be $15.0 \pm 0.2 \text{ eV}$. Several other measurements include, $14.7 \pm 0.1 \text{ eV}$; A. Foffani, S. Pignataro, B. Cantone, and F. Grasso. Z. Physik. Chem. (Frankfurt) 45, 79 (1965) and $15.2 \pm 0.2 \text{ eV}$; D. R. Bidinosti and N.S. McIntyre, Can. J. Chem., 45, 641 (1967).
26. D.B. Jacobson and B. S. Freiser J. Am. Chem. Soc., 107, 72 (1985).
27. L.F. Halle, F.S. Klein, and J.L. Beauchamp, J. Am. Chem. Soc., 106, 2543 (1984).
28. Binding energies of propene and H_2O to metal ions may be estimated using a correlation scheme between binding energies of molecules to CpNi^+ (Cp = cyclopentadienyl) and proton; R.R. Corderman and J.L. Beauchamp, J. Am. Chem. Soc., 98, 3998 (1976). We estimate $D^\circ(\text{CpNi}^+ \text{-OH}_2) \sim 31 \text{ kcal mol}^{-1}$ and $D[\text{CpNi}^+ \text{-(CH}_3\text{CH=CH}_2)] \geq 44 \text{ kcal mol}^{-1}$ from this correlation.
29. $\Delta H_f^\circ(\text{cyclopropane}) = 12.73 \text{ kcal mol}^{-1}$ and $\Delta H_f^\circ(\text{propene}) = 4.88 \text{ kcal mol}^{-1}$ from Ref. 10.
30. $\Delta H_f^\circ(\text{CH}_2) = 93.7 \text{ kcal mol}^{-1}$ from Ref. 25.
31. C.E. Moore, "Atomic Energy Levels" (National Bureau of Standards, Washington, D.C., 1971).
32. C.J. Cassady and B.S. Frasier, J. Am. Chem. Soc., 106, 6176 (1984).
33. S. Benson, "Thermonuclear Kinetics" (J. Wiley, New York, 1968).
34. $\Delta H_f^\circ(\text{Cr}^+) = 250.3 \text{ kcal mol}^{-1}$ from; H.M. Rosenstock, K. Draxl, B.W.

Steiner, and J.T. Herron, J. Phys. Chem. Ref. Data Suppl., 6 (1977).

CHAPTER IV

REACTIONS OF TRANSITION METAL IONS WITH METHYL SILANES
IN THE GAS PHASE; THE FORMATION AND CHARACTERISTICS OF STRONG
TRANSITION METAL-SILYLENE BONDS

REACTIONS OF TRANSITION METAL IONS WITH METHYL SILANES
IN THE GAS PHASE; THE FORMATION AND CHARACTERISTICS OF STRONG
TRANSITION METAL-SILYLENE BONDS

Heon Kang,¹ Denley B. Jacobson, and J.L. Beauchamp^{*}

The Arthur Amos Noyes Laboratory of Chemical Physics,²
California Institute of Technology, Pasadena, California 91125

M.T. Bowers^{*}

Department of Chemistry, University of California,
Santa Barbara, California 93106

^{*}To whom correspondence should be addressed.

Abstract

Reactions of transition metal ions (Ti, V, Cr, Fe, Co, and Ni) with organosilanes are investigated in the gas phase using an ion beam apparatus. Co^+ and Ni^+ react with silane to yield metal silylenes as exothermic products. Collision-induced dissociation studies of the product CoSiH_2^+ and nascent CoSiH_4^+ adducts provide additional information concerning the product structure and reaction mechanisms. Product kinetic energy releases for dehydrogenation of nascent MSiH_4^+ ($\text{M} = \text{Co}, \text{Ni}$) are measured to further characterize the H_2 elimination process. Reactions with methyl silanes lead to formation of metal silylenes as major reaction channels, along with several other processes including hydride abstraction, dehydrogenation, and methane loss. Reactions with hexamethyl disilane are also investigated, with major products indicating Si-Si bond cleavage. An examination of the reaction enthalpies for the observed metal silylene products provides estimates for metal ion-silylene bond energies, which include $D^\circ(\text{M}^+-\text{SiH}_2) = 56 \pm 6 \text{ kcal mol}^{-1}$ ($\text{M} = \text{Co}, \text{Ni}$). Correlation between the metal ion-silylene bond energies and the electronic structure of the metal ions supports a bonding scheme in which silylene donates its lone pair electrons to an empty 4s orbital of the metal center. For Co^+ and Ni^+ , back-donation of paired 3d electrons from the metal into the empty 3p orbital on silicon is suggested to account for the stronger bond deduced for these metals.

Introduction

Studies of molecular transformations involving the reactions of silicon compounds at transition metal centers are numerous. Hydrosilation, for example, which results in the addition of Si-H bonds to unsaturated hydrocarbons, is catalyzed by transition metal complexes.³⁻⁵ However, catalytic hydrosilations are often very complex and their mechanisms are not well understood. Oxidative addition of a Si-H bond to the metal center is presumed to be an obligatory step in the hydrosilation process and direct evidence for this reaction is provided by several spectroscopic studies at low temperatures.^{6,7} Nevertheless, relatively little is known about the nature, strengths, and specific reactions leading to the formation and rupture of single and multiple bonds between transition metals and silicon.

Recent studies of the reactions of transition metal ions with small organic molecules in the gas phase have been very successful in providing valuable information concerning the reaction mechanisms⁸⁻¹³ and thermochemistry of organometallic fragments in the absence of complicating solution phenomena.¹⁴⁻¹⁷ In the present work, we have examined reactions of several first-row transition metal ions with a series of methyl silanes in the gas phase. A surprising observation, with no precedent in condensed phase chemistry, is prevalent formation of transition metal silylenes as major products. The silicon center in organosilanes completely dominates the observed reactions, which are very different from the reactions of transition metal ions with alkanes in the gas phase.^{9,10,16} These differences can be attributed to the special stability of metal silylenes. Correlation of metal-silicon bond energies with the electronic structures of the metal ions provides interesting insights into the nature of transi-

tion metal-silylene bonds. Kinetic energy release distributions for dehydrogenations of nascent CoSiH_4^+ and NiSiH_4^+ clusters were also measured. These results yield information on the exit channel dynamics.¹⁸

Experimental

The ion-beam apparatus used for these investigations is described in detail elsewhere.¹⁹ Briefly, transition metal ions, Ti^+ , V^+ , Cr^+ , Fe^+ , Co^+ , and Ni^+ are generated from inorganic compounds, TiCl_4 , VOCl_3 , $\text{Cr}(\text{CO})_6$, $\text{FeCl}_3(\text{anhy})$, $\text{CoCl}_2(\text{anhy})$, and $\text{NiCl}_2(\text{anhy})$, respectively, by surface ionization. Ions are extracted from the source, mass, and energy selected, and allowed to interact with the target gas in a collision chamber. Product ions scattered in the forward direction are focused into a quadrupole mass filter, and detected using a channeltron electron multiplier operated in a pulse counting mode. Ion signal intensities are corrected for the mass discrimination of the quadrupole mass filter. The surface ionization source minimizes the production of excited state metal ions which can often react differently from ground state species.^{17,20,21} The relative populations of the electronic states of metal ions are estimated by assuming a Boltzmann distribution at the source temperature employed, 2000-2600 °K (Table I). CH_3SiH_3 was prepared by reducing CH_3SiCl_3 with LiAlH_4 .²² The other silicon compounds were obtained commercially and used without further purification. A sample of CH_3SiD_3 was kindly provided by Professor F.S. Rowland (U.C. Irvine).

Product translational energy releases for dehydrogenation of nascent CoSiH_4^+ and NiSiH_4^+ adducts were obtained using a reverse geometry double focusing mass spectrometer (VG Instruments ZAB-2F).²⁴ Cobalt and nickel

Table I. LOWER ELECTRONIC STATES OF TRANSITION METAL
IONS AND THEIR RELATIVE POPULATIONS

Metal				Filament	Population,
Ion	State ^a	Configuration	Energy, eV ^b	Temperature, °K	%
Ti ⁺	X ⁴ F	3d ² 4s	0.00	2290	62
	4F	3d ³	0.11		36
	2F	3d ² 4s	0.56		2
	2D	3d ² 4s	1.05		<1
V ⁺	X ⁵ D	3d ⁴	0.00	2290	81
	5F	3d ³ 4s	0.34		19
	3F	3d ³ 4s	1.08		<1
Cr ⁺	X ⁶ S	3d ⁵	0.00	2000	100
	6D	3d ⁴ 4s	1.52		<1
Fe ⁺	X ⁶ D	3d ⁶ 4s	0.00	2560	74
	4F	3d ⁷	0.25		25
	4D	3d ⁶ 4s	0.98		1
	4P	3d ⁷	1.64		<1
Co ⁺	X ³ F	3d ⁸	0.00	2560	78
	5F	3d ⁷ 4s	0.43		22
	3F	3d ⁷ 4s	1.21		<1
Ni ⁺	X ² D	3d ⁹	0.00	2490	98
	4F	3d ⁸ 4s	1.09		2
	2F	3d ⁸ 4s	1.68		<1

^aData from Ref. 23.

^bState energies cited are averaged over J states.

ions were formed from 150 eV electron impact on $\text{Co}(\text{CO})_3\text{NO}$ and CpNiNO (Cp = cyclopentadienyl), respectively. Metal-silane adducts were formed in a high-pressure source operated typically at $<3 \times 10^{-3}$ torr of total pressure. Under these conditions metal-silane clusters were formed and extracted from the source before undergoing subsequent collisions. The source was operated under nearly field-free conditions to avoid imparting translational energy to the reactant species. Ions exited the source, were accelerated to 8 KV, and mass selected. Products resulting from the decomposition of mass selected ions in the second field-free region between the magnet and electric sectors were detected by scanning the energy of the electric sector. Kinetic energy release distributions were obtained from metastable peak shapes recorded under conditions in which the energy resolution of the main beam did not contribute significantly to the observed metastable peak widths.²⁵

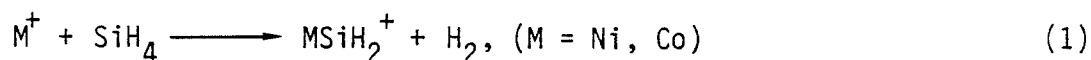
Collision-induced dissociation (CID)²⁶ studies were also performed on nascent CoSiH_4^+ adducts as well as CoSiH_2^+ to probe their structures and fragmentation patterns. CID experiments used He as the target gas admitted into the collision cell situated at the focal point between the magnetic and electric sectors until 50% attenuation of the main beam intensity was observed.

It is important to point out that neutral products are not detected in these experiments. However, except where noted below, the identity of these products can usually be inferred without ambiguity. In addition, these experiments provide no direct structural information about the ionic products. The CID studies in addition to thermochemical arguments can often distinguish possibilities for isomeric structures.

Results and Discussion

In the present study, the transition metal ions, Ti^+ , V^+ , Cr^+ , Fe^+ , Co^+ , and Ni^+ are reacted with silane, the methyl silanes, and hexamethyl disilane in the gas phase. Reactions observed in these systems are considered in the following section, along with plausible mechanisms. In general, Ni^+ and Co^+ are observed to be most reactive toward organosilanes, followed by Ti^+ , V^+ , and Fe^+ . The specific reactions of Ti^+ and V^+ distinguish these ions from the late transition metals. Cr^+ is unreactive with organosilanes, as is the case with hydrocarbons.²⁷ This is followed by an examination of reaction thermochemistry in which several transition metal-silylene bond energies are bracketed. Finally, these bond energies are related to the valence electronic structures of the metal ions to deduce a bonding scheme for transition metal silylenes.

Silane. The products observed in the exothermic reactions with organosilanes are shown in Table II. Both Co^+ and Ni^+ react with silane at low energies resulting in dehydrogenation, reaction 1. Experimental cross sections for these products exhibit typical exothermic behavior, which decrease with increasing kinetic energy as shown in Figure 1.



V^+ , Cr^+ , and Fe^+ are all unreactive with silane. Ti^+ reacts exothermically with silane according to reaction 1, however, the experimental cross section is very small ($\sigma < 0.8 \text{ \AA}^2$).

Collision-Induced Dissociation (CID) of $CoSiH_2^+$, formed in reaction 1, yields reactions 2-4. The small amount of $CoSiH^+$ and $CoSi^+$, processes

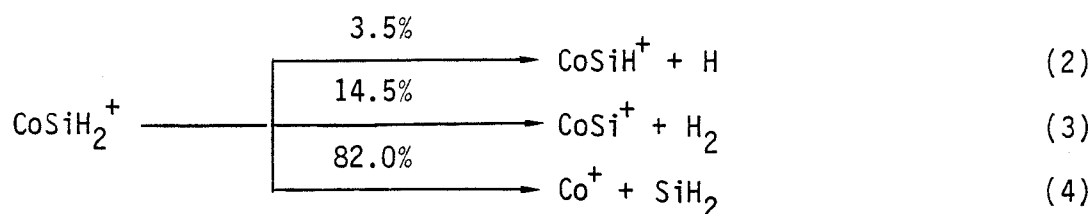


Table II. LOW ENERGY PRODUCT DISTRIBUTIONS FOR REACTIONS OF
TRANSITION METAL IONS WITH SILICON COMPOUNDS.^a

Metal	Neutral Reactant					
Ion	<u>SiH₄</u>	<u>SiH₃Me</u>	<u>SiH₂Me₂</u>	<u>SiHMe₃</u>	<u>SiMe₄</u>	<u>Si₂Me₆</u>
	[17] ^b	[34]	[126]	[120]	[110]	[370]
Ni ⁺	H ₂ (100) ^c	H ₂ (100)	H ₂ (95) CH ₄ (5)	H ₂ (9) CH ₄ (30) NiH(61)	NiMe(100)	SiHMe ₃ (66) SiMe ₄ (34)
	[3.7]	[117]	[64]	[190]	[47]	[300]
Co ⁺	H ₂ (100)	H ₂ (100)	H ₂ (95) CH ₄ (5)	H ₂ (12) CH ₄ (33) CoH(55)	CoMe(100)	SiHMe ₃ or CoMe(97) SiMe ₄ (3)
			[43]	[23]		[180]
Fe ⁺	n.r.	n.r.	H ₂ (100)	H ₂ (40) CH ₄ (60)	n.r.	SiHMe ₃ (15) SiMe ₄ (85)
Cr ⁺	n.r.	n.r.	n.r.	n.r.	n.r.	n.r.
		[1.9]	[17]	[7.6]	[2.7]	[280]
V ⁺	n.r.	H ₂ (100)	H ₂ (45) CH ₄ (55)	H ₂ (100)	H ₂ (10) CH ₄ (90)	H ₂ (23) 2H ₂ (8) CH ₄ (10) CH ₄ ,H ₂ (20) SiC ₂ H ₈ (10) SiC ₃ H ₁₀ (29)

Table II, cont'd.

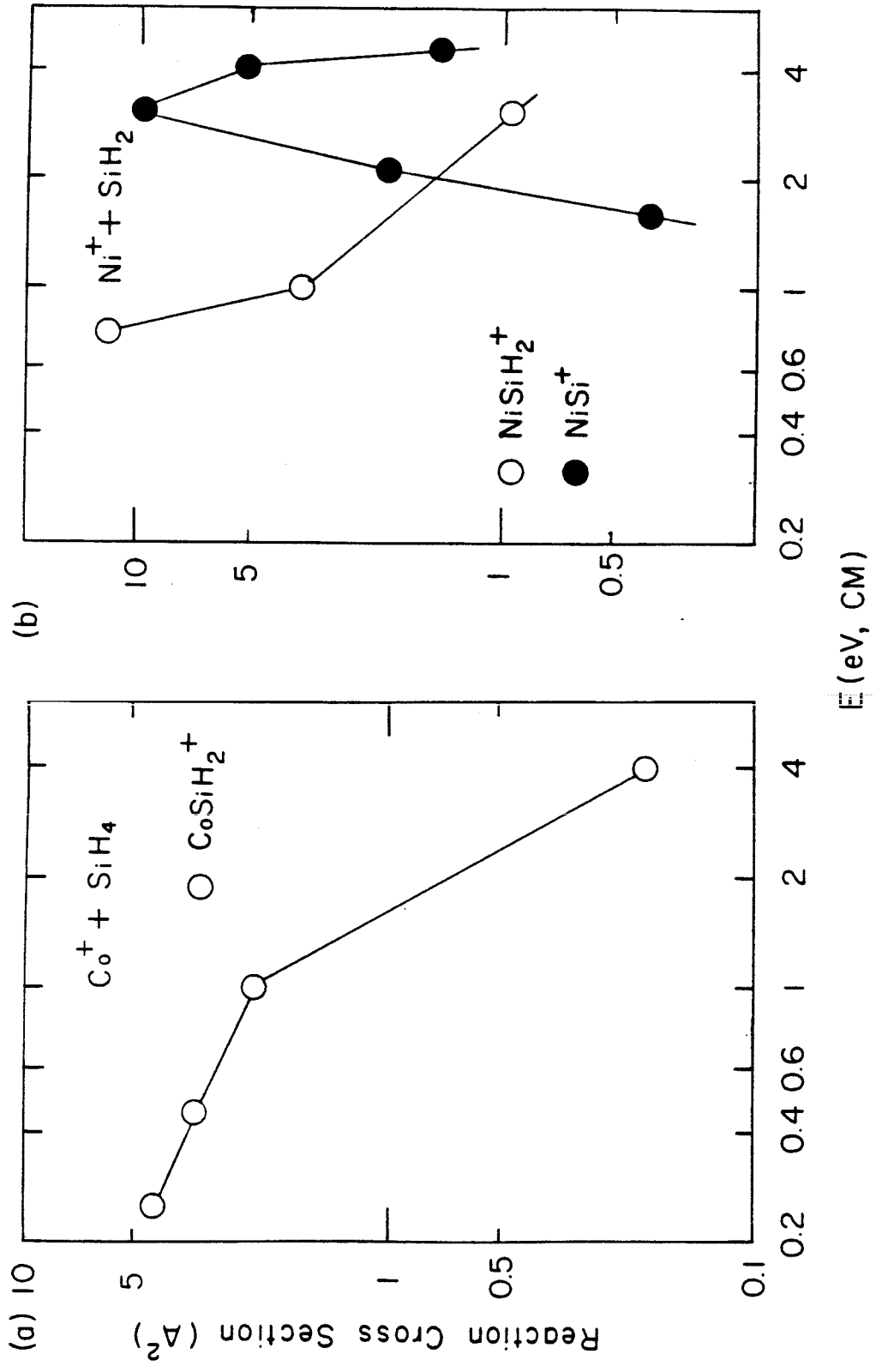
Metal	Neutral Reactant					
	<u>SiH₄</u>	<u>SiH₃Me</u>	<u>SiH₂Me₂</u>	<u>SiHMe₃</u>	<u>SiMe₄</u>	<u>Si₂Me₆</u>
Ti ⁺	[0.8]	[57]	[95]	[133]	[44]	[310]
	H ₂ (100)	H ₂ (94)	H ₂ (58)	H ₂ (95)	H ₂ (66)	H ₂ (18)
		CH ₄ (6)	CH ₄ (42)	CH ₄ (5)	CH ₄ (34)	2H ₂ (5)
						CH ₄ (17)
						CH ₄ ,H ₂ (31)
						SiC ₂ H ₈ (11)
						SiC ₃ H ₁₀ (18)

^aOnly the neutral products are listed. The product distribution was measured at 0.5 eV center of mass kinetic energy.

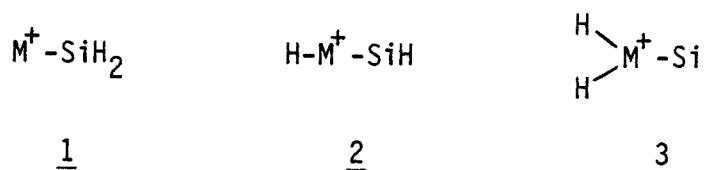
^b[Total cross section, Å²].⁵⁰

^c% of total reaction.

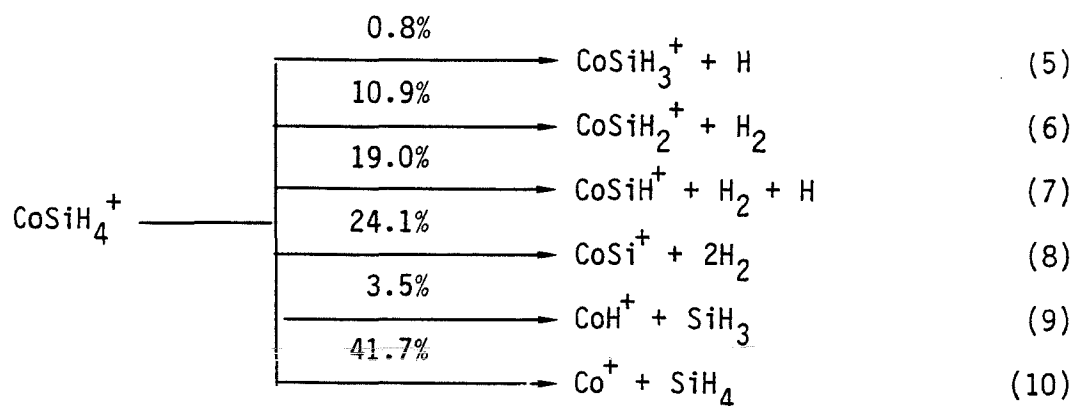
Figure 1. Variation in experimental cross section as a function of center of mass kinetic energy for (a) the reaction of Co^+ with silane, and (b) the reaction of Ni^+ with silane.



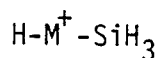
2 and 3, suggest that the structure of CoSiH_2^+ can be formulated as a cobalt-silylene complex, 1. If the CoSiH_2^+ structure were better described by either 2 or 3, then processes 2 and 3 would be expected to dominate.



CID of the nascent CoSiH_4^+ cluster yields processes 5-10.



Processes 5 and 9 may indicate competitive dissociations from intermediate 4, which may be formed by insertion of Co^+ into a Si-H bond.

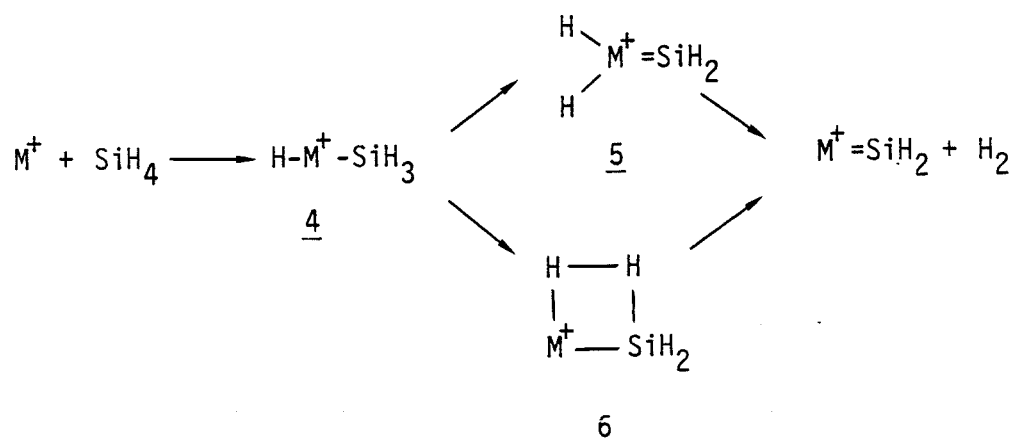


4

CoSiH_3^+ , formed by process 5, probably dissociates further into CoSiH^+ and H_2 as indicated in process 7, and hence yield of CoSiH_3^+ may actually be much higher. This implies $D^\circ(\text{Co}^+ - \text{SiH}_3) - D^\circ(\text{Co}^+ - \text{H}) = 52 \text{ kcal mol}^{-1}$.⁹ With this bond energy, insertion of Co^+ into the silane Si-H bond is energetically favorable.

A mechanism for the dehydrogenation of silane is presented in Scheme I and involves the proposed insertion of a metal ion into the

Scheme I



Si-H bond as an initial step forming 4. This is then followed by an α -hydrogen transfer forming 5 which can eliminate H_2 to yield $\text{M}=\text{SiH}_2^+$ ($\text{M} = \text{Co}, \text{Ni}$).²⁸ Alternatively, dehydrogenation may proceed through the four-centered intermediate 6 in Scheme I. Such four-centered intermediates have been proposed in studies of the H/D exchange reaction of Cl_2MH ($\text{M} = \text{Sc}, \text{Ti}, \text{Ti}^+$) with D_2 using generalized valence bond methods.²⁹ In addition, Watson³⁰ has recently observed an interesting methane exchange reaction which may proceed through a four-centered transition state. The 1,1-dehydrogenation of silane can be a facile process leading to the formation metal-silylene, because the reaction enthalpy for generating

silylene from silane (reaction 11) is only 50 kcal mol⁻¹ (Table III).

This can be compared with carbene formation from methane, reaction 12,



which requires 112 kcal mol⁻¹, rendering 1,1-dehydrogenation a very demanding process in the corresponding reactions of metal ions with methane.³²

The variation of product abundances as a function of kinetic energy for reactions of Co⁺ and Ni⁺ with silane are shown in Figure 1. For the cobalt system only a decrease in the Co=SiH₂⁺ product is observed with increasing energy and no other products are detected ($\sigma < 0.3 \text{ \AA}^2$). For the nickel system, however, NiSi⁺ is observed at higher energy as an endothermic product. This result suggests that dehydrogenation of Ni=SiH₂⁺ is more facile than Co=SiH₂⁺.

The kinetic energy release distributions associated with the metastable loss of H₂ from nascent CoSiH₄⁺ and NiSiH₄⁺ clusters are shown in Figure 2. Elimination of H₂ from the intermediate 5 or 6 is the last step in the postulated mechanism, Scheme I. The shape and average kinetic energy release distributions are quite distinct for these two systems. The kinetic energy distribution for H₂ eliminated from NiSiH₄⁺ is narrow in comparison to the corresponding process involving cobalt. The cobalt system yields a higher average kinetic energy ($\langle \text{KE} \rangle = 0.146 \text{ eV}$) than the nickel system ($\langle \text{KE} \rangle = 0.089 \text{ eV}$). The maximum kinetic energy release for eliminated H₂ is approximately 0.4-0.5 eV in both systems. The origins of the different shapes of the distributions in Figure 2 are not well understood, and may reflect distinctly different potential energy surfaces for the two reactions.³³ In this case the results suggest that there is

Table III. THERMOCHEMICAL DATA USED IN THE TEXT

	kcal mol ⁻¹	ref		kcal mol ⁻¹	ref
D(H ₃ Si-H)	90.3	a	$\Delta H_f(\text{SiH}_4)$	8.2	a
D(H ₃ Si-Me)	88	a	$\Delta H_f(\text{SiH}_3\text{Me})$	-7	a
D(Me ₃ Si-SiMe ₃)	80.5	a	$\Delta H_f(\text{SiH}_2\text{Me})$	-23	a
$\Delta H_f(\text{CH}_4)$	-17.9	b	$\Delta H_f(\text{SiHMe}_3)$	-39	a
$\Delta H_f(\text{C}_2\text{H}_4)$	12.5	b	$\Delta H_f(\text{SiMe}_4)$	-55	a
$\Delta H_f(\text{CH}_2)$	93.7	e	$\Delta H_f(\text{SiMe}_6)$	-87	b
			$\Delta H_f(\text{SiH}_2)$	58	a
			$\Delta H_f(\text{SiHMe})$	39	c
			$\Delta H_f(\text{SiMe}_2)$	26	a
			$\Delta H_f(\text{CH}_2=\text{SiMe}_2)$	7	a
			$\Delta H_f(\text{CH}_2=\text{SiH}_2)$	39	a
			$\Delta H_f(\text{SiH}_3^+)$	236	d

^aRef. 31.

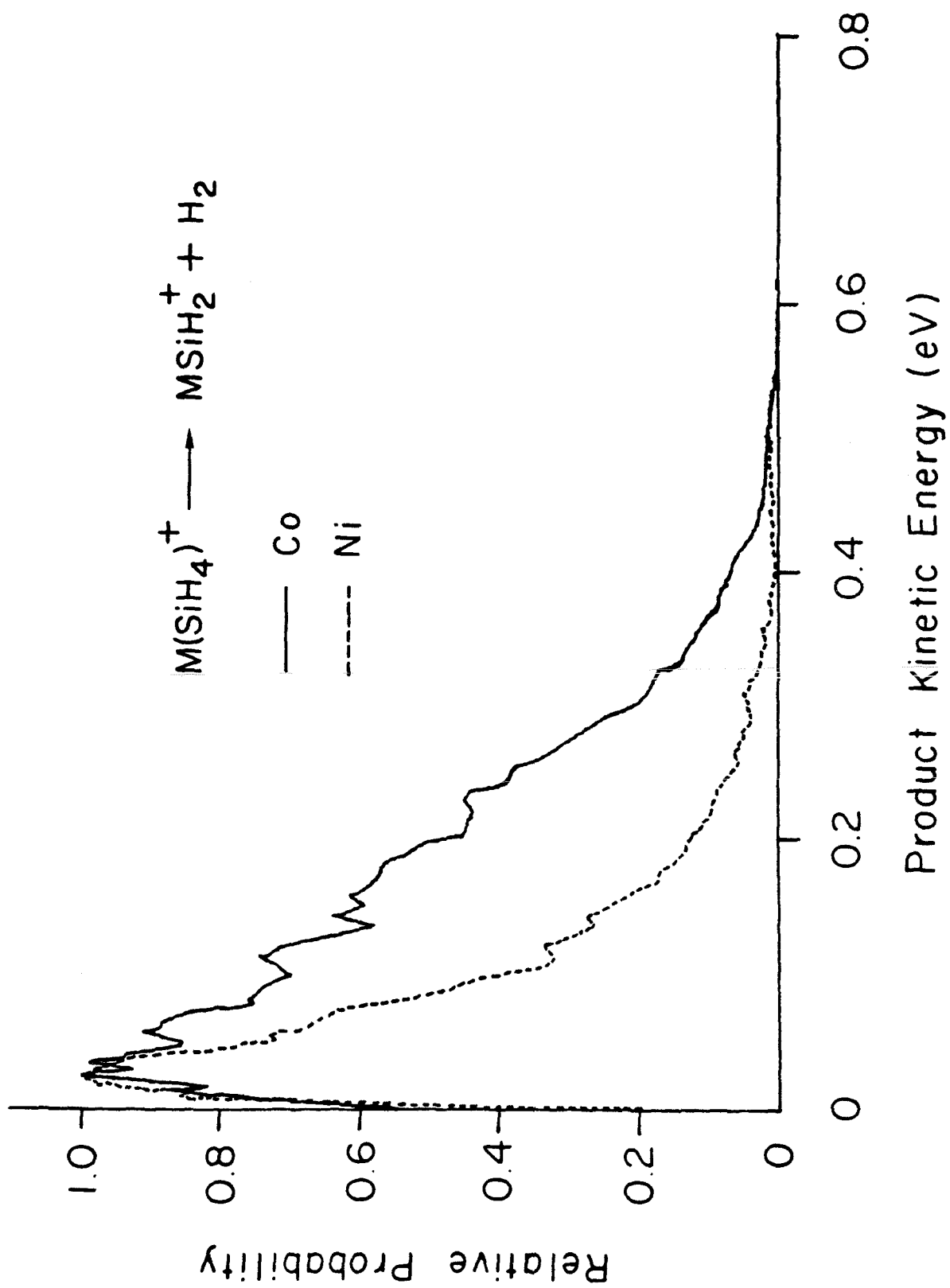
^bRef. 48.

^cestimated from the values of Ref. 31.

^dRef. 41.

^eRef. 49.

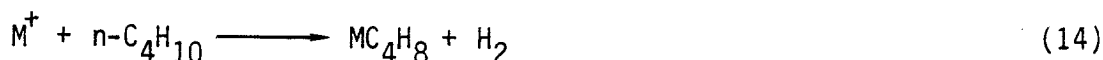
Figure 2. Product translational energy distributions for the metastable loss of H_2 from nascent CoSiH_4^+ (—) and NiSiH_4^+ (···) adducts. The maximum probability is set equal to unity in each case.



a larger barrier for addition of H_2 to $CoSiH_2^+$ than to $NiSiH_2^+$. These barriers can have origins in specific electronic correlation of reactants, intermediates, and products.³⁴ For comparison, the barrier for the addition of H_2 to singlet SiH_2 , process 13, has been calculated using basis

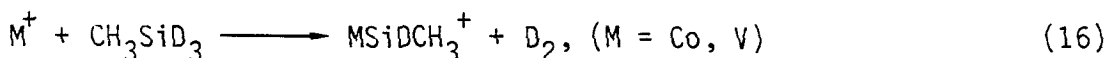
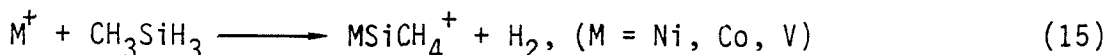


sets of double-zeta quality and CI techniques to be 6.3 kcal/mol at 600 °K.³⁵ In a related study the metastable dehydrogenation of n-butane by Co^+ and Ni^+ , reaction 14, yielded kinetic energy release distributions

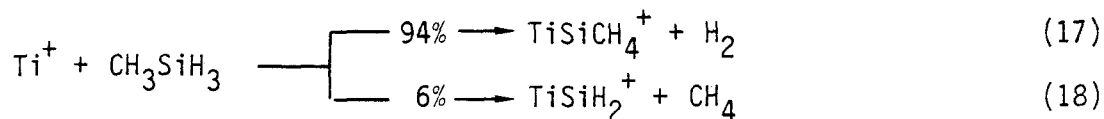


which were essentially identical.¹⁸ This result indicates that both systems may involve very similar potential energy surfaces for the major dehydrogenation processes of n-butane.

Methyl-Substituted Silanes. Ni^+ , Co^+ , and V^+ undergo exothermic reactions with CH_3SiH_3 to yield $M(SiCH_4)^+$ and H_2 (reaction 15). An



examination of these reactions using CH_3SiD_3 results in D_2 loss for Co^+ and V^+ , indicating exclusively a 1,1-dehydrogenation process (reaction 16).³⁶ The observed 1,1-dehydrogenation process suggests that the product is a metal silylene ($M=SiDCH_3^+$). Formation of the other isomers such as metal silaethylene complex $[M(SiH_2=CH_2)^+]$ and metal silylmethylene $[M=CH(SiCH_3)^+]$ would be expected to yield HD and H_2 losses, respectively.³⁷ Ti^+ reacts with methyl silane to yield both H_2 and CH_4 losses (reactions 17, 18). In the same reaction using CH_3SiD_3 , D_2 and CH_3D



losses are observed. This is again consistent with the formulation of product structures as metal silylenes, $\text{Ti}=\text{SiDCH}_3^+$ and $\text{Ti}=\text{SiD}_2^+$. Fe^+ or Cr^+ does not undergo an exothermic reaction with methyl silane.

The observed processes can be rationalized by the mechanisms proposed in Scheme II using the reactions of Ti^+ as an example. Ti^+ may first insert into a Si-D bond of CH_3SiD_3 forming an intermediate 7. Then, D_2 loss can result from either α -D transfer to the metal center (9) or, alternatively, the dissociation of a four-centered intermediate (10). 7 may either undergo α -methyl transfer (11) or form a four-centered intermediate 12 to eliminate CH_3D . Initial insertion of Ti^+ into a Si-Me bond can also be postulated, with loss of CH_3D occurring via intermediate 11 or 13.

Products observed at different collision energies in the reactions with methyl silane are shown in Figure 3. Most of the metal ions except Cr^+ react with methyl silane at high energies to yield minor products of endothermic reactions. Although Fe^+ does not yield products involving exothermic reactions with methyl silane, several products are observed at high energies including FeSi^+ , FeSiH^+ , and FeCH_3^+ . Similar products are observed for Co^+ and Ni^+ at high energies, including MSi^+ , MSiH^+ , and MCH_3^+ ($\text{M} = \text{Co}, \text{Ni}$), illustrating very similar reactivities between Fe, Co, and Ni. On the other hand, Ti^+ and V^+ yield quite different high energy products from those of the late transition metals. Double dehydrogenation product $\text{M}(\text{SiCH}_2)^+$ ($\text{M} = \text{Ti}$ and V) is unique for these metals. Metal silicides (MSi^+) are not produced from these metals.

Scheme II

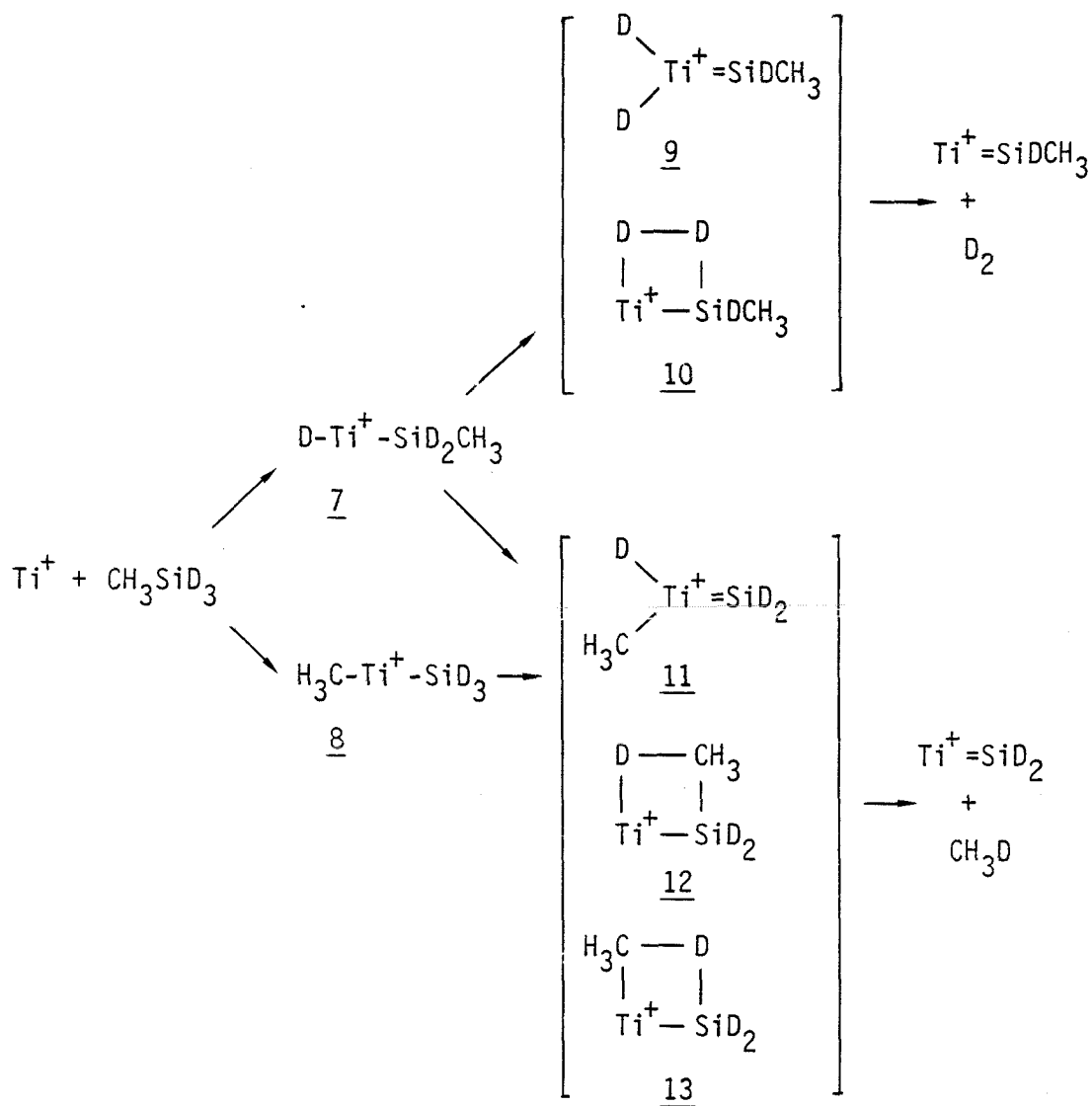
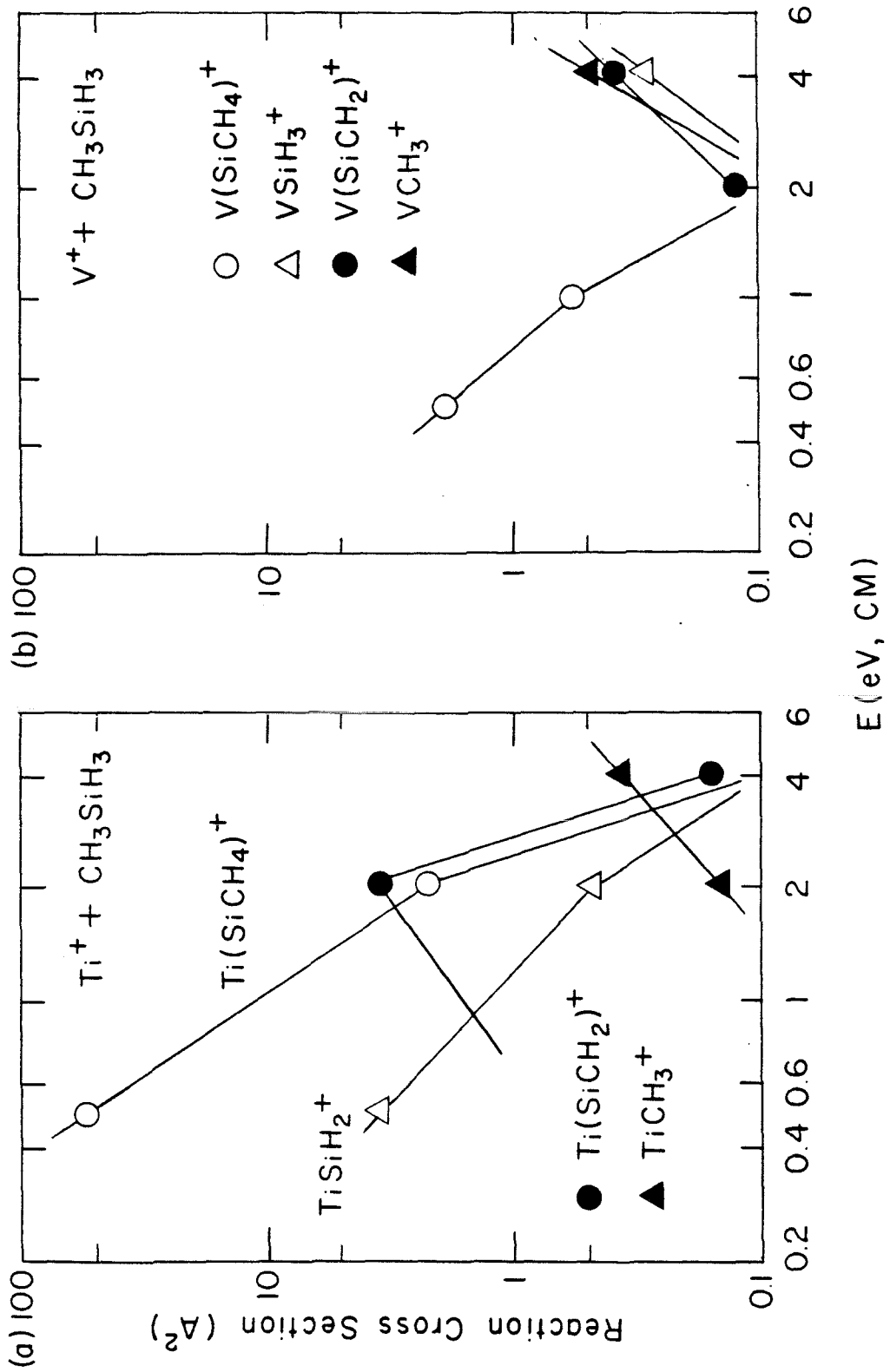
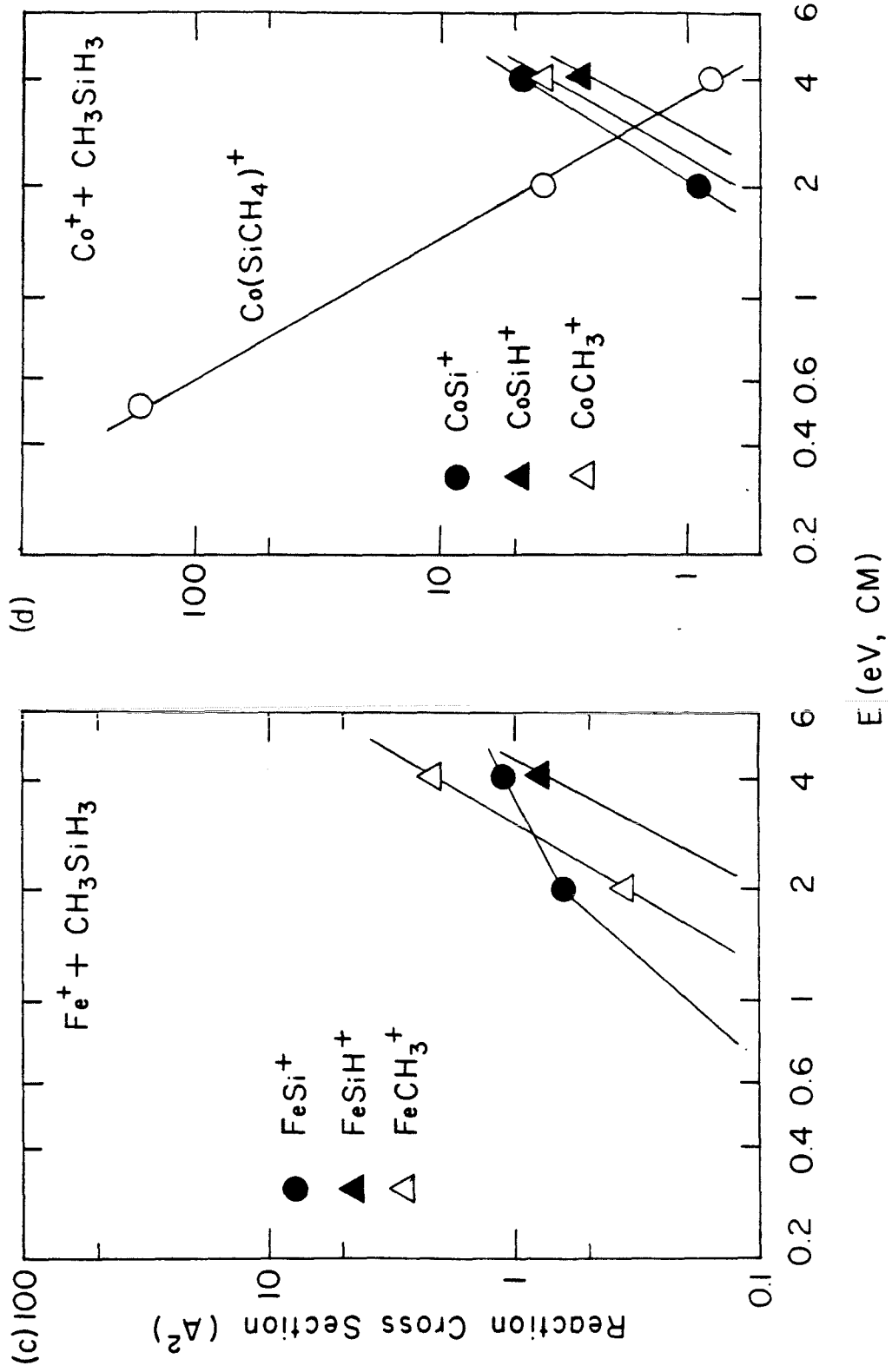
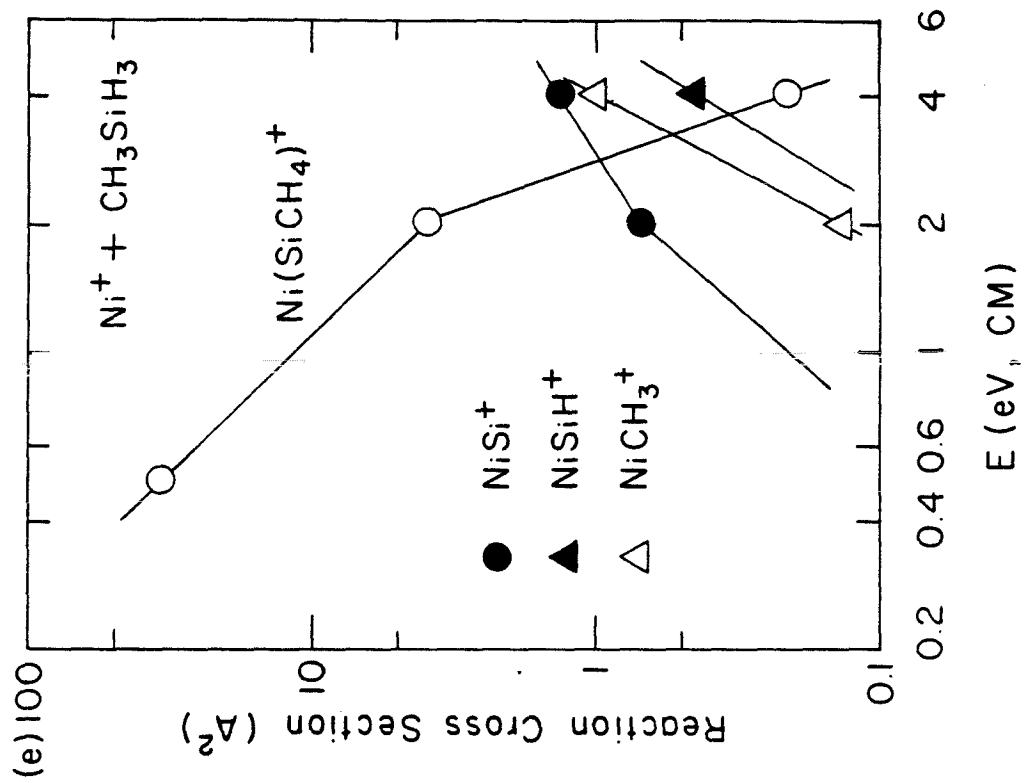


Figure 3. Variation in experimental cross section as a function of center of mass kinetic energy for the reactions of (a) Ti^+ with methyl silane, (b) V^+ with methyl silane, (c) Fe^+ with methyl silane, (d) Co^+ with methyl silane, and (e) Ni^+ with methyl silane.





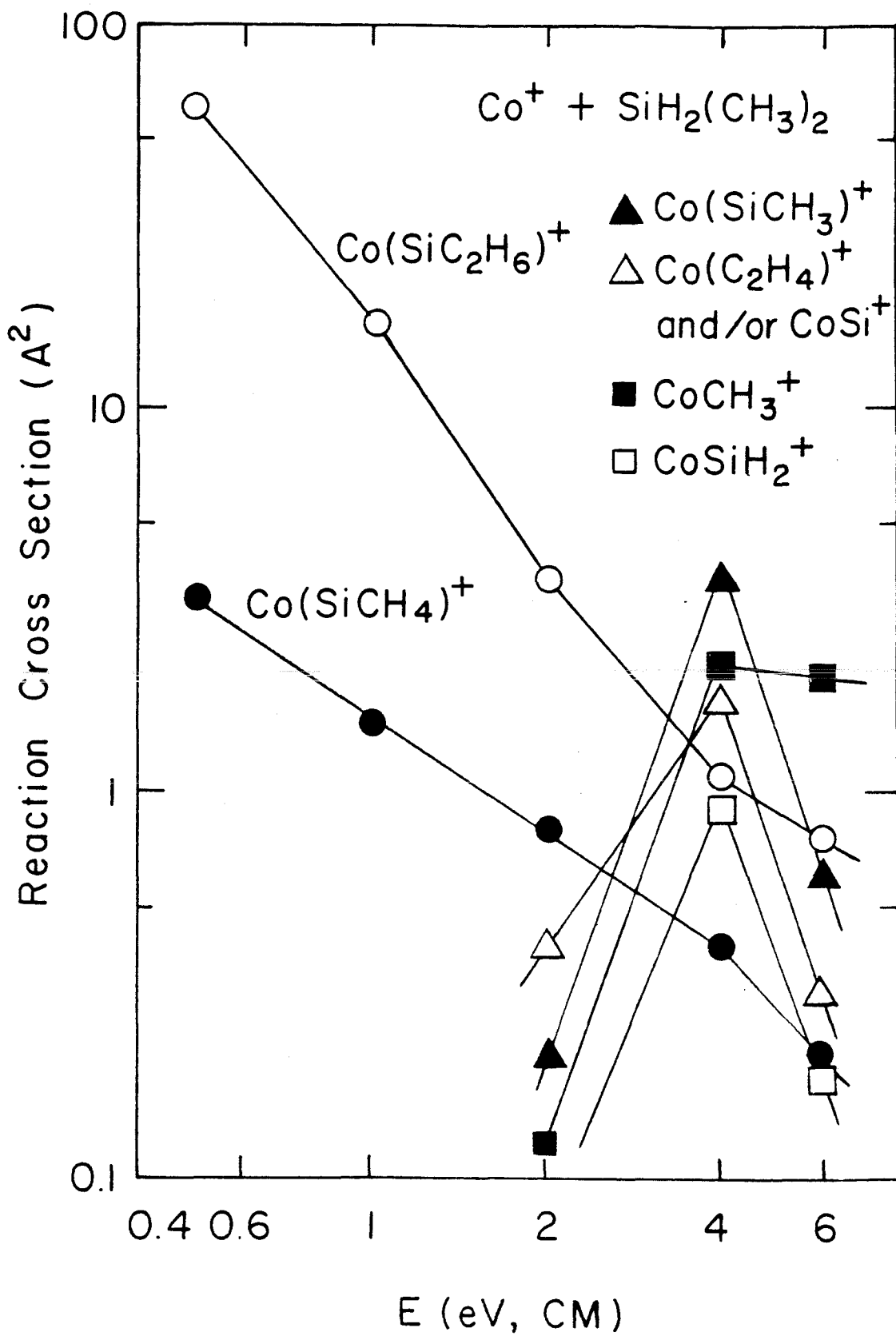


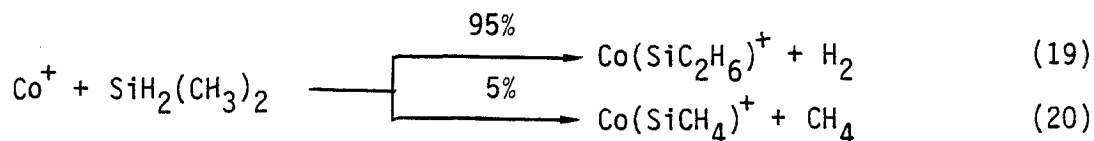
A common high energy product for all of these metals is MCH_3^+ ($M = Ti, V, Fe, Co,$ and Ni), which might be expected to be formed by the dissociation of a Si-C bond insertion intermediate (8 in Scheme II) via an endothermic bond cleavage at high energies. Considering that $MSiH_3^+$ is not produced except for V, this could imply $D^\circ(M^+-CH_2) > D^\circ(M^+-SiH_3)$. Alternatively, this observation could also imply that the bond cleavage product M^+-SiH_3 further dissociates to yield other products, as indicated by the formation of MSi^+ and $MSiH^+$ ($M = Fe, Co,$ and Ni) at high energies. The reaction of V^+ yields comparable amounts of VCH_3^+ and $VSiH_3^+$. Assuming that the structure is V^+-SiH_3 , $D^\circ(V^+-SiH_3) - D^\circ(V^+-CH_3) = 49 \text{ kcal mol}^{-1,21}$ is implied.

It is interesting to compare the reactions of methyl silane and those of ethane. Reaction of Ti^+ with methyl silane, for example, yields $Ti=SiH_2^+$ and $Ti=SiHCH_3^+$, the metal silylenes. On the other hand, reaction of Ti^+ with ethane yields the metal-ethene complex $Ti(CH_2=CH_2)^+$ and the corresponding metal carbene species $Ti=CHCH_3^+$ is not produced.¹⁰ This is confirmed by the reaction of Ti^+ with CH_3CD_3 , which eliminates predominantly HD in a 1,2-dehydrogenation process.³⁸ It has been suggested that $M=CHCH_3^+$ ($M = Fe, Co$) species readily rearrange to the corresponding $M(\text{ethene})^+$ isomer.³⁹

Reactions of $Ti^+, V^+, Co^+,$ and Ni^+ with dimethyl silane yield H_2 and CH_4 loss as exothermic products. Reaction of Fe^+ exhibits H_2 loss as the only product channel. Both exothermic and endothermic products formed in the reaction of Co^+ with dimethyl silane are shown as an example in Figure 4. The exothermic products include $Co(SiC_2H_6)^+$ and $Co(SiCH_4)^+$ (reactions 19, 20). These products can be rationalized by a mechanism

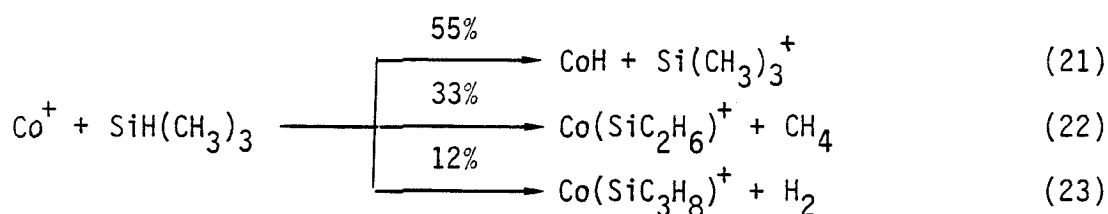
Figure 4. Variation in experimental cross section as a function of center of mass kinetic energy for the reaction of Co^+ with dimethyl silane.





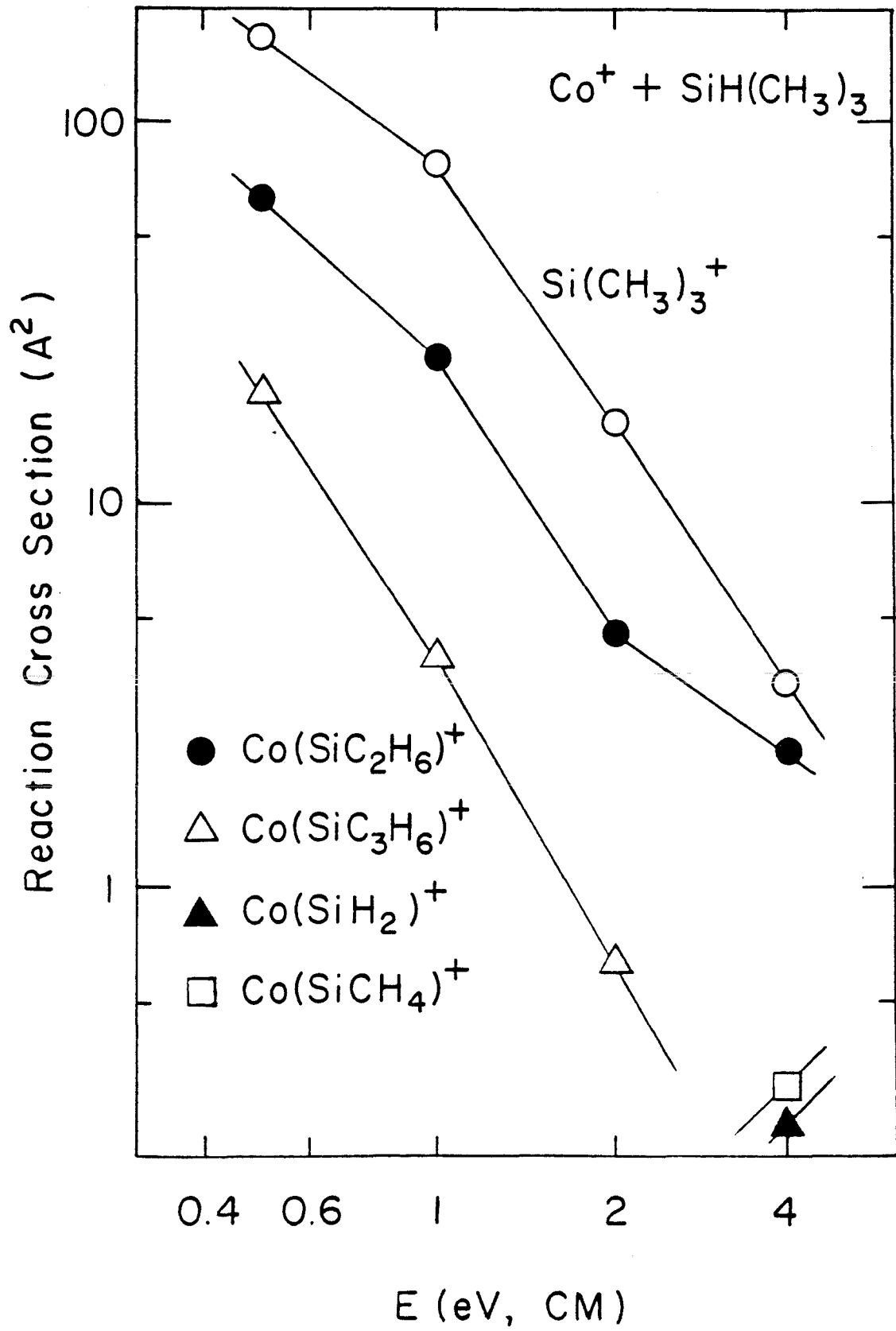
analogous to Scheme II, which involves an initial insertion of Co^+ into a Si-H or Si-C bond followed by an α -Me or α -H transfer. Assuming similar pathways for the reactions with methyl silane and dimethyl silane, the products $\text{M}(\text{SiC}_2\text{H}_6)^+$ and $\text{M}(\text{SiCH}_4)^+$ observed for Ti, V, Fe, Co, and Ni are assumed to be metal silylenes. High energy products in the reaction of Co^+ with dimethyl silane include $\text{Co}(\text{SiCH}_3)^+$, CoCH_3^+ , $\text{Co}(\text{C}_2\text{H}_4)^+$ and/or CoSi^+ , and CoSiH_2^+ . Formation of CoCH_3^+ may result from direct bond cleavage of a Si-C insertin intermediate analogous to 8 in Scheme II. Formation of the other products may involve further molecular rearrangements in the high energy intermediates.

Trimethyl silane shows somewhat different reactivity than mono- and dimethyl silanes. Reaction of Co^+ with trimethyl silane, reactions 21-23, leads to formation of $\text{Si}(\text{CH}_3)_3^+$ as the major product channel, along with



methane loss and dehydrogenation. These three product channels dominate the reaction and only small amounts of $\text{Co}(\text{SiCH}_4)^+$ and $\text{Co}(\text{SiH}_2)^+$ are formed at high energies (Figure 5). The product $\text{Si}(\text{CH}_3)_3$ results from hydride abstraction by Co^+ to generate CoH as a neutral product (reaction 21). The hydride abstraction reaction is observed only for Co^+ and Ni^+ , indicating $D^\circ(\text{M}^+ - \text{H}^-) > D^\circ(\text{SiMe}_3^+ - \text{H}^-)$ for these metals. This observation

Figure 5. Variation in experimental cross section as a function of center of mass kinetic energy for the reaction of Co^+ with trimethyl silane.



is consistent with the fact that heterolytic M^+-H^- bond dissociation energy is higher for Ni and Co than for the other first-row transition metals (Table IV). The $Me_3Si^+-H^-$ heterolytic bond dissociation energy of $218 \text{ kcal mol}^{-1}$ is calculated using Equation 24, with $AP(SiMe_3^+) = 10.20 \pm 0.03 \text{ eV}$ obtained from spectrometry measurements.⁴¹ This value provides somewhat higher estimates for the heterolytic bond dissociation energies for

$$D^\circ(Me_3Si^+-H^-) = AP(SiMe_3^+) - EA(H) \quad (24)$$

nickel and cobalt hydride than the values summarized in Table IV.

Reaction 23, in which H_2 is eliminated, yields the ion product $Co(SiC_3H_8)^+$. The dehydrogenation process is observed to be the major channel in the reaction of Ti^+ and V^+ . The structures of the ionic products $M(SiC_3H_8)^+$ ($M = Ti, V, Fe, Co,$ and Ni) are not known. A metal-dimethyl silaethylene complex $[M(H_2C=SiMe_2)^+]$ may be thermodynamically possible. Since formation of dimethyl silaethylene from trimethyl silane (reaction 25) requires 46 kcal mol^{-1} (Table III), the exothermic formation of $M(H_2C=SiMe_2)^+$ would require a binding energy between the metal



ion and dimethyl silaethylene greater than this value. Binding energy between Co^+ and the corresponding alkane, 2-methyl propene, is estimated to be $50 - 55 \text{ kcal mol}^{-1}$.⁸ For comparison, reactions with 2-methyl propane exhibit H_2 loss as a major process for all of these metals.^{9,10,16} Isotopic labeling has been used to confirm a 1,2-dehydrogenation of 2-methyl propane in several instances.^{9(b)}

Reactions of Ni^+ and Co^+ with tetramethyl silane yield $SiMe_3^+$ as the only exothermic product. Cross section data for the Ni system are shown

Table IV. HETEROLYTIC M^+-H^- BOND DISSOCIATION ENERGIES^a

	<u>Sc</u>	<u>Ti</u>	<u>V</u>	<u>Cr</u>	<u>Mn</u>	<u>Fe</u>	<u>Co</u>	<u>Ni</u>
$D^{\circ}(M^+-H^-),$	163	178	178	179	196	194	206	214
kcal mol ⁻¹							>218 ^b	>218 ^b

^a Ref.40.

^bthis study.

in Figure 6. This product represents formal methyl anion abstraction from tetramethyl silane by Co^+ or Ni^+ . As discussed in the case of trimethyl silane, a lower limit for M^+-Me^- heterolytic bond dissociation energy can be estimated as $D^\circ(\text{M}^+-\text{Me}^-) > D^\circ(\text{Me}^--\text{SiMe}_3^+) = 229 \text{ kcal mol}^{-1}$ ($\text{M} = \text{Co}, \text{Ni}$).⁴² Using this value, homolytic bond dissociation energies $D^\circ(\text{Co}-\text{Me}) > 54 \text{ kcal mol}^{-1}$ are derived.⁴³ Both Ti^+ and V^+ react with tetramethyl silane to lose H_2 and CH_4 . Although Fe^+ undergoes a facile reaction with 2,2-dimethyl propane to lose methane, no exothermic reaction is observed with tetramethyl silane.

Hexamethyl disilane. The reactions with hexamethyl disilane ($\text{Me}_3\text{Si}-\text{SiMe}_3$) exhibit very large experimental cross sections for product formation, which indicates that these reactions are extremely facile. Fe^+ , Co^+ , and Ni^+ yield products of exothermic reactions which include $\text{M}(\text{SiC}_3\text{H}_8)^+$ and $\text{M}(\text{SiC}_2\text{H}_6)^+$ ($\text{M} = \text{Fe}, \text{Co}, \text{and Ni}$). Figure 7 presents cross section data for the reaction of Ni^+ with hexamethyl disilane as an example of these late transition metal systems. The observed products in these systems indicate that cleavage of the weak Si-Si bond ($80.5 \text{ kcal mol}^{-1}$)³¹ completely dominates the reaction pathways. The reactions of Ti^+ and V^+ , on the other hand, are distinguished from those of Fe^+ , Co^+ , and Ni^+ , yielding a variety of products including dehydrogenation, methane loss, as well as Si-Si bond cleavage products.

Bond Energies. As is amply illustrated by the above results, metal silylenes are often observed as a major product in the reactions of atomic metal ions with methyl silanes. By examining the reaction thermochemistry for the observed products, the dissociation energies of the metal-silylene bonds can be obtained. For example, the reactions of Co^+ and Ni^+ with silane yield $\text{M}=\text{SiH}_2^+$ as an exothermic product (reaction 1 and Figure 1).

Figure 6. Variation in experimental cross section as a function of center of mass kinetic energy for the reaction of Ni^+ with tetramethyl silane.

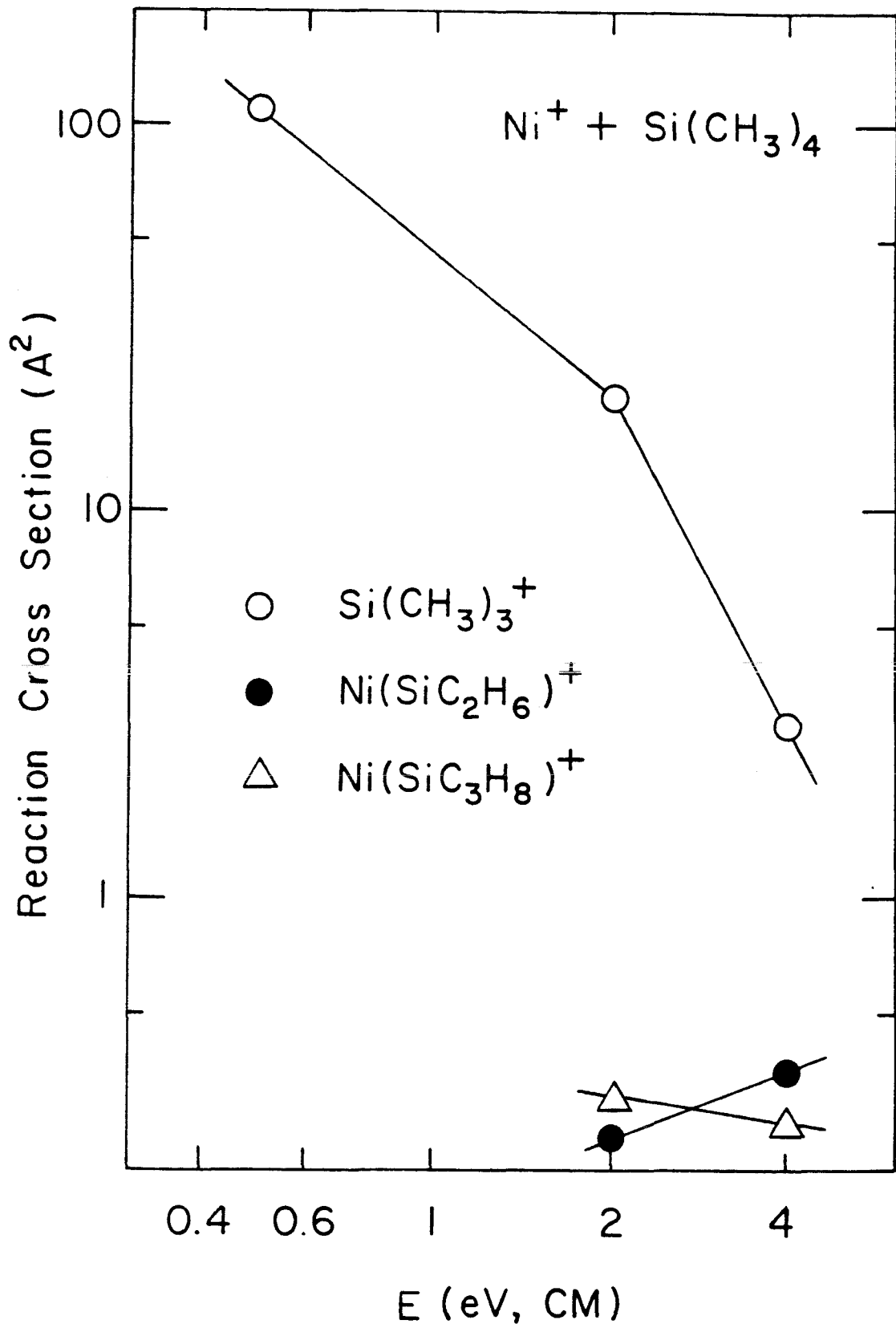
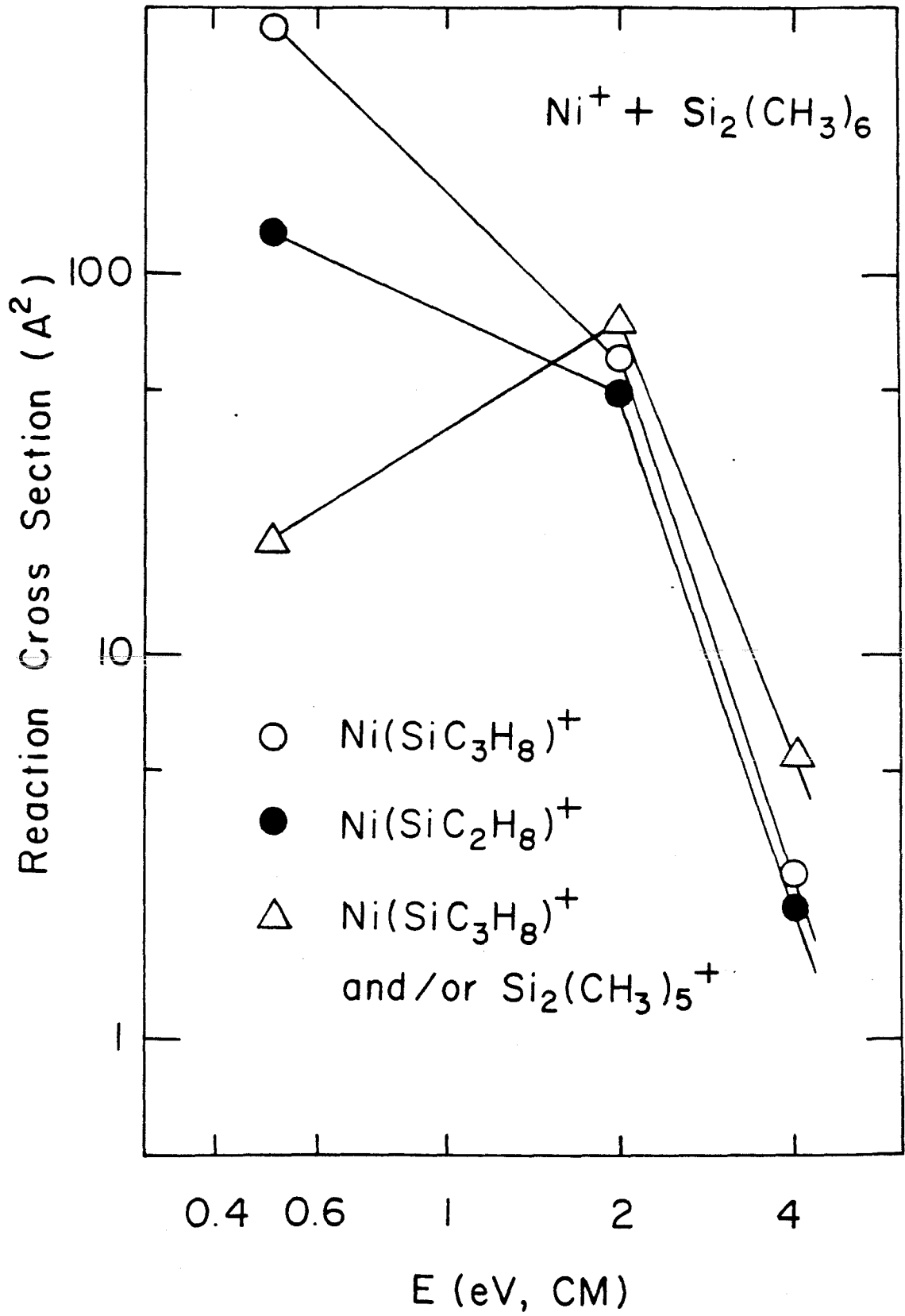


Figure 7. Variation in experimental cross section as a function of center of mass kinetic energy for the reactions of Ni^+ with hexamethyl disilane.



This provides a lower limit for the M^+-SiH_2 bond energy ($M = Co, Ni$) of 50 kcal mol^{-1} (Table V). Similarly, a lower limit for the $M^+-SiHCH_3$ bond dissociation energy can be obtained from the exothermic formation of this species in the reactions with methyl silane (reaction 15). In several reactions with the methyl silanes and hexamethyl disilane, $M(SiC_2H_6)^+$ is produced as an exothermic product. On the condition that the structure is a metal silylene $M=Si(CH_3)_2^+$, this provides a lower limit for the metal-silylene bond energy (Table V). Interestingly, the reactions with dimethyl silane yield $M=SiH_2^+$ as a high energy product for Fe^+ , Co^+ and Ni^+ . Cross sections for the formation of these products exhibit the typical behavior of an endothermic reaction, which is shown in Figure 4 for $Co=SiH_2^+$. Provided that no substantial energy barrier is present which might inhibit the formation of $M=SiH_2^+$ at low energy, the endothermicity of $M=SiH_2^+$ formation provides an upper limit of 61 kcal mol^{-1} for the $M=SiH_2^+$ bond energy ($M = Fe, Co, \text{ and } Ni$). The bond dissociation energies estimated in this fashion are summarized in Table VI along with the reactions used to infer the various limits. Reaction enthalpies used in this determination may require additional attention. One of the important quantities in deriving these reaction enthalpies is the controversial heat of formation of SiH_2 , for which several values are reported, including 58 kcal mol^{-1} ,³¹ and 81 kcal mol^{-1} .⁴⁴ Considering the probable experimental uncertainties in these measurements, we have chosen to use the value from Ref.31, $\Delta H_f^\circ(SiH_2) = 58 \text{ kcal mol}^{-1}$.

The Nature of Transition Metal-Silylene Bond. The present study shows two distinct features of transition metal silylenes. First, the transition metal silylenes are fairly stable, which often renders metal silylenes as major products in the reactions of transition metal ions

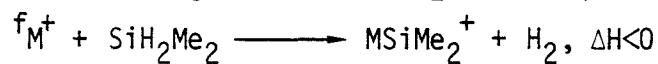
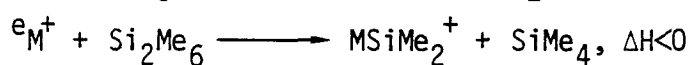
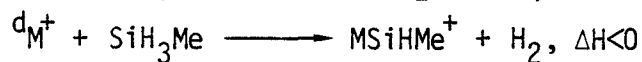
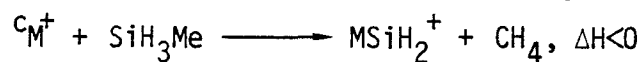
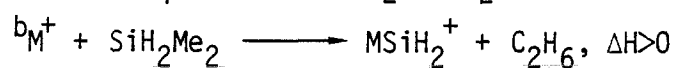
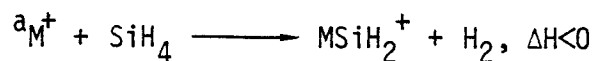
Table V. REACTION ENTHALPIES FOR THE FORMATION OF SILYLENES
FROM SEVERAL SILICON COMPOUNDS, kcal mol⁻¹,^a

Silicon Compound	Eliminated Fragment			
	H ₂	CH ₄	C ₂ H ₆	Si(CH ₃) ₄
SiH ₄	50			
CH ₃ SiH ₃	49	47		
SiH ₂ (CH ₃) ₂	49	47	61	
SiH(CH ₃) ₃		47	61	
Si(CH ₃) ₄			61	
Si ₂ (CH ₃) ₆				58

^aRef. 31.

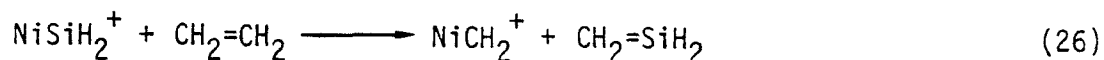
Table VI. TRANSITION METAL ION-SILYLENE BOND ENERGIES

Metal Ion	Ground State Electronic Configuration (Term) ^g	Bond Energies, kcal mol ⁻¹		
		M^+-SiH_2	$M^+-SiHCH_3$	$M^+-Si(CH_3)_2$
Ni ⁺	d ⁹ (² D)	56±6 ^{a,b}	>46 ^d	>58 ^e
Co ⁺	d ⁸ (³ F)	56±6 ^{a,b}	>46 ^d	>58 ^e
Fe ⁺	s ¹ d ⁶ (⁶ D)	<61 ^b		>58 ^e
V ⁺	d ⁴ (⁵ D)		>46 ^d	>49 ^f
Ti ⁺	s ¹ d ² (⁴ F)	>47 ^c	>46 ^d	>49 ^f



^g Ref. 23.

with the silanes. The stability of metal silylenes may be illustrated further by the enthalpy change of reaction 26, for which $\Delta H^\circ = 32 \text{ kcal}$



mol^{-1} .⁴⁵ Second, the metal-silylene bond is stronger for Ni^+ and Co^+ than the other transition metal ions studied, as illustrated by the exothermic formation of $\text{M}=\text{SiH}_2^+$ ($\text{M} = \text{Ni}$ and Co) from silane. These observations provide a basis to describe the bonding between transition metal ions and silylene as follows.

Silylene has a singlet ground state (1A_1) and a low-lying triplet excited state at -0.81 eV ($18.6 \text{ kcal mol}^{-1}$).⁴⁶ The ground state silylene is expected to form a donor-acceptor type σ -bond to the metal ion by donating its lone-pair electrons to the metal center. Hence, metal ions with an empty 4s orbital (ground state derived from a $3d^n$ valence electronic configuration) can make a strong metal-silylene bond by accepting the lone-pair electrons from silylene. Observation of the strong bond for $\text{Ni}^+(3d^9)$ and $\text{Co}^+(3d^8)$ supports this conjecture.

In addition to accepting lone-pair electrons from silylene, both Ni^+ and Co^+ can also back-donate electrons from their paired $3d_{\pi}$ orbital to the empty $3p_{\pi}$ orbital of silicon, enhancing the transition metal-silylene bond strength. The π -backbonding strength could be estimated by subtracting a typical n-donor σ -bond energy from the measured metal-silylene bond energy. Unfortunately, bond dissociation energies between bare transition metal ions and the second-row element n-donor bases are not available. Bond dissociation energies between CpNi^+ ($\text{Cp} = \text{cyclopentadienyl}$) and several n-donor bases (B) may be useful for this purpose. CpNi^+ also has an empty 4s orbital which acts as an acceptor for lone-

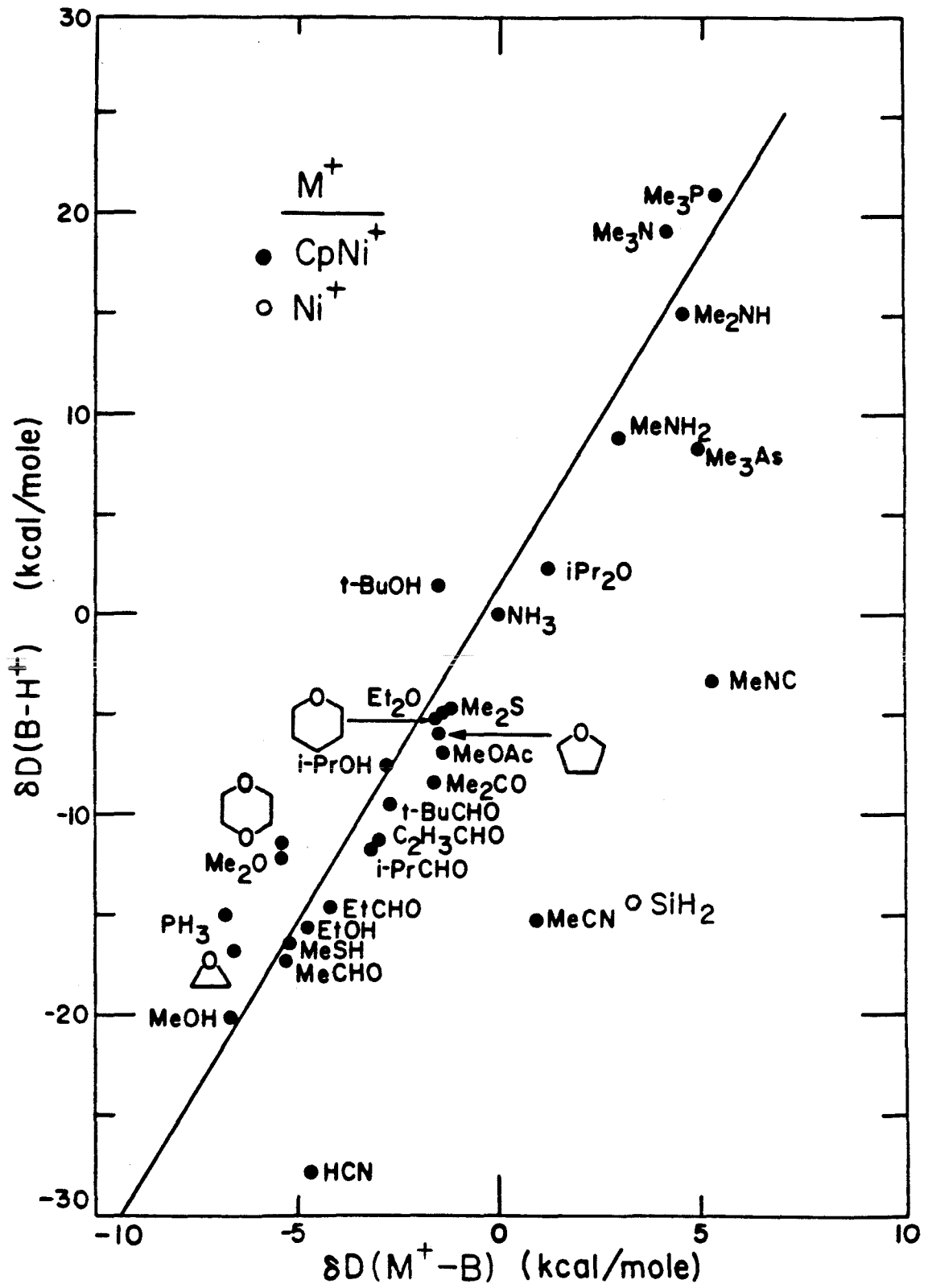
pair electrons. Previous studies using ion cyclotron resonance spectrometry in our laboratory have revealed a linear correlation between the CpNi^+ -B bond energies and the proton affinities of B (Figure 8).⁴⁷ Proton affinity of SiH_2 is calculated from Equation 27 to be $188 \text{ kcal mol}^{-1}$.

$$\text{PA}(\text{SiH}_2) = \Delta H_f(\text{SiH}_2) + \Delta H_f(\text{H}^+) - \Delta H_f(\text{SiH}_3^+) \quad (27)$$

When the Ni^+ - SiH_2 bond energy obtained in the present study is included in Figure 8, it can be noticed that the Ni^+ - SiH_2 bond is stronger than normal σ -donor bonds to CpNi^+ . The greater preference for bonding to CpNi^+ is also exhibited by HCN, MeCN, MeNC, and Me_3As , which are expected to have π -bonding ability. Although this analysis may be rather qualitative due to the intrinsic difference between atomic Ni^+ and CpNi^+ , it provides an illustration that Ni^+ - SiH_2 bond may have a substantial π -bonding character.

One way to test the validity of the bonding analysis for transition metallsilylenes described above is to apply this scheme to the other metal ions. Fe^+ and Ti^+ have $4s^1 3d^n$ valence electronic configurations and we expect that their metal-silylene bond strength is weakened due to the half-filled 4s orbital. This argument is supported by the absence of FeSiH_2^+ as well as a very small amount of TiSiH_2^+ formation from the exothermic reactions of Ti^+ with silane. Although the ground state of V^+ is derived from a $3d^4$ electronic configuration with an empty 4s orbital, V^+ is unreactive toward silane. Comparing V^+ with Ni^+ and Co^+ , V^+ has only singly occupied 3d orbitals. Hence, the amount of back-donation in the metal-silylene bond may be reduced for V^+ compared with Ni^+ or Co^+ . Cr^+ has a stable $3d^5$ valence electronic configuration and may not initiate reaction toward silane or methyl-substituted silanes by the insertion into

Figure 8. Comparison of two scales of molecular basicity; binding energies of molecules to H^+ , $D(B-H^+)$, and to metal ions, $D(M^+-B)$. Relative binding energies referenced to NH_3 , $\delta D(B-H^+)$ and $\delta D(M^+-B)$, are shown. The data are taken from Reference 47.



a Si-H or Si-Me bond. We have previously found that the Cr^+ is unreactive toward alkanes for the same reason.²⁷

Conclusion

The present results are the first experimental observation and bond energy determination of transition metal silylenes. The metal silylenes are the major products from the reactions of transition metal ions with the silanes, providing a contrast to the formation of metal-alkene complexes from the reactions of transition metal ions with alkanes. This difference in reactivity is attributed to the thermodynamically less demanding process of generating silylene from the silanes compared to carbene formation from the corresponding alkanes. Metal-silylene bond dissociation energies, estimated by examining the reaction thermochemistry associated with metal silylene formation, are stronger for Co^+ and Ni^+ than for the other metal ions. The bonding between transition metal ions and silylene is described by σ -donation of lone pair electrons from the ground state silylene to the metal center, and π -backdonation of paired 3d electrons from the metal into the empty 3p orbital of Si is invoked to account for the strengthened Ni^+-SiH_2 and Co^+-SiH_2 bonds.

Acknowledgment

We gratefully acknowledge the support of the National Science Foundation under Grants CHE 8407857 (J.L.B.) and CHE (M.T.B.). Graduate fellowship support by the Korean Government (H.K., 1980-84) is gratefully acknowledged.

References

1. Present address; Department of Chemistry, University of Houston, 4800 Calhoun Road, Houston, Texas 77004.
2. Contribution No.
3. Khan, M.M.T.; Martell, A.E., "Homogeneous Catalysis by Metal Complexes", Vol. 2 (Academic Press, 1974), p.66
4. Collman, J.P.; Hegedus, L.S., "Principles and Applications of Organotransition Metal Chemistry" (University Science Books, 1980), p. 384.
5. Noll, W., "Chemistry and Technology of Silicons" (Academic Press, 1986).
6. Fernandez, M-J.; Bailey, P.M.; Bentz, P.O.; Ricci, J.S.; Koetzle, T.F.; Maitlis, P.M., J. Am. Chem. Soc. (1984), 106, 5458.
7. Fernandez, M-J.; Maitlis, P.M., Organometallics (1983), 2, 164.
8. Hanratty, M.A.; Beauchamp, J.L.; Illies, A.J.; and Bower, M.T., J. Am. Chem. Soc. (in press).
9. (a) Halle, L.F.; Armentrout, P.B.; Beauchamp, J.L., Organometallics (1982), 1, 963. (b) Houriet, R.; Halle, L.F.; Beauchamp, J.L., Organometallics (1983), 2, 1818.
10. Byrd, G.D.; Burnier, R.O.; Freiser, B.S., J. Am. Chem. Soc. (1982), 104, 3565.
11. Jacobson, D.B.; Freiser, B.S., J. Am. Chem. Soc., (1985), 107, 4373 and references therein.
12. Larsen, B.S.; Ridge, D.F., J. Am. Chem. Soc. (1984), 106, 1912.
13. Walba, D.M.; Depuy, C.H.; Grabowski, J.J.; and Bierbaum, V.M., Organometallics (1984), 3, 498.
14. Aristov, N.; Armentrout, P.B., J. Am. Chem. Soc. (1984), 106, 4065.

15. Sallans, L.; Lane, K.R.; Squires, R.R.; Freiser, B.S., J. Am. Chem. Soc. (1984), 106, 4065.
16. Armentrout, P.B.; Beachamp, J.L., J. Am. Chem. Soc. (1981), 103, 784.
17. Mandich, M.L.; Halle, L.F.; Beauchamp, J.L., J. Am. Chem. Soc. (1984), 106, 4403.
18. Hanratty, M.A.; Beauchamp, J.L.; Illies, A.J.; Bowers, M.T., J. Am. Chem. Soc. (1985), 107, 1788.
19. Armentrout, P.B.; Beauchamp, J.L., J. Chem. Phys. (1981), 74, 2819.
20. Halle, L.F.; Armentrout, P.B.; Beauchamp, J.L., J. Am. Chem. Soc. (1981), 103, 962.
21. Aristov, N.; Armentrout, P.B. (to be published).
22. Gaspar, P.P.; Levy, C.A.; Adair, G.M., Inorg. Chem. (1970), 9, 1272.
23. Moore, C.E., "Atomic Energy Levels" (National Bureau of Standards, Washington, D.C., 1949).
24. For a description of the experimental instrumentation and methodology, see: (a) Illies, A.J.; Bowers, M.T., Chem. Phys. (1982), 65, 281. (b) Illies, A.J.; Jarold, M.F.; Bass, L.M.; Bowers, M.T., J. Am. Chem. Soc. (1983), 105, 5775.
25. For details of the kinetic energy release calculations, see: Jarold, M.F.; Illies, A.J.; Kirchner, N.J.; Wagner-Redeker, W.; Bowers, M.T.; Mandich, M.L.; Beauchamp, J.L., J. Phys. Chem. (1983), 87, 2213.
26. For a general discussion of collision-induced dissociation, see: Cooks, R.G., "Collision Spectroscopy" (Plenum Press, New York, 1978).
27. Beauchamp, J.L., unpublished results.

28. We use $M=SiH_2^+$ in representing metal silylenes to be consistent with the valence of silicon atom. However, this should not be interpreted as two σ -bonds between the metal and silicon, because, as discussed in the text, the metal-silylene bond is considered as σ -donation of a lone-pair orbital of silylene to a metal and in some cases additional Π -back-donation from metal to silicon.
29. Steigerwald, M.L.; Goddard, W.A., III, *J. Am. Chem. Soc.* (1984), 106, 308.
30. Watson, P.L., *J. Am. Chem. Soc.* (1983), 105, 6491.
31. Walsh, R., *Acc. Chem. Res.* (1981), 14, 246.
32. 1,1-Dehydrogenation process is not observed in the gas phase reactions of the first row transition metal ions with methane.
33. See, for example: Jarold, M.F.; Bass, L.M.; Kemper, P.R.; van Koppen, P.A.M.; Bowers, M.T., *J. Am. Chem. Soc.* (1983), 78, 3756.
34. See, for example: (a) Blomberg, M.R.A.; Brandemark, U.; Siegbahn, P.E.m., *J. Am. Chem. Soc.* (1983), 105, 5557. (b) Blomberg, M.R.A.; Siegbahn, P.E.M.; Bauschlicher, C.W., *J. Chem. Phys.* (1984) 81, 1373.
35. Sax, A.; Olbrich, G., *J. Am. Chem. Soc.* (1985), 107, 4868.
36. Ni^+ was not included in this study because of the limited amount of CH_3SiD_3 available for the experiment.
37. Although the energy difference between methyl silylene and silaethylene is controversial in both experimental and theoretical results, they reasonably agree that heat of formation of methyl silylene is lower than that of silaethylene by a few $kcal\ mol^{-1}$ or almost equal; Schaefer, H.F., *Acc. Chem. Res.* (1982), 15, 283.
38. Tolbert, M.A.; Beauchamp, J.L. (unpublished result).

39. Jacobson, D.B.; Freiser, B.S., J. Am. Chem. Soc. (in press).
40. Martinho Simoes, J.A.; Beauchamp, J.L., Chemical Reviews (to be published).
41. Cordermann, R.R., Ph.D. Thesis, California Institute of Technology (1977).
42. Calculated using $D(\text{Me}_3\text{Si}^+-\text{Me}^-) = AP(\text{SiMe}_3^+) - EA(\text{Me})$; $AP(\text{SiMe}_3^+) = 10.03 \pm 0.04$ eV from Murphy, M.K.; Beauchamp, J.L., J. Am. Chem. Soc. (1977), 99, 2085; $EA(\text{CH}_3) = -0.08$ eV from Ellison, G.B.; Engelking, P.C.; Lineberger, W.C., J. Am. Chem. Soc. (1978), 100, 2556.
43. Calculated using $D^\circ(\text{M}-\text{Me}) = D^\circ(\text{M}^+-\text{Me}^-) + EA(\text{Me}) - IP(\text{M})$.
44. Saalfeld, F.E.; McDowell, M.V., Inorg. Chem. (1967), 6, 96.
45. $D^\circ(\text{Ni}^+-\text{CH}_2) = 86 \pm 6$ kcal mol⁻¹ from Ref. 9(a).
46. Meadows, J.H.; Schaefer III, H.F., J. Am. Chem. Soc. (1976), 98, 3998.
47. Corderman, R.R.; Beauchamp, J.L., J. Am. Chem. Soc. (1976), 98, 3998.
48. Pedley, J.B.; Rylance, J., "Sussex-N.P.L. Computer Analyzed Thermochemical Data: Organic and Organometallic Compounds" (Univ. of Sussex, 1977).
49. Rosenstock, H.M.; Draxl, K.; Steiner, B.W.; Herron, J.T., J. Phys. Chem. Ref. Data. Suppl. (1977), 6.
50. The experimental cross sections are sometimes larger than the values estimated using Langevin-Gioumouis-Stevenson model for ion-molecule reactions. The disagreement, especially for hexamethyl disilane, might indicate experimental uncertainties in measuring absolute reaction cross sections.

CHAPTER V

PULSED LASER EVAPORATION AND IONIZATION OF SOLID METAL TARGETS.
IMPLICATIONS FOR STUDYING THE GAS-PHASE
REACTIONS OF LASER-GENERATED ATOMS AND IONS

PULSED LASER EVAPORATION AND IONIZATION OF SOLID METAL
TARGETS. IMPLICATIONS FOR STUDYING THE GAS-PHASE
REACTIONS OF LASER-GENERATED ATOMS AND IONS

Heon Kang and J.L. Beauchamp*

Contribution No. 7147 from Arthur Amos Noyes Laboratory of
Chemical Physics, California Institute of Technology, Pasadena,
California 91125.

Abstract

Intense beams of metal ions and atoms are generated by a CO₂ TEA laser focused onto solid Al and Ni targets to give power densities of $10^7 - 10^9$ watts cm⁻². Beam composition is determined using a quadrupole mass spectrometer, and time-of-flight measurements yield ion and atom kinetic energy distributions. Kinetic energies of multiply charged ions increase in proportion to the square of their charge multiplicities. A novel source design is described in which a parabolic reflector focuses the laser beam onto a small metal target and evaporated atoms are sampled through a small aperture in the reflector. By varying the power density, pulsed atom beams are produced with kinetic energies variable between 0.1 and 10 eV. Several aspects of employing the laser-generated ions and atoms in ion cyclotron resonance experiments and as a beam source for gas-phase reaction studies are discussed.

Introduction

Pulsed-laser evaporation and ionization of solid metal targets has become an important experimental technique for generating metal atoms and ions for gas-phase studies. A high-power laser pulse can increase the instantaneous surface temperature within the focused area well above the boiling point of the metal, resulting in the generation of an intense pulse of metal atoms and ions. It was first demonstrated by Friichtenicht that energetic and intense metal atom beams can be produced in this fashion.¹ More recently, the combination of this methodology with a pulsed nozzle has yielded supersonic beams of cold metal atoms and clusters.^{2,3} Laser-generated ions have been used extensively in ion cyclotron resonance (ICR) studies of the reactions of these species with small organic molecules in the gas phase.^{4,5}

Conventionally, metal atom beams have been generated mainly by thermal evaporation from oven sources, which are able to evaporate some of the relatively low boiling point metals.⁶ Unless seeded beam techniques are employed, the kinetic energies of the evaporated metal atoms are limited by accessible oven temperatures. In addition to other differences, pulsed-laser evaporation techniques have four distinct advantages when compared to thermal oven sources. First, metal atoms produced by pulsed-laser evaporation have kinetic energies which can be varied more widely over the range appropriate to study chemical reactions (0.1–10 eV). Second, the kinetic energy can be easily varied by changing laser parameters. Third, *any* solid material, regardless of its boiling temperature, can be evaporated and, in addition, ionized. As a fourth and final point, the laser heating is localized to a small area of the target surface, and the remainder of the apparatus remains at ambient temperature during an experiment.

Even with the prominent attributes noted above, there are still important facets of the experiment which remain to be characterized. These include the origin of the high kinetic energies of laser-generated metal atoms and ions, the relationship between kinetic energies and laser-power densities, characterization of the internal state distribution of the beam, and the effect of target geometries and surface conditions on the experiment. On the practical side, laser-evaporated target material often deposits on the window through which the laser light is introduced and eventually blocks the radiation. To avoid this problem, Friichtenicht¹ used a target in which a thin metal film was deposited on a transparent substrate. Irradiation through the substrate evaporated the metal atoms from the opposite face. This arrangement requires that the target be repositioned after each shot. In the present paper we describe a source geometry which avoids fogging the window and yields a metal atom beam propagating in the same direction as the laser beam, but which does not require target repositioning between laser pulses. In this source (Figure 1) atoms and ions emitted from the target are sampled with a quadrupole mass spectrometer through a small aperture at the center of a parabolic mirror. We report ion and atom kinetic energy distributions determined at various laser power densities using time-of-flight techniques. The implications of the present experiments for studies of the chemistry of laser-evaporated atoms and ions are briefly discussed.

Experimental Section

The experimental apparatus is shown schematically in Figure 1. A CO₂ TEA laser (Tachisto TAC II) is operated multimode at 10.6 μm, delivering up to 1 J pulse⁻¹. The laser pulse consists of an initial 50-ns peak which contains about 40% of the total pulse energy, followed by a 500-ns tail. Laser light enters through a NaCl window and is focused onto a metal target by a front surface 1.7-cm focal length parabolic reflector. Both aluminum (mp = 660 °C, bp = 2467 °C) and nickel (mp = 1453 °C, bp = 2732 °C) are used as target materials. Laser-produced atoms and ions pass through a 2-mm-diameter aperture in the center of the parabolic reflector and are detected by a quadrupole mass spectrometer (EAI Quad 300). The ionizer of the mass spectrometer is located 25 cm from the metal target. The laser power density at the metal surface is varied by translating the target with respect to the mirror. Ionic species among the metal vapor components are directly mass selected by the quadrupole mass filter and detected by an off-axis channeltron electron multiplier (Galileo Electrooptics CEM 4700). For the detection of neutral particles, an electric field is applied across two deflection plates to remove ionic species. The remaining neutral species are identified after being ionized by electron impact. Time-of-flight (TOF) spectra were recorded with a Textronix 5223 digitizing oscilloscope. Mass spectra were recorded by using a boxcar integrator with a gate width sufficient to include the entire spectrum of TOF values while scanning the mass spectrometer. Ion collection efficiency is enhanced by a positively biased grid installed between the quadrupole rods and electron multiplier as shown in Figure 1. The system pressure is maintained below 1×10^{-7} torr by a 50 L s⁻¹ ion pump.

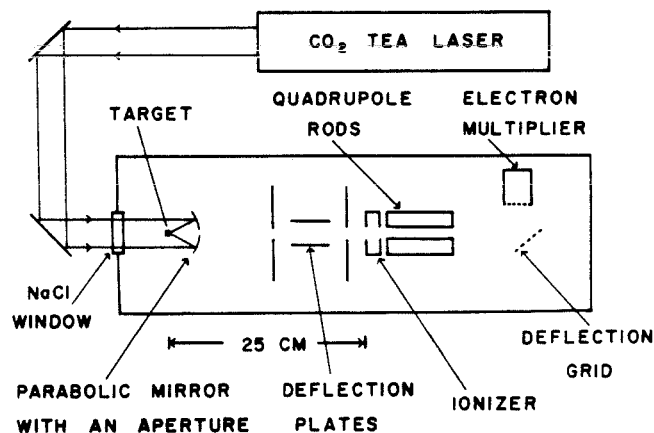


Figure 1. Schematic diagram of the apparatus employed for studies of laser-generated atoms and ions.

Results

The range of ionic species observed in the evaporation of a Ni target at a laser power density of $1 \times 10^8 \text{ W cm}^{-2}$ is shown in Figure 2. Multiply charged ions comprise a significant fraction of the observed ion abundances. The distortion in the recorded Ni isotope ratios for the fast multiply charged ions is due to the limited response time of the boxcar integrator. Reduction of the laser power density either by reduction of total pulse energy or by changing the laser focus results in a decrease of multiply charged ions relative to singly charged ions. When the laser power density is below $2 \times 10^7 \text{ W cm}^{-2}$, ionic species are not produced. It is almost impossible, however, to obtain *only* singly charged ions. Kinetic energies of these ions are measured by using a TOF method. Since the time scale for ion production is much shorter than the time scale for the ions to reach the detector, TOF spectra are converted readily to kinetic energy distributions. Figures 3 and 4 show kinetic energy distributions of laser-generated Al and Ni ions at 1×10^8 and $3 \times 10^8 \text{ W cm}^{-2}$, respectively. They clearly demonstrate the increase of ion kinetic energies with the increase of ionic charge multiplicity. The area under the energy distribution curve is proportional to the number of each ionic species reaching the detector. No attempt was made to correct for the effect of ion kinetic energy on quadrupole transmission and ion detection efficiencies. A correction was made for the variation of neutral atom ionization probability with kinetic energy. Kinetic energy distributions were recorded from single TOF measurements. As a result, the shape of the kinetic energy distribution curve could change slightly for each laser pulse. The TOF distributions were not averaged since they were found to change somewhat from pulse to pulse and occasionally exhibited nonreproducible structure. An example of this behavior is shown with the data in Figure 4. The

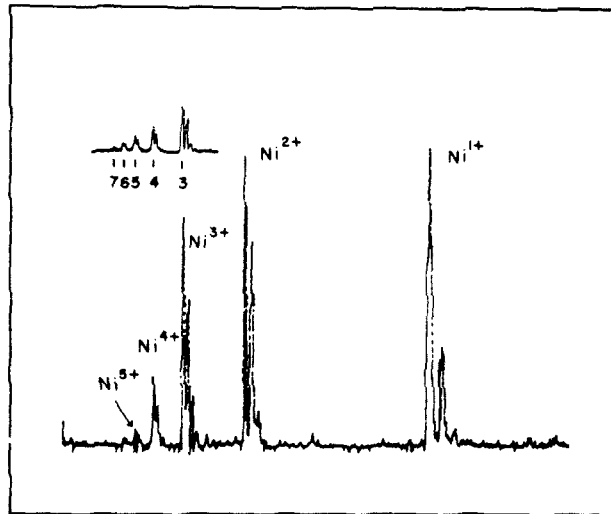


Figure 2. Mass spectrum of ionic species produced by a CO_2 TEA laser pulse focused onto a solid Ni target. Laser power density is approximately $1 \times 10^8 \text{ W cm}^{-2}$ at the target surface. The numbers represents charge multiplicities of each ionic species.

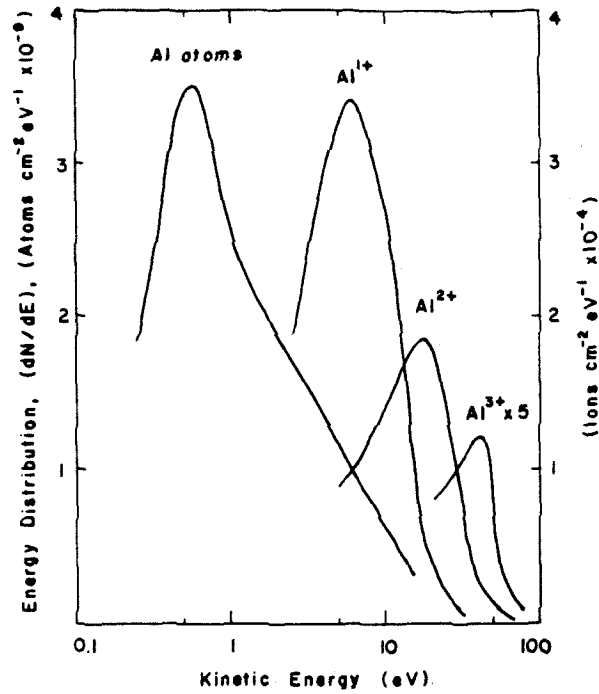


Figure 3. Kinetic energy distributions of Al ions and atoms. A laser pulse of total energy 0.4 J is focused onto an Al target to give a power density of $1 \times 10^8 \text{ W cm}^{-2}$. The particle beam flux is measured at 25 cm from the target. The area under the curve represents the number of the each species detected at this distance. The numbers are approximately 4×10^5 , 5×10^5 , and 1×10^5 ions $\text{cm}^{-2} \text{ pulse}^{-1}$ for Al^{1+} , Al^{2+} , Al^{3+} , and 2×10^{10} atoms $\text{cm}^{-2} \text{ pulse}^{-1}$ for Al atoms, respectively.

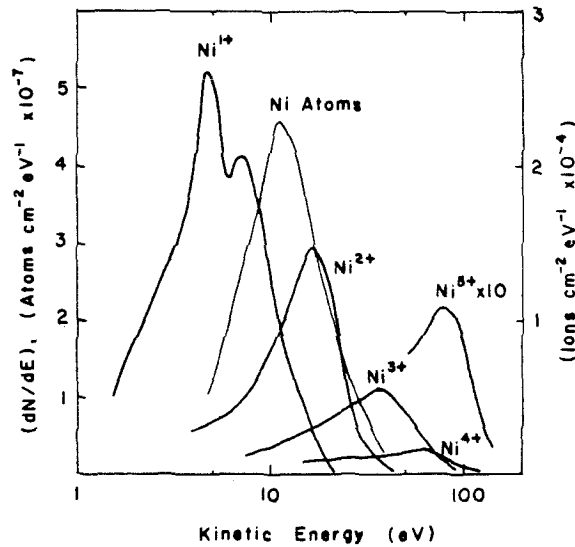


Figure 4. Kinetic energy distributions of Ni ions and atoms. A laser pulse of total energy 0.6 J is focused to give a power density of $3 \times 10^8 \text{ W cm}^{-2}$. The numbers of these species at 25 cm are approximately 2×10^5 , 2×10^5 , 2×10^5 , and 1.4×10^5 ions $\text{cm}^{-2} \text{ pulse}^{-1}$ for Ni^{1+} , Ni^{2+} , Ni^{3+} , and Ni^{4+} , and 8×10^8 atoms $\text{cm}^{-2} \text{ pulse}^{-1}$ for Ni atoms, respectively.

total number of ions produced from the target by a single laser pulse in Figures 3 and 4 can be roughly estimated by assuming that spatial distribution of ejected ions follows a $\cos \theta$ function,⁷ which gives 1×10^{11} and 4×10^{10} ions for Al and Ni, respectively.

A different target geometry where the target surface was set at a nominal 45° to both laser beam and detector, which were perpendicular to each other, was also employed for several studies of ion production. Laser light was focused by a 9.5-cm-focal-length lens onto the target. With this arrangement, the yields and kinetic energy distributions of species with different charge multiplicities are identical with results from the parabolic mirror target geometry shown in Figures 2-4. However, distinct differences are observed in the yields of neutral atoms generated from the two target geometries. Figure 5 presents data for Al atoms generated with different target geometries and laser conditions. The source incorporating the parabolic mirror yields highly energetic Al atoms (curves B and C), whose kinetic energy distribution can be shifted simply by changing the laser power density on the target. In contrast, the 45° geometry source produces a kinetic energy distribution characteristic of thermally evaporated species (curve A) and high kinetic energy atoms are not observed. Failure to detect energetic Al atoms with the 45° geometry target at any laser power density indicates that energetic atoms propagate preferentially along the laser beam and that their flux toward the detector, which is perpendicular to the laser beam, is negligible. The yield of low-energy Al atoms (curve A) decreases and finally disappears after about 10 consecutive laser pulses. Under these conditions, the observed Al ion signals do not vary significantly. The focused laser radiation evaporates the metal target and eventually leads to the formation of a small pinhole in the surface. It appears that neutral atoms are evaporated inside the aperture and cannot be detected in a direction perpendicular to the hole axis. Ion formation occurs when the metal vapor cloud absorbs sufficient laser radiation to form a plasma.^{7,8} This apparently occurs above the surface and leads to ion signals which are not affected by pinhole formation. An obvious advantage of the parabolic mirror geometry is that both laser beam and detector are located on the same axis, permitting observation of the maximum flux of energetic atoms. Consistent signal intensities are obtained even after an extended period of irradiation leads to pinhole formation.

In contrast to the data obtained for Al atoms, the Ni atom TOF distributions varied significantly from pulse to pulse. This made it difficult to characterize the variation in kinetic energy distributions with laser power densities. A laser power density of $3 \times 10^8 \text{ cm}^{-2}$ was found to be optimum for Ni atom production.

Atom angular distributions could not be measured with the apparatus shown in Figure 1. Pinhole formation probably leads to a distribution which is much narrower than $\cos \theta$. Total numbers of Al and Ni atoms produced by a single laser pulse in Figures 3 and 4 are estimated by assuming $\cos \theta$ angular distribution to be 1×10^{15} and 4×10^{13} atoms, respectively, which are interpreted as upper limits. No dimers or larger clusters were observed in the present studies. We estimate that dimers are less than 1% of the atomic species for both neutrals and ions.

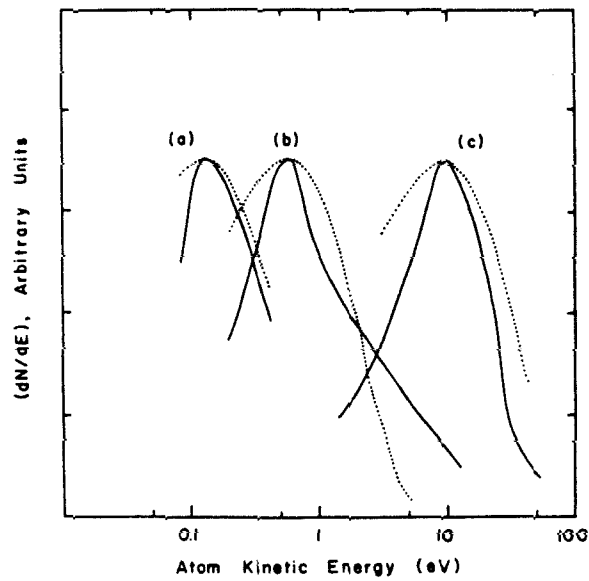


Figure 5. Kinetic energy distributions of Al atoms produced under different conditions of laser power density and target geometry. (a) 45° target geometry at a laser power density of $1 \times 10^8 \text{ W cm}^{-2}$. (b) Parabolic mirror geometry at $1 \times 10^8 \text{ W cm}^{-2}$. (c) Parabolic mirror geometry at $5 \times 10^8 \text{ W cm}^{-2}$. Envelopes of Maxwell-Boltzmann distributions are shown with dotted lines, representing temperatures of 2×10^3 , 9×10^3 , and $1.5 \times 10^4 \text{ K}$ for a, b, and c, respectively.

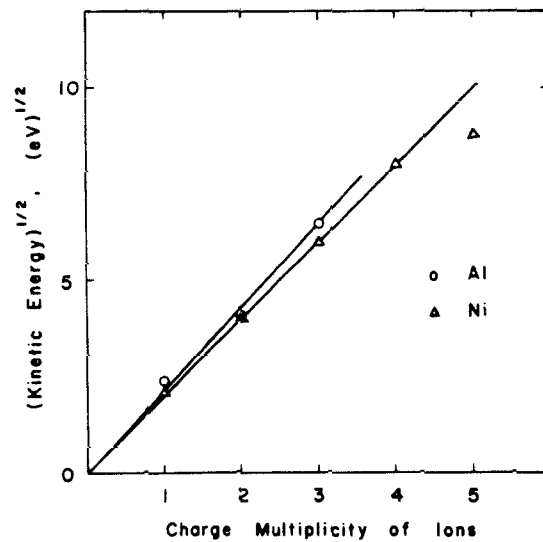


Figure 6. Variation of the most probable ion kinetic energies with charge multiplicity for Al (O) and Ni (Δ) ions presented in Figure 3. The slopes yield electron temperatures of 9.3 and 8.0 eV for Al and Ni, respectively.

Discussion

Kinetic energies greater than several eV are not unusual for laser-generated atoms and ions. The mechanisms leading to generation of such high kinetic energy species, however, have been a subject of controversy. The phenomena associated with ion production are better understood and a quantitative analysis of the present data is possible. This will be presented first, followed by a discussion of neutral atom production.

Consider the events which lead to ion production. The initial interaction of high-power laser radiation with the metal surface generates an evaporated atom cloud together with a few electrons and ions. Further absorption of energy by the expanding cloud results in formation of a high-density pulsed plasma. Electrons in the plasma are accelerated by absorption of laser radiation (inverse Bremsstrahlung process). Production of multiply charged ions in the pulsed plasma results from sequential excitation processes involving collisions of ions with energetic electrons. The lighter electrons escape from the expanding ionized gas, forming a negatively charged sheath around the plasma. The electric field between the negative sheath and the positive core of the quasi-neutral plasma accelerates the ions to final kinetic energies which depend on ion charges and masses. A theoretical analysis of this ion acceleration mechanism¹⁰ predicts that if the plasma contains a minor ion component of mass m and charge multiplicity z in addition to a major ion species of mass M and charge multiplicity Z , then the most probable kinetic energy of the accelerated minor ion component (E_{mp}) can be represented by eq 1, the ion kinetic

$$E_{mp} = (Mz^2/2mZ)T_e \quad (1)$$

energy being a function of ion charge multiplicity, ion mass, and the plasma electron temperature, T_e , which has the same units as E_{mp} . This is confirmed by the data shown in Figure 6, with the square root of the most probable kinetic energy varying linearly with the ion charge. Interestingly, *all* of the ionic species fit the correlation suggested by eq 1, and not just the minor components. The slopes represent electron temperatures of 9.3 and 8.0 eV for the Al and Ni plasma at laser power densities of 1×10^8 and 3×10^8 W cm⁻², respectively. The electron temperature is not to be interpreted as an equilibrium temperature of the laser-generated atom cloud, however, since only a small fraction (10^{-3} - 10^{-4}) of the cloud is ionized at the laser power densities employed.

The production of energetic atoms at high power densities has been observed with the source incorporating the parabolic mirror in the present work and the thin-film targets used in earlier studies. The detailed mechanism of fast atom production is not yet understood. Charge exchange of plasma-accelerated ions as they pass through the slower atom cloud can give rise to fast atoms, but the ion/neutral ratio and measured kinetic energy distributions do not support this mechanism for the majority of the observed fast atoms. Energetic atoms have the following noteworthy characteristics. First, their kinetic energy distributions are distinctly narrower than Maxwell-Boltzmann distributions which match the most probable kinetic energies. These are shown for the Al atom results in Figure 5. Second, the atoms appear to propagate preferentially back along the laser beam, even when it is inclined with respect to the surface normal. Laser-generated atoms with an angular distribution narrower than $\cos \theta$ were also observed in experiments employing the thin-film target geometry.^{1,11} Friichtenicht and co-workers were able to develop a theoretical model which fit their experimentally observed particle velocity distributions.¹² Their model is based on the following

assumptions. The laser-evaporated vapor cloud expands against the target substrate and imparts momentum to it, thereby giving the center of mass of the vapor cloud a constant velocity normal to the surface. During the initial expansion, particles in the vapor cloud equilibrate at a certain temperature resulting in a thermal velocity distribution which would appear spherically symmetric to an observer moving with the center of mass. The center-of-mass velocity and the equilibrium temperature can be adjusted to fit their model to experimental data. They estimated that the equilibrium temperature inferred from this model could be several times lower than would be implied by the measured on-axis kinetic energy distribution.

A significant consideration in employing laser-generated metal ions and atoms for gas-phase reaction studies is the internal state distribution of the beam, since electronically excited species can react very differently from ground-state species.⁹ If the kinetic energy distributions of the energetic atoms observed in the present study are characteristic of equilibrium temperatures of the laser-generated vapor clouds, then a significant fraction of the particles are expected to be in electronically excited states. This problem is reduced in severity if Fritichtenicht's analysis can be applied to the present study and the equilibrium temperature of the atom cloud is indeed lower than the kinetic temperature.

The mechanism of ion production discussed above leaves little doubt that electronically excited species will be present in laser-generated ion clouds. Gas-phase reaction studies employing laser-generated atoms and ions, including mainly ICR studies of the reactions of transition-metal ions with organic molecules,^{4,5} and atom beam-gas collision studies using chemiluminescence detection methods¹³ have not provided indications that the presence of electronically excited reactant species is a major problem. This may, in part, be due to the fact that relatively long time scales are associated with these experiments (about 50 μ s for the beam-gas collision studies and up to several seconds for the ICR studies), permitting even relatively slow radiative decay processes to relax excited-state species in the beam.

As an additional point, the high kinetic energies of laser-generated metal ions have some interesting implications for the ICR studies of these ions. In most experiments only ions with kinetic energies below 1 eV are efficiently confined due to the low trapping voltages employed. Discrimination against multiply charged ions is particularly severe, and it should be possible to observe and study these species by employing higher trapping voltages. Even the simply charged ions have a broad kinetic energy distribution (Figures 3 and 4), however, which may have a pronounced effect in subsequent reactions.¹⁴

Acknowledgment. H.K. thanks the Korean Government for a graduate fellowship (1980-83). This work was supported by a grant from the National Science Foundation (CHE-8407857). Acknowledgment is made to the donors of the Petroleum Research Fund, administered by the American Chemical Society, for partial support of this work.

Registry No. Al, 7429-90-5; Ni, 7440-02-0.

- (1) Fichtenicht, J. F. *Rev. Sci. Instrum.* **1974**, *45*, 51.
- (2) Dietz, T. G.; Ducan, M. A.; Powers, D. E.; Smalley, R. E. *J. Chem. Phys.* **1981**, *74*, 6511. Michalopoulos, D. L.; Geusic, M. E.; Hansen, S. G.; Powers, D. E.; Smalley, R. E. *J. Chem. Phys.* **1982**, *76*, 3914. Powers, D. E.; Hansen, S. G.; Geusic, M. E.; Pulu, A. C.; Hopkins, J. B.; Dietz, T. G.; Duncan, M. A.; Langridge-Smith, P. R. R.; Smalley, R. E. *J. Phys. Chem.* **1982**, *86*, 2556. Powers, D. E.; Hansen, S. G.; Geusic, M. E.; Michalopoulos, D. L.; Smalley, R. E. *J. Chem. Phys.* **1983**, *78*, 2866. Morse, M. D.; Hansen, G. P.; Langridge-Smith, P. R. R.; Zheng, Lan-Sun; Geusic, M. E.; Michalopoulos, D. L.; Smalley, R. E. *J. Chem. Phys.* **1984**, *80*, 5400.
- (3) Gole, J. L.; English, J. H.; Bondybey, V. E. *J. Phys. Chem.* **1982**, *86*, 2560. Bondybey, V. E.; English, J. H. *J. Chem. Phys.* **1982**, *76*, 2165. Bondybey, V. E.; Schwartz, G. P.; English, J. H. *J. Chem. Phys.* **1983**, *78*, 11. Bondybey, V. E.; English, J. H. *J. Chem. Phys.* **1984**, *80*, 568.
- (4) Cody, R. B.; Burnier, R. C.; Reents, W. D., Jr.; Carlin, T. J.; McCrery, D. A.; Lengel, R. K.; Freiser, B. S.; *Int. J. Mass Spectrom. Ion Phys.* **1980**, *33*, 37. Burnier, R. C.; Byrd, G. D.; Freiser, B. S. *Anal. Chem.* **1980**, *52*, 1641. Jacobson, D. B.; Freiser, B. S. *J. Am. Chem. Soc.* **1984**, *106*, 3891, 3900 and references contained therein.
- (5) Uppal, J. S.; Johnson, D. E.; Staley, R. H. *J. Am. Chem. Soc.* **1981**, *103*, 508. Kappes, M. M.; Staley, R. H. *J. Phys. Chem.* **1981**, *85*, 942; Jones, R. W.; Staley, R. H. *J. Phys. Chem.* **1982**, *86*, 1387.
- (6) Fontijn, A.; Felder, W. In "Reactive Intermediates in the Gas Phase: Generation and Monitoring"; Setser, D. W., Ed.; Academic Press: New York, 1979; Chapter II.
- (7) Ready, J. F. "Effects of High-Power Laser Radiation"; Academic Press: New York, 1971.
- (8) Ready, J. F. "Industrial Applications of Lasers"; Academic Press: New York, 1978; Chapter 4.
- (9) Halle, L. F.; Armentrout, P. B.; Beauchamp, J. L. *J. Am. Chem. Soc.* **1981**, *103*, 962.
- (10) Gurevich, A. V.; Pariiskaya, L. V.; Pitaevskii, L. P. *Sov. Phys.—JETP (Engl. Transl.)* **1983**, *36*, 274.
- (11) Marmar, E. S.; Cecchi, J. L.; Cohen, S. A. *Rev. Sci. Instrum.* **1975**, *46*, 1149.
- (12) Utterback, N. G.; Tang, S. P.; Fichtenicht, J. F. *Phys. Fluids* **1976**, *19*, 900.
- (13) Wicke, B. G.; Tang, S. P.; Fichtenicht, J. F. *Chem. Phys. Lett.* **1978**, *53*, 304. Tang, S. P.; Utterback, N. G.; Fichtenicht, J. F. *J. Chem. Phys.* **1976**, *64*, 3833; Wicke, B. G. *J. Chem. Phys.* **1983**, *78*, 6036.
- (14) Armentrout, P. B.; Beauchamp, J. L. *J. Am. Chem. Soc.* **1981**, *103*, 784.